universität wien

DISSERTATION

Titel der Dissertation

Interaction of tumor necrosis factor-alpha with an antibody and of albumin with cholate investigated by FTIR attenuated total reflection spectroscopy

Verfasser

Mag. Norbert HASSLER

angestrebter akademischer Grad

Doktor der Naturwissenschaften (Dr. rer. nat.)

Wien, 2008

Studienkennzahl lt. Studienblatt:	A 091 419
Dissertationsgebiet lt. Studienblatt:	Chemie
Betreuer:	Univ. Prof. Dr. Urs Peter Fringeli

In memoriam

Prof. Urs Peter Fringeli

(1939 – 2008)

Table of contents

Danksagung

Die vorliegende Arbeit wurde am Institut für Biophysikalische Chemie an der Fakultät für Chemie der Universität Wien unter der Anleitung von Prof. Dr. Urs Peter Fringeli durchgeführt. Mein besonderer Dank gilt daher Prof. Fringeli für die stete Unterstützung bei der Planung von Experimenten und für die kritische Diskussion von Ergebnissen. Trotz seiner schweren Erkrankung war er auch nach seiner Emeritierung stets für seine Doktoranden da. Daher ist es umso trauriger, dass er den Abschluss nicht mehr miterleben durfte. Wir werden ihn nicht nur als Professor, sondern auch als guten Freund in Erinnerung behalten.

Insgesamt danke ich der gesamten Arbeitsgruppe, Ass.-Prof. Dr. Dieter Baurecht, Dr. Gerald Reiter (derzeit am Max Planck Institute of Colloids and Interfaces in Golm), Dr. Jasmina Matijašević und Ing. Regina Prossinagg, für das angenehme und freundschaftliche Arbeitsklima. Alle haben in unterschiedlicher, sich ergänzender Weise mit dazu beigetragen, dass diese Arbeit entstehen konnte. Prof. Annette Rompel, der Nachfolgerin von Prof. Fringeli, danke ich für ihre Unterstützung beim Abschluss meines Doktoratsstudiums.

Bei Prof. Dieter Falkenhagen und Dr. Viktoria Weber vom Zentrum für Biomedizinische Technologie der Donau-Universität Krems bedanke ich mich für die Bereitstellung des humanen Tumornekrosefaktors-alpha (hTNF-α) und des hTNF-α-Antikörpers.

Schließlich bedanke ich mich bei meinen Eltern und meinem Bruder für die Unterstützung während des Studiums.

Zusammenfassung

FTIR-Spektroskopie, kombiniert mit der Methode der abgeschwächten Totalreflexion (ATR), wird zunehmend zur Erforschung von oberflächennahen Vorgängen benützt. Zur Untersuchung von Biomembranen, Monoschichten und dünnen Filmen werden sehr empfindliche Methoden benötigt, um deren Oberflächenkonzentrationen und molekulare Strukturen zu bestimmen. In dieser Arbeit wurde die Wechselwirkung zweier Proteine untereinander und eines Proteins mit einem Liganden, die in einer phosphatgepufferten Saline (PBS) gelöst waren, untersucht. Zu diesem Zweck wurden zwei Techniken angewendet: die single-beam-sample-reference (SBSR) Spektroskopie und die konzentrationsmodulierte Anregungs-(c-ME)-Spektroskopie. Gemeinsam führen diese zu optimaler Hintergrundkompensation und verbessertem Signal-Rausch-Verhältnis.

Im ersten Teil wird die Erkennung des immobilisierten humanen Tumornekrosefaktors-alpha (TNF-alpha), eines wichtigen Vermittlers der zellulären Immunantwort, durch den monoklonalen Antikörper Infliximab beschrieben. Rinderserumalbumin (BSA) wurde verwendet, um die unspezifische Bindung des Antikörpers an das multiple interne Reflexionselement (MIRE) zu verhindern. Die durch die SBSR-Technik erhaltenen Spektren ermöglichten die Unterscheidung der beteiligten Proteine auf Grund ihrer unterschiedlichen Amid-Banden. Das molekulare Bindungsverhältnis zwischen immobilisiertem TNF-alpha und dem spezifisch gebundenen Antikörper betrug 5.3.

Im zweiten Teil dieser Arbeit wurde die Wechselwirkung von Cholat mit adsorbiertem humanem Serumalbumin (HSA) untersucht. Cholat gehört zu den Gallensäuren und ist ein Ligand von HSA, dem am häufigsten vorkommenden Protein im Blut. Um die reversible Reaktion von immobilisiertem HSA auf periodische Konzentrationsänderungen von Cholat zu bestimmen, wurde c-ME-Spektroskopie

angewendet. Die Antwort des Protein-Ligand-Systems wurde dabei mittels zeitaufgelöster FTIR-Spektroskopie gemessen und die anfallenden Daten einer phasen-sensitiven Detektion (PSD) unterworfen. Dadurch konnten störende Signalkomponenten, die nicht die gleiche Frequenz wie die Anregung hatten, eliminiert werden. Die erzielte Empfindlichkeit lag im Mikro-Absorbanzbereich, was eine Grundbedingung darstellt, um spezifische Wechselwirkungen auf molekularem Niveau aufzulösen. Um Informationen über Bindungskapazität und –verhalten zwischen immobilisiertem Serumalbumin und Cholat zu erhalten, wurden die Modulationsexperimente mehrere Male im Cholatkonzentrationsbereich zwischen 0.3 mM und 20 mM durchgeführt. Dabei konnte eine Zunahme alpha-helikaler Strukturen von HSA als Folge der Cholatbindung beobachtet werden. Bindungskurven können auch durch Surface-plasmon-resonance (SPR) erhalten werden. Obwohl die c-ME Spektroskopie höheren experimentellen Aufwand als SPR erfordert, liegt ihr Vorteil im Zugang zu Informationen über strukturelle Änderungen im Rezeptor, die durch die Ligandenbindung verursacht wurden. Der Hintergrundkompensation wurde besondere Aufmerksamkeit gewidmet, um überlappende spektrale Beiträge von gelöstem und an HSA gebundenem Cholat zu trennen.

Summary

FTIR attenuated total reflection (ATR) spectroscopy is increasingly used for investigations of processes at or near a surface. Very sensitive techniques are needed, particularly if biomembranes, monolayers, and thin films are studied with respect to surface concentration and molecular structure. In this work the interaction of two proteins and of a protein with a ligand dissolved in a phosphate buffered saline (PBS) was investigated. For this purpose two techniques were used; single beam sample reference (SBSR) spectroscopy and concentration-modulated excitation (c-ME) spectroscopy, resulting in an optimum background compensation and signal-to-noise ratio.

First the recognition of immobilized human tumor necrosis factor-alpha (TNF-alpha), an important mediator of cellular immune response, by a monoclonal antibody known as Infliximab was studied. Bovine serum albumin (BSA) was used to avoid unspecific bonding of the antibody. Differences in the amide bands enabled the discrimination of the proteins by their spectra obtained by SBSR spectroscopy. The molecular ratio of the bonding between TNF-alpha adsorbed to a multiple internal reflection element (MIRE) and the corresponding antibody resulted in 5.3.

In the second part of this work the interaction of cholate with adsorbed HSA was investigated. Cholate belongs to the bile acids and is a ligand of human serum albumin (HSA), the most abundant protein in blood. c-ME spectroscopy was applied to study the reversible reaction of immobilized HSA to periodic changes of the concentration of cholate. The response of the system was measured with time-resolved FTIR spectroscopy and then processed by a phase-sensitive detection (PSD), thus eliminating disturbing signal components, which did not have the same frequency like the excitation itself. The achieved sensitivity was in the micro-absorbance range, a prerequisite for studying specific interactions on a molecular level. In order to get information about bonding capacity and behaviour between immobilized albumin and cholate, modulation experiments were performed several times with concentrations of cholate in the range of 0.3 mM to 20 mM. An increase of alpha-helical structures of HSA was observed upon cholate bonding. Bonding curves are determined usually by surface plasmon resonance (SPR). Although c-ME spectroscopy requires higher experimental effort than SPR, its advantage is the access to information about structural changes in the receptor caused by ligand bonding. Special attention was paid to background compensation in order to separate overlapping spectral contributions of dissolved and HSA-bonded cholate.

1 Introduction

1.1 Background and aim of this work

This work was inspired by Prof. Urs Peter Fringeli of the Institute for Biophysical Chemistry of the University of Vienna and by Prof. Dieter Falkenhagen and Dr. Viktoria Weber of the Center for Biomedical Technology of the Danube University of Krems. Collaboration between the Institute for Biophysical Chemistry and the Center for Biomedical Technology to investigate the mechanisms of sepsis was established for several years [1,2]. First we investigated the interaction of human tumor necrosis factor-α (TNFα) with a monoclonal antibody known as Infliximab. The antibody was produced to remove excess TNFα from the blood system in the case of overexpression because an elevated concentration of TNFα is involved in the development of many diseases (see Section 1.2). The aim of the work was to find out whether adsorbed TNFα is still recognized by the antibody and if it is possible to determine surface concentrations of both proteins, which is a precondition to evaluate the ratio between TNFα and antibody bond to TNFα. Antigen-antibody interactions are usually investigated by enzyme linked immunosorbent assays (ELISA). In the first part of this work we transferred a simplified version of ELISA to FTIR attenuated total reflection (ATR) spectroscopy.

Encouraged by good results Prof. Fringeli made the proposal to build up a system for concentration-modulated excitation spectroscopy (c-MES) to study the interaction of an immobilized receptor and a ligand in aqueous environment. Such a system can serve as an additional and complementing technique to surface plasmon resonance (SPR) because it provides both the bonding curve of the receptor-ligand interaction and structural information about the influence of the ligand on the receptor. So far, one question remained: Which receptor-ligand system should be taken?

At the time of this question the Center for Biomedical Technology developed an extracorporeal liver support system ("artificial liver") [3]. In such a system human serum albumin (HSA) plays an important part in blood cleaning, however, not HSA in solution, as in blood, but HSA immobilized on cellulose. Therefore, information about the bonding capacity and behaviour between immobilized albumin and metabolites like bilirubin, bile acids, and ammonia is of great medical interest. In the case of liver failure these substances bonded to albumin must be removed from the blood by the artificial blood cleaning system.

For this reason we decided to select HSA as receptor, and cholate, a bile acid, as ligand for the system to be investigated. Procedures for covalent immobilization of proteins on Ge surfaces were established using aminosilanes and carbodiimide [4]. To exclude chemical modifications of the receptor caused by covalent immobilization, in this work the simplest technique of immobilization was used, i.e. adsorption of the receptor.

In the second part of this PhD thesis I investigated the interaction of cholate with HSA adsorbed to a multiple internal reflection element (MIRE). FTIR ATR spectroscopy was used to get quantitative information on effects initiated by specific interaction. The experimental setup may also serve as a model reactor for artificial blood cleaning. In order to achieve a spectroscopic sensitivity above that of conventional difference spectroscopy, modulated excitation (ME) FTIR ATR spectroscopy was applied [5]. Excitation of HSA was performed by periodically exchanging the cholate solution and pure buffer in an ATR cuvette.

1.2 Human tumor necrosis factor alpha (hTNFα)

First the deathly action on cancer cell of this cytokin was discovered. Today it is known that hTNFα plays an important part as mediator in cellular immune response and

inflammation. It is involved in the progress of a lot of diseases like septic shock, cancer, AIDS, rheumatoid arthritis and malaria. It acts as a positive stimulant for the immune system, but it is also responsible for the loss of weight of patients in the course of chronic infections (cachexia). If it is overexpressed, especially caused by infection of Gram negative bacteria, it can lead to death because of septic shock. The participation in the development of autoimmune diseases is also discussed [6].

The sequence of amino-acid residues and the three-dimensional structur is known [7]. hTNFα is a homotrimeric protein with a molecular weight of 52.1 kDa. The subunits are hold together because of hydrophobic interactions. A ribbon representation is shown in Fig. 1. The protein has the shape of a cone with a basal plane of about 2400 $Å^2$ ($d \approx 55$ Å) and a height of 55 Å. The main secondary structural element is the antiparallel β-sheet (45%). Other structural elements are β-turns and random conformations, but there is no α-helix.

1.3 Anti-hTNFα antibody (AB)

The monoclonal antibody has its origin from a human-murine cell line and is available as Infliximab (Remicade®). It is clinically applied for therapy in rheumatoid arthritis and Crohn's disease. The antibody belongs to the IgG1 subclass and has a molecular weight of 146 kDa. The main secondary structural element is the β-sheet (50%). The α-helix content is less than 5% [8].

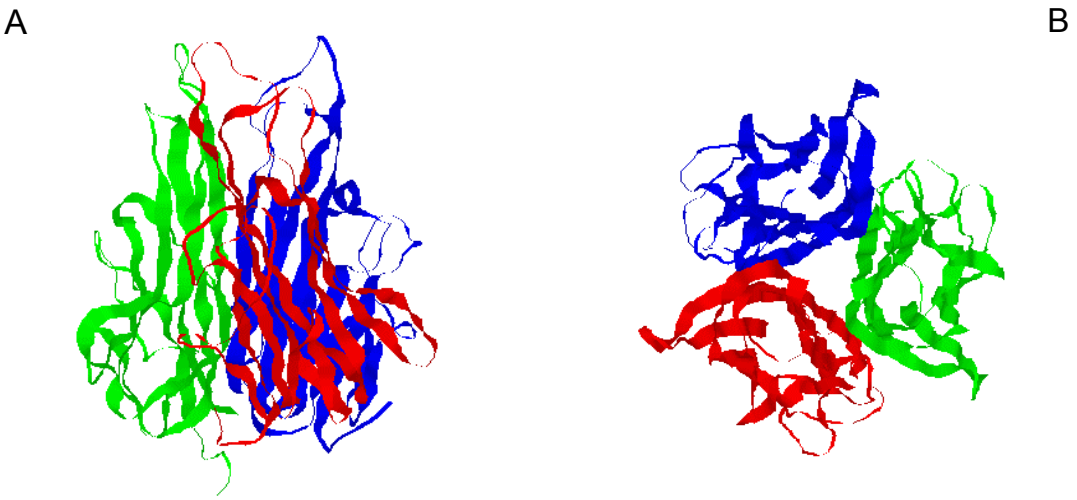

Fig. 1: Ribbon representation of the trimeric hTNFα consisting of antiparallel β-sheets (45%), β-turns and random conformation; there are no α-helices. A: front view. B: view from the top. Data from x-ray structure analysis (PDB-file 1TNF [7]) viewed with RasWin Molecular Graphics 2.6. Fig. from [9].

1.4 Serum albumins (BSA and HSA)

Bovine (BSA) and human (HSA) serum albumin belong to the group of serum albumins and exhibit almost the same inner composition, as it was proved by sequence homology. Both proteins are monomeric with a molecular weight of 66.4 kDa and consist of 583 (BSA) and 585 (HSA) amino acid residues, respectively. The main structural element of albumins is the α-helix (BSA: 68 %, HSA: 67%), the content of β-turns is 17 % in BSA and 10% in HSA. These proteins have no β-sheets. Whereas BSA is important because of its role as model protein and its many in-vitro applications, HSA was investigated in a lot of clinical, metabolic, and genetic studies [10].

The shape of BSA is shown in Fig. 2. The cigar-like appearance with the dimensions of 140 Å x 40 Å x 40 Å was derived from hydrodynamic data [11]. Since x-ray investigations on crystals are not available so far, these dimensions were used to calculate

the theoretical surface concentration, which can be achieved in the case of 100 % coverage of the MIRE.

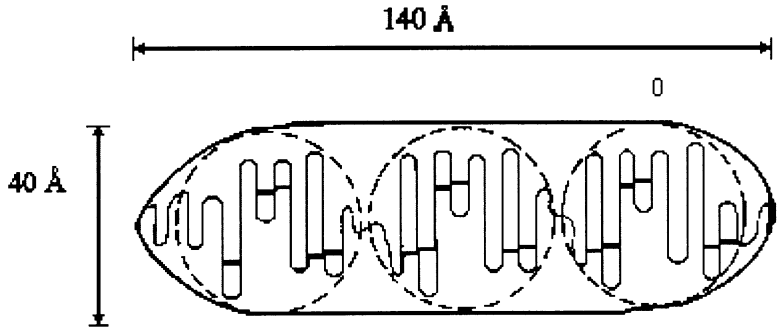

Fig. 2: Schematic representation of BSA derived from hydrodynamic measurements resulting in a size of 140 Å x 40 Å x 40 Å. Dashed circles denote three homologous domains, each of them consisting of 9 loops connected by disulfide bonds. Fig. from [11].

As a principal component of blood with a concentration of about 40 mg/ml, HSA (Fig. 3) belongs to one of the most studied proteins [10,12]. It is mainly responsible for the maintenance of blood pH [13] and for the bonding and transport of many metabolites in the blood circuit. As found by x-ray studies, its threedimensional shape can be approximated as an equilateral triangle with sides of ~80 Å and a depth of ~30 Å [12]. The difference in appearance and dimensions compared to BSA is explained by the fact that hydrodynamic measurements are performed on albumin in solution, whereas in x-ray studies the proteins are crystallized and, therefore, have a reduced mobility. The real shape depending on the qualities of the surrounding medium is supposed to be between these limits.

Although HSA has a high degree of conformational flexibility, its structure exhibits remarkable resistance against denaturation [14], which is a precondition to perform long time experiments. On hydrophilic surfaces it adsorbs as monomolecular film [15].

The most outstanding property of albumins is their ability to bond many different ligands reversibly; one of it is cholate, the anion of cholic acid at the pH of blood. Belonging to the bile acids, it is produced from cholesterol in the liver and stored in the gall bladder. Its main function is to solubilize lipids of food in progress of digestion. A list of HSA bonding ligands is shown in Table 1.

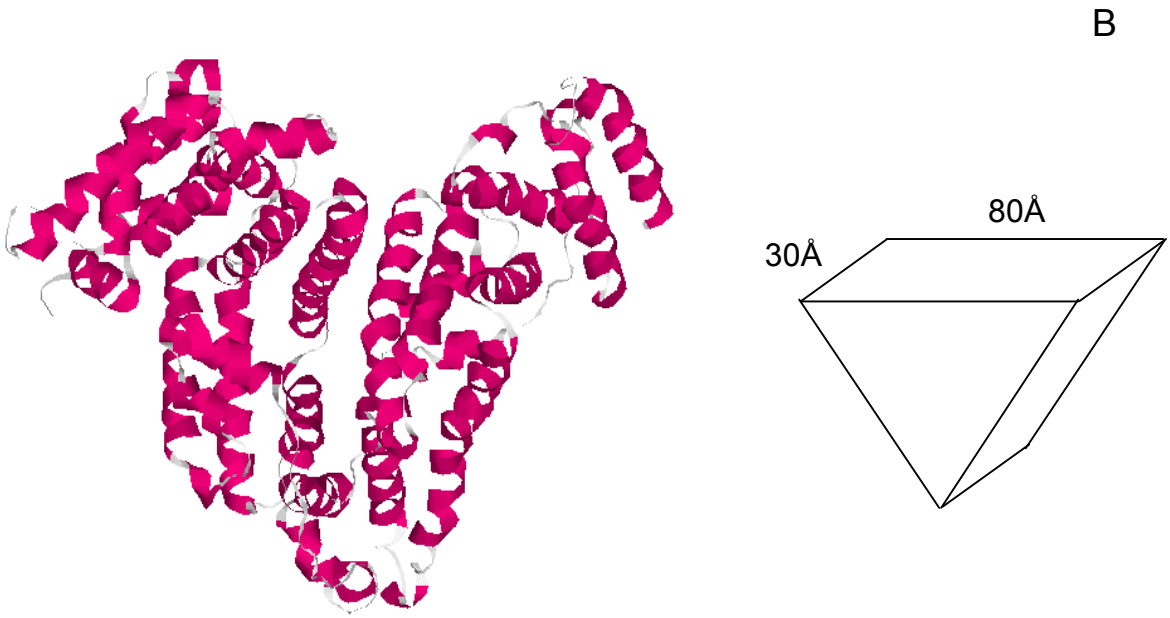

Fig. 3. Human serum albumin (HSA). (A) Ribbon representation of HSA. Red ribbons denote α-helices of the molecule. The image was calculated by RasWin Molecular Graphics 2.6 using x-ray data (PDB file 1BJ5). (B) Schematic representation of HSA emphasizing the three dimensional shape of one molecule. It can be approximated as an equilateral triangle with sides of ~80 Å and a "thickness" of ~30 Å. Fig. from [9].

1.5 Cholate

Cholate has a molecular weight of 430.6 g/mol and is a so called natural detergent (Fig. 4). Considering that its basic constitution is like a cholesterol, the molecular structure reveals areas with hydrophobic and hydrophilic qualities, explaining the solubilizing properties by its stereochemical characteristics [16]. It is known from equilibrium dialysis

that 1 mol HSA in solution bonds 2.8 mol cholate with an association constant of 3300 ($K_{a,1}$) and 12.0 mol with an association constant of 300 ($K_{a,2}$) [17].

Table 1. A small selection of ligands of human serum albumin (HSA) [10].

Compound	Association constant, K_A (M^{-1})	n	Reference
Long-chain fatty acids[a]	(1–69) × 10^7	1	Richieri *et al.* (1993)
Eicosanoids (PGE_1)	7 × 10^4	2	Unger (1972)
Bile acids[b]	(3–200) × 10^3	3	Roda *et al.* (1982)
Steroids			
Cortisol[c]	5 × 10^3	2	Yates and Urquhart (1962)
Progesterone[c]	3.6 × 10^5	1	Ramsey and Westphal (1978)
Testosterone[c]	2.4 × 10^4	1	Pearlman and Crepy (1967)
Aldosterone	3.2 × 10^3	1	Richardson *et al.* (1977)
Bilirubin	9.5 × 10^7	1	Brodersen (1982)
Hematin	1.1 × 10^8	1	Adams and Berman (1980)
L-Thyroxine	1.6 × 10^6	1	Kragh-Hansen (1981)
L-Tryptophan	1.0 × 10^4	1	McMenamy and Oncley (1958)
25-OH-Vitamin D_3	6 × 10^5	1	Bikle *et al.* (1986)
1,25-$(OH)_2$-Vitamin D_3	5 × 10^4	1	Bikle *et al.* (1986)
Aquocobalamin	2 × 10^7	1	Lien and Wood (1972)
Folate	9 × 10^2		Soliman and Olesen (1976)
Ascorbate	3.5 × 10^4	0.1	Molloy and Wilson (1980)
Copper(II)	1.5 × 10^{16}	1	Masuoka *et al.* (1993)
Zinc(II)	3.4 × 10^7	1	Masuoka *et al.* (1993)
Calcium	15.1 × 10^2	1	Kragh-Hansen and Vorum (1993)
	6.5 × 10^2	3	
Magnesium	1 × 10^2	12	Pedersen (1972a)
Chloride	7.2 × 10^2	1	Scatchard and Yap (1964)
	6.1 × 10^1	4	

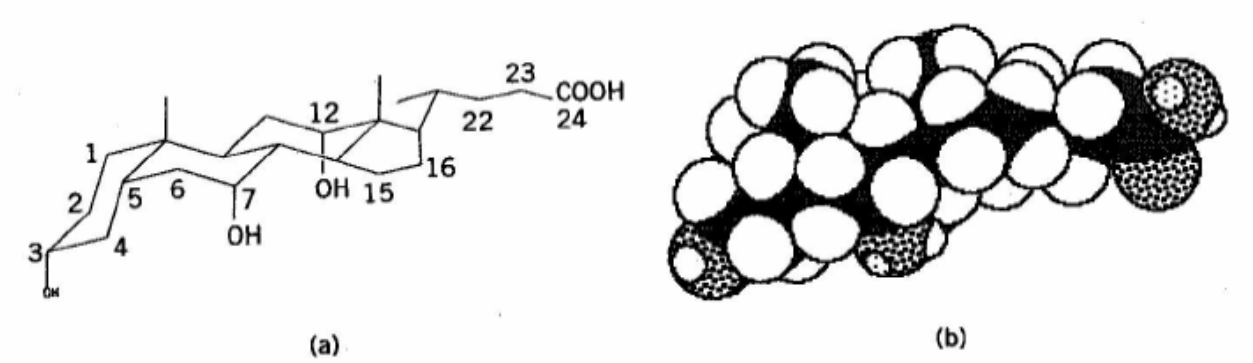

Fig. 4. Stereochemistry of cholate. (a) Chemical structure. (b) Molecular model. The molecule shows two faces: a hydrophilic and a hydrophobic one explaining the amphibatic properties of cholate. Fig. from [16].

2 Theory

2.1 ATR Spectroscopy – Basic considerations

The phenomenon of total internal reflection occurs during the crossing of a beam of light between optically differently permeable media with the refractive indices n_1 and n_2 in case of following conditions: The beam has to cross the media from the optically denser to the rarer medium ($n_1 > n_2$), and the angle of incidence θ has to exceed the critical angle ($\theta > \theta_c$). The critical angle θ_c is determined by the refractive indices of the two media: $\sin \theta_c = n_2/n_1 = n_{21}$.

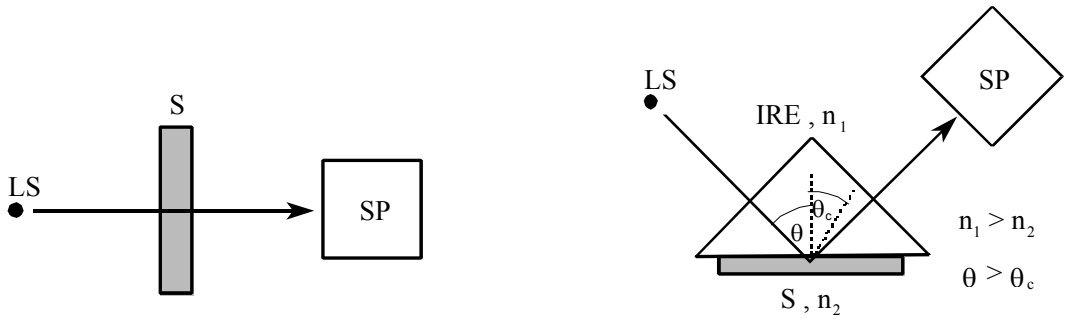

a. TRANSMISSION b. INTERNAL REFLECTION

Fig. 5. Comparison of transmission (a) and internal reflection (b) technique. In a transmission experiment the sample is penetrated totally by the light beam, whereas in case of internal reflection the beam is reflected at the interface between denser and rarer media. θ: angle of incidence, θ_c: critical angle, n_1, n_2: refractive index of internal reflection element (IRE) and sample (S). Abbreviations: LS, light source; SP, spectrometer; IRE, internal reflection element (ATR crystal). Fig. from [18].

Fig. 5 shows a schematic comparison of transmission and internal reflection. While in case of transmission the light penetrates the sample completely, internal reflection causes total reflection of the beam at the interface between denser and rarer media. On that condition an electromagnetic field still exists beyond the reflecting interface in the rarer medium. This field exhibits the frequency of the incoming light, but the amplitude of the

electric field E is reduced exponentially with the distance z from the surface according to eq. (1).

$$E = E_0 \, e^{-\frac{z}{d_p}} \qquad (1)$$

The penetration depth d_p is given by

$$d_p = \frac{\lambda_1}{2\pi \left(\sin^2 \theta - n_{21}^2\right)^{\frac{1}{2}}} \qquad (2)$$

λ_1 denotes the wavelength of the beam in medium (1), which is in this case the internal reflection element. According to eq. (2) the penetration depth is in the range of λ_1.

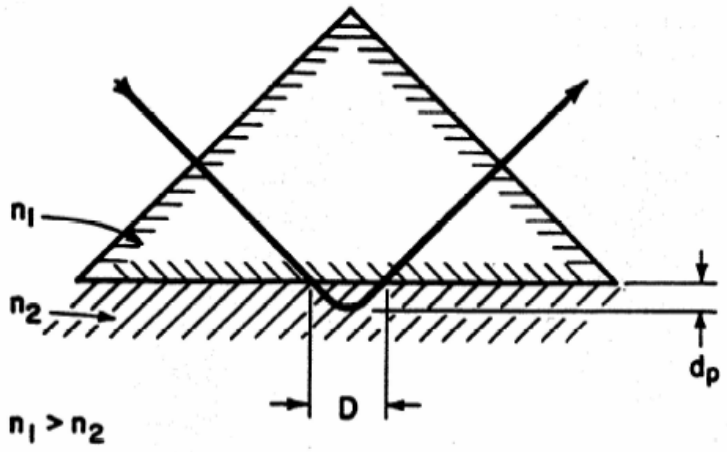

Fig. 6: Path of ray of light in case of total internal reflection. The ray penetrates a fraction of a wavelength (d_p) beyond the reflecting surface into the rarer medium of refractive index n_2, and there is a certain displacement D upon reflection. Fig. from [19].

Fig. 6 emphasizes the displacement D of the reflected ray, referred to as Goos-Hänchen displacement [20], as a result of the internal reflection. The electromagnetic field in the rarer medium is denoted as evanescent wave and consists of electric field components along all three axes of the rectangular coordinate system attached to the ATR plate (see Fig. 7), whereas the incident plane wave only exhibits electric field components in the plane perpendicular to the direction of propagation. Two selected directions of the

incident electric field vector are chosen via a polarizer, namely parallel (||, pp) and perpendicular (⊥, vp) to the plane of incidence.

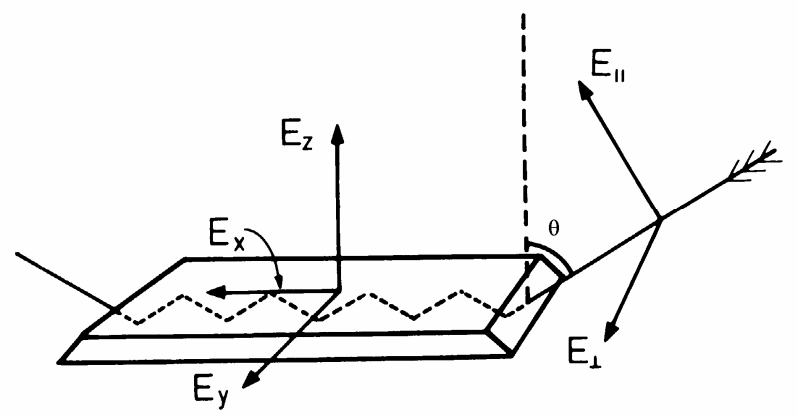

Fig. 7: Multiple internal reflection element (MIRE) with plate-fixed koordinate system. From geometrical considerations, it follows that $E_{||}$ results in E_x and E_z components, and $E_\perp$ in the E_y component of the evanescent field, respectively. θ, angle of incidence; $E_{||}$, E parallel (pp) and $E_\perp$, E perpendicular (vp) polarized components of the electric field of incident light; E_x, E_y, E_z, electric field components with respect to the plate fixed-coordinate system ($E_{||} \rightarrow E_x, E_z$, $E_\perp \rightarrow E_y$). Fig. from [21].

The relative electric field components $E^r_{0x2,0y2,0z2}$ in the rarer medium (2) at z=0, i.e. the interface of media (1) and (2), resulting from the ratio between the absolute field components E_{0x2}, E_{0z2}, E_{0y2} and $E_{1||}$, $E_{1\perp}$, are given by Fresnel's equations [22]. Eq. (3) holds exactly for nonabsorbing media (1) and (2), but is also a good approximation for weak absorbing samples. For bulk rarer medium (2) it follows that

$$E^r_{0x2} = \frac{E_{0x2}}{E_{1||}} = \frac{2\cos\theta\left(\sin^2\theta - n_{21}^2\right)^{1/2}}{\left(1-n_{21}^2\right)^{1/2}\left[\left(1+n_{21}^2\right)\sin^2\theta - n_{21}^2\right]^{1/2}}$$

$$E^r_{0z2} = \frac{E_{0z2}}{E_{1||}} = \frac{2\cos\theta\sin\theta}{\left(1-n_{21}^2\right)^{1/2}\left[\left(1+n_{21}^2\right)\sin^2\theta - n_{21}^2\right]^{1/2}} \qquad (3)$$

$$E^r_{0y2} = \frac{E_{0y2}}{E_{1\perp}} = \frac{2\cos\theta}{\left(1-n_{21}^2\right)^{1/2}}$$

with $(E^r_{02||})^2 = (E^r_{0x2})^2 + (E^r_{0z2})^2$ and $(E^r_{02\perp})^2 = (E^r_{0y2})^2$

In presence of a thin film (2) fixed to the surface of the reflection element (1) the evanescent wave penetrates also into the surrounding medium (3). Provided that the layer thickness d is small compared to the penetration depth d_p the so-called thin layer approximation can be applied. It supposes that the electric field in the rarer medium is influenced by media 1 and 3 only and that the thin layer (2) is taken into account as a dielectric inserted into this field (see Fig. 8). For a thin immobilized layer (2) in contact with bulk rarer medium (3) it follows that

$$E^r_{0x2} = \frac{E_{0x2}}{E_{1\|}} = \frac{2\cos\theta\left(\sin^2\theta - n_{31}^2\right)^{1/2}}{\left(1-n_{31}^2\right)^{1/2}\left[\left(1+n_{31}^2\right)\sin^2\theta - n_{31}^2\right]^{1/2}}$$

$$E^r_{0z2} = \frac{E_{0z2}}{E_{1\|}} = \frac{2\cos\theta\,\sin\theta\,n_{32}^2}{\left(1-n_{31}^2\right)^{1/2}\left[\left(1+n_{31}^2\right)\sin^2\theta - n_{31}^2\right]^{1/2}} \qquad (4)$$

$$E^r_{0y2} = \frac{E_{0y2}}{E_{1\perp}} = \frac{2\cos\theta}{\left(1-n_{31}^2\right)^{1/2}}$$

with $(E^r_{02\|})^2 = (E^r_{0x2})^2 + (E^r_{0z2})^2$ and $(E^r_{02\perp})^2 = (E^r_{0y2})^2$

In these equations, n_{ik} denotes the ratio of refractive indices n_i/n_k of medium i and k, where i,k = 1,2,3 stand for ATR plate, thin film and surrounding medium, respectively. For bulk rarer medium only, i.e. in absence of a layer, index (3) must be replaced by (2), thus resulting in eq. (3). Equations are taken from [18].

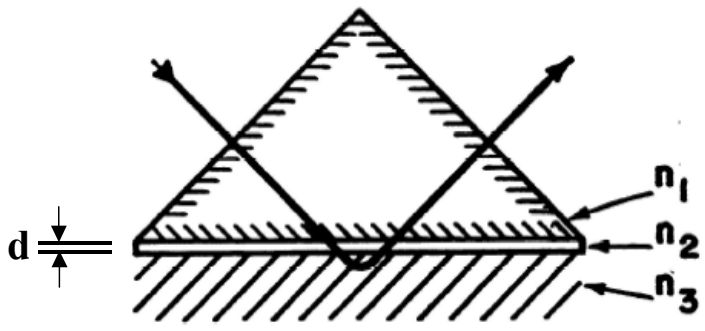

Fig. 8: A thin layer of thickness d<dp with refractive index n_2 is fixed on the surface of the internal reflection element. Fig. from [19].

2.2 Quantitative analysis of thin layers

2.2.1 Isotropic samples – The concept of effective thickness

The Lambert-Beer law is used for quantitative analysis in transmission spectroscopy according to eq. (5).

$$T = \frac{I}{I_0} = 10^{-A} = 10^{-\varepsilon c d_e} \qquad (5)$$

T and A denote transmission and absorbance, respectively. I_0 and I stand for intensity of light before and after sample. c and ε denote concentration and the molar absorption coefficient.

The quantity d_e stands for the effective thickness and indicates the thickness of a sample that would result in the same absorbance in a hypothetical transmission experiment, as obtained with the original ATR experiment. The concept of effective thickness was first used by Harrick [19] and further developed and applied in [18, 23]. It enables the application of Lambert-Beer's law on ATR spectra.

For a layer of thickness d extended from $z = z_i$ to $z = z_f$ ($d = z_f - z_i$) one obtains:

$$d_e = \frac{n_2}{n_1 \cos\theta} \cdot \frac{d_p}{2} \cdot \left(e^{-\frac{2z_i}{d_p}} - e^{-\frac{2z_f}{d_p}} \right) \cdot (E_{02}^r)^2 \qquad (6)$$

The relative electric field in the sample $(E_{02}^r)^2$ stands either for pp light $(E_{02\parallel}^r)^2$ or for vp light $(E_{02\perp}^r)^2$. It should be noted that such a simple expression for the effective thickness is only available for polarized light. For a bulk medium extended from $z_i = 0$ to $z_f = \infty$ eq. (6) results in

$$d_e^{bulk} = \frac{1}{\cos\theta} \frac{n_2}{n_1} \frac{d_p}{2} (E_{02}^r)^2 \qquad (7)$$

If an immobilized layer (z_i=0, z_f = d) with thickness d is small compared to the penetration depth of the evanescent wave (d<<d_p), the remaining exponential in eq. (6) can be linearized. Then d_e results in

$$d_e^{th,iso} = \frac{1}{\cos\theta}\frac{n_2}{n_1} d\,(E_{02}^r)^2 \qquad (8)$$

It should be noted that $d_e^{th,iso}$, contrary to d_e^{bulk}, is no longer dependent on wavelength because d_p is cancelled after linearization.

The corresponding effective thicknesses for parallel and perpendicular polarized incident light differ by the factor

$$\frac{d_{e_{l\|}}}{d_{e\perp}} = \frac{(E_{0x2}^r)^2 + (E_{0z2}^r)^2}{(E_{0y2}^r)^2} \qquad (9)$$

For a bulk isotropic medium this factor is 2.0 provided that the angle of incidence θ is 45°. The effective thickness achieved with unpolarized light is a linear combination of $d_{e_{l\|}}$ and $d_{e\perp}$, where the ratio is dependent on the pre-polarization by optical components of the spectrometer. Therefore, simple application of the Lambert-Beer law to ATR data requires the use of polarized incident light. A detailed analysis is given in [18].

2.2.2 Oriented samples – Determination of structure

If polarized incident IR light is used to record spectra, absorbances of oriented samples are not only dependent on the number of molecules per area, but also on the arrangement of the sample. The peak absorbance or the integrated absorbance of a given band is the experimentally accessible quantity required for the determination of surface concentration and orientation of samples. The integrated absorbance of a given band is proportional to the square of the scalar product between the transition dipole moment $\vec{M}$ and the electric field $\vec{E}$ of radiation.

$$\int_{band} A(\nu)d\nu = c\, d\int \varepsilon(\nu)d\nu \quad \propto \quad \left(\frac{\vec{E}}{|\vec{E}|}\cdot\vec{M}\right)^2 = |\vec{M}|^2 \cdot \cos^2(\vec{M},\vec{E}) \qquad (10)$$

The transition dipole moment $\vec{M}$ is the change of the molecular transition dipole moment during a vibriational transition. Eq. (10) is the basis for orientation measurements, since the area of an absorbance band is directly related to the angle between $\vec{M}$ and $\vec{E}$.

In orientation measurements the relevant parameter for data analysis is the so-called dichroic ratio R.

$$R(\tilde{\nu}) = \frac{\int A_{pp}(\tilde{\nu})\, d\tilde{\nu}}{\int A_{vp}(\tilde{\nu})\, d\tilde{\nu}} \qquad (11)$$

$\int A_{pp}(\tilde{\nu})\, d\tilde{\nu}$ and $\int A_{vp}(\tilde{\nu})\, d\tilde{\nu}$ denote the integrated absorbences of a given absorption band measured with pp and vp incident light, respectively. Peak absorbences may also be used instead of integrated absorbances. Assuming a liquid crystalline ultrastructure (LCU) of the sample with uniaxial orientation along the normal to the MIRE (z-axis), one obtains for the dichroic ratio the following expression:

$$R(\tilde{\nu}) = \frac{\int A_{pp}(\tilde{\nu})\, d\tilde{\nu}}{\int A_{vp}(\tilde{\nu})\, d\tilde{\nu}} = \frac{(E^r_{0x2})^2}{(E^r_{0y2})^2} + 2\frac{(E^r_{0z2})^2\overline{\langle\cos^2\Theta\rangle}}{(E^r_{0y2})^2\left(1-\overline{\langle\cos^2\Theta\rangle}\right)} \qquad (12)$$

$\overline{\langle\cos^2\Theta\rangle}$ denotes the average over the mean squares of the cosines of the angles between the transition dipole moments of a given vibration and the z-axis of the laboratory coordinate system, which is fixed to the MIRE. The xy-plane is parallel to the surface of the MIRE, with the x-axis directing along the light propagation. A detailed analysis of the theory of orientation measurements and examples of its application are given in [23] and [1,24], respectively.

2.2.3 Determination of surface concentrations and error calculation

The volume concentration c and the surface concentration Γ are related to each other via the thickness of the sample d. By introducing Lambert-Beer's law one obtains

$$c = \frac{\Gamma}{d} = \frac{\int A(\tilde{\nu})d\tilde{\nu}}{N\nu\, d_e^{th} \int \varepsilon(\tilde{\nu})d\tilde{\nu}} \qquad (13)$$

$\int A(\tilde{\nu})\, d\tilde{\nu}$ denotes the integrated absorbance of a distinct absorption band measured with parallel (pp) and perpendicular (vp) polarized incident light, respectively. N and ν are the mean number of the active internal reflections and the number of equal functional groups per molecule. $\int \varepsilon(\tilde{\nu})\, d\tilde{\nu}$ denotes the decadic integrated molar absorption coefficient of the band. d_e^{th} is the effective thickness of the layer depending on the structure of the layer as well as on the polarization of incident light [23]. Therefore, the surface concentration Γ can be expressed by using the dichroic ratio R determined by experiments and the relative electric field strengths (see eqs. (3) and (4)).

$$\Gamma = \frac{d \int A(\tilde{\nu})\, d\tilde{\nu}}{3N\nu\, d_e^{th,\,iso} \int \varepsilon(\tilde{\nu})\, d\tilde{\nu}} \left[2 - \frac{(E_{0x2}^r)^2}{(E_{0z2}^r)^2} + R \frac{(E_{0y2}^r)^2}{(E_{0z2}^r)^2} \right] \qquad (14)$$

As presented in eq. (14), the surface concentration Γ can be seen as the projection of the molecules in the volume defined by unit area and height d of the real sample. $d_e^{th,\,iso}$ denotes the effective thickness of an isotropic layer of real thickness d, as given by eq. (8). Equations are taken from [24].

Input parameters and uncertainties used in all calculations such as the angle of incidence, refractive indices, integrated molar absorption coefficients, and the number of active internal reflections are listed in Table 2.

Uncertainties of results were evaluated by calculation of standard deviations or straightforward error propagations. Analytical expressions for partial derivatives were

determined by means of the Symbolic Mathematical Toolbox of MATLAB [25], whereas the final numeric calculation of overall uncertainties was performed by means of the standard MATLAB software.

Table 2. Magnitudes and uncertainties of input parameters used in evaluations of surface concentrations and dichroic ratios.

Parameter	Symbol	Magnitude	Uncertainty[a]
Angle of incidence [deg]	θ	45.00	1.50
Refractive index of germanium MIRE	n_1	4.00	0.00
Refractive index of an adsorbed protein layer	n_2	1.45	0.05
Refractive index of the aqueous environment at 1547 cm^{-1} / at 1405 cm^{-1}	n_3	1.33 / 1.31	0.05
Integrated molar absorption coefficient of amide II [cm mol^{-1}] [21]. Linear baseline. Range of integration: 1598 ± 1 – 1482 ± 1 cm^{-1}.	$\int \varepsilon_{amideII}\, d\tilde{\nu}$	8.25×10^6	2.90×10^5
Integrated molar absorption coefficient of $\nu_s(COO^-)$ of cholate in PBS [cm mol^{-1}]. Linear baseline. Range of integration: 1484 ± 2 - 1350 ± 2 cm^{-1}.	$\int \varepsilon_{(COO^-)}\, d\tilde{\nu}$	1.36×10^7	1.36×10^6
Number of carboxylic groups per cholate molecule	ν	1	0
Number of active internal reflections using a reflection element of 1.5 / 2.0 mm thickness	N	26.8 / 19.6	1.0

[a] The limit of confidence is approximately 90%.

2.2.4 Solvent compensation

In ATR spectroscopy the quality of absorbance spectra of thin layers measured in the presence of solvents depends on a good compensation of solvent bands, especially if the solvent absorbs in the same spectral regions as the thin layer of interest. In a typical experiment an absorbance spectrum of a thin layer is calculated using a spectrum of the solvent as reference recorded in absence of the layer. The evaluation of the interaction between TNFα and the anti-TNFα antibody was performed in this traditional way. We found out that in this case neglecting of solvent compensation contributed 0.5 - 1% to the errors of surface concentrations only.

In case of evaluation of the bonding curve characterizing the interaction between adsorbed HSA and cholate the omission of solvent correction produced a systematic error of results up to about 6% (see Table 8, p. 76). Therefore, for a more precise quantitative evaluation of thin films we considered the overcompensation of the solvent due to its displacement by the layer.

Since according to eq. (2) the evanescent field produced by the IR beam on the surface of the reflection element penetrates proportionally to the wavelength of the beam into the rarer medium, basic ATR theory has to be applied for an accurate compensation of the solvent.

As long as the solvent behaves as weak absorbing, i.e. the Napierian absorption index κ of the complex refractive index $\hat{n} = n + i\kappa$ fulfills the condition $\kappa < 0.1$, quantitative analysis may be performed with the concept of effective thickness. The effective thickness d_e represents a hypothetical thickness for a transmission cell in order to result in the same absorbance as obtained per one internal reflection in the ATR experiment. A general expression of the effective thickness for a layer of thickness d of a weak absorbing medium ranging from z_i to z_f ($d = z_f - z_i$) is given by eq. (6).

During measuring an absorbance spectrum of the solvent, which serves as reference for the calculation of the thin layer spectrum, the solvent is in direct contact with the reflexion element. Now the thickness d can be considered as infinite with $z_i = 0$ and $z_f = \infty$. From eq. (6) and eq. (7) it follows that the corresponding absorbance spectrum of the solvent is given by

$$A(\tilde{\nu}) = N \cdot \varepsilon(\tilde{\nu}) \cdot c \cdot d_e^{bulk}(\tilde{\nu}) \qquad (15)$$

$A(\tilde{\nu})$ denotes absorbance, $\varepsilon(\tilde{\nu})$ is the molar absorbance coefficient, c denotes molarity, and N is the number of active internal reflections.

After adsorption of a layer on the reflexion element a thin film of solvent in the amount of the thickness d of the layer is displaced. Considering eq. (6) the solvent starts now at $z_i = d$ and $z_f = \infty$. Therefore, the effective thickness d_e of the solvent at presence of a layer is described by

$$d_e = \frac{n_2}{n_1 \cos\theta} \cdot \frac{d_p}{2} \cdot e^{-\frac{2d}{d_p}} \cdot E_0^{r2} \qquad (16)$$

Eq. (6) and (16) differ in the factor $e^{-\frac{2d}{d_p}}$ only. Therefore, the overcompensated absorbance spectrum of the solvent $A_{overcomp}(\tilde{\nu})$ taking the replacement by the layer into account is given by

$$A_{overcomp}(\tilde{\nu}) = N \cdot \varepsilon(\tilde{\nu}) \cdot c \cdot d_e^{bulk}(\tilde{\nu}) \cdot e^{-\frac{2d}{d_p}} \qquad (17)$$

In principle, the layer thickness d is accessible via the surface concentration Γ, the molecular mass M_r, and the specific layer density ρ according to $d = \Gamma \cdot M_r / \rho$. In this work the layer thickness d was adjusted by the operator in such a way that the resulting spectrum of the layer showed a reasonable compensation in the spectral region of the stretching vibration ν of the aqueous solvent (for an example, see Fig. 28, p. 62). It should be noted that thickness d does not reflect the real thickness of the layer, but the amount of

replaced solvent. A MATLAB program used for calculation of solvent compensations is listed in Section 7.1. A procedure correcting the overcompensation of a silan layer is presented in [26].

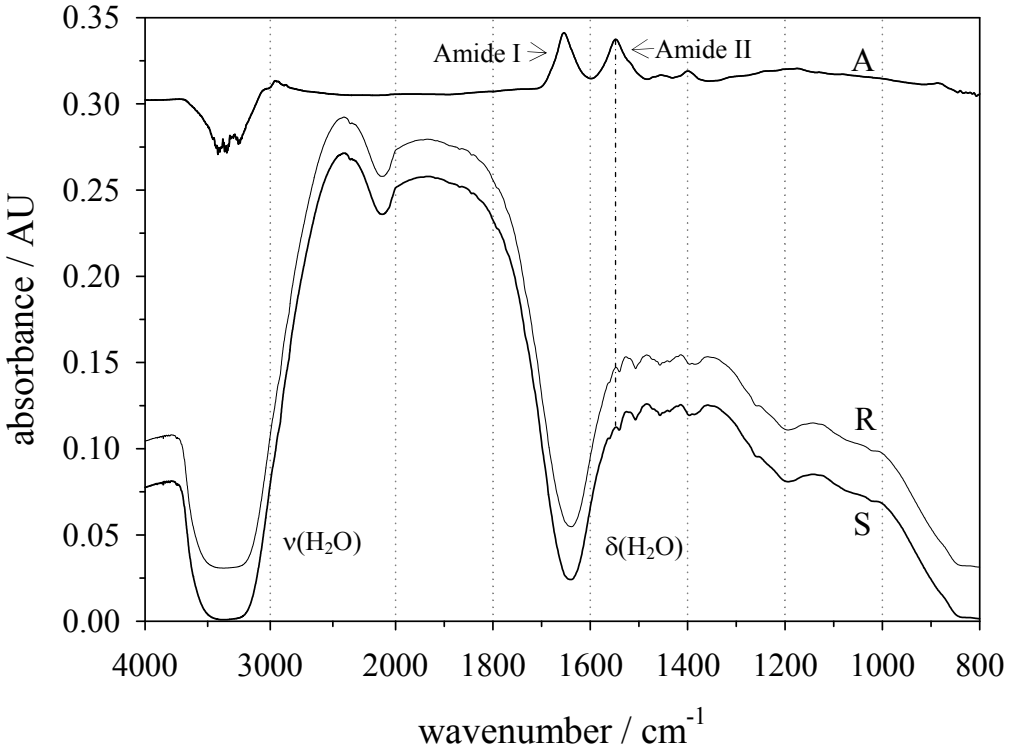

Fig. 9. Water incompensation as a result of adsorption of proteins to the surface of the reflection element.
R: Intensity spectrum of the R compartments containing PBS. This spectrum is shifted upward for clarification.
S: Intensity spectrum of the S compartments of the reflection element featuring an adsorbed albumin layer. The S compartments were also filled with PBS.
R and S spectra show that the water stretching vibration $\nu(H_2O)$ at ~3400 cm^{-1} is responsible for complete absorption of energy. In this region no other OH stretching vibrations can be detected. At the water bending vibration (~1645 cm^{-1}) only 10% of whole energy is available. Since the amide I band is placed in the center of this vibration, it is influenced very strongly even by small water incompensations. Therefore, this band cannot be used for quantitative evaluations. In case of a good water compensation between R and S compartments, the amide II band at ~1550 cm^{-1} is not affected because it is located at the edge of $\delta(H_2O)$.
R and S spectra have a relative scale of energy.
A: IR ATR absorbance spectrum of S and R according to A = -log(S/R). The negative band of $\nu(H_2O)$ is the result of buffer replacement by the adsorbed protein layer in the S compartments. A solvent compensation procedure, as presented in this Section can correct the amount of replaced buffer, but not the changed structure of water in the surrounding of the protein (hydration water) making such compensation calculations incomplete.

Quantitative analysis of protein layers in aqueous environment is faced with the following problem (Fig. 9): Water as a main component of buffers absorbs at 3400 cm^{-1} (stretching vibration, ν) and at 1645 cm^{-1} (bending vibration, δ). IR spectra of proteins are dominated by two bands, the amide I (1630-1660 cm^{-1}) and the amide II (1520-1550 cm^{-1}) band. Quantification by amide I is not possible because it is covered completely by $\delta(H_2O)$, even if water is accurately compensated between R and S compartments of the flow-through cell. The amide II band can be used for determination of surface concentrations because it is less influenced by $\delta(H_2O)$. However, small incompensations always occur because an adsorbing layer removes buffer from the surface of the MIRE, as it is seen at the negative ν (H_2O) in spectrum A of Fig. 9. A solvent compensation procedure can correct the amount of replaced buffer, but not the changed structure of water in the surrounding of the protein (hydration water) making such compensation calculations incomplete.

2.3 Modulated excitation spectroscopy (MES)

Modulated excitation spectroscopy, also denoted as modulation spectroscopy, is a sensitive technique to investigate reversible reactions. The method is based on the stimulation of the system by a periodic alteration of an external parameter, such as temperature [27], pressure, electric field [28], or concentration [29,30]. Then the system will respond periodically at the frequency of the stimulation and with higher harmonics, depending on the Fourier components of the stimulation and non-linearities of the system. A setup for modulated excitation (ME) spectroscopy is shown in Fig. 10.

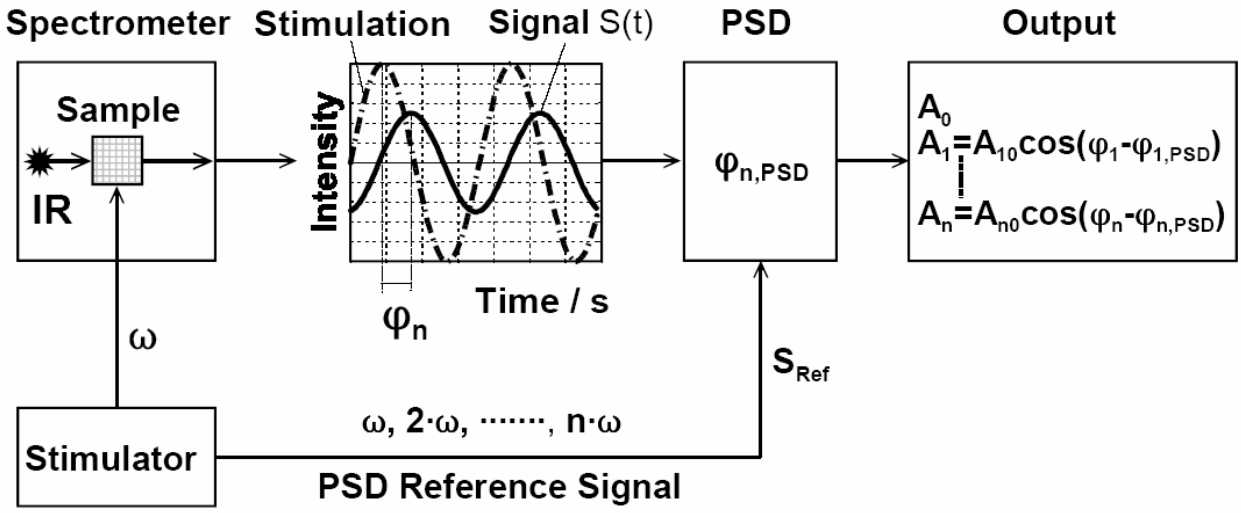

Fig. 10: Schematic setup for modulated excitation (ME) spectroscopy. A periodic excitation is exerted on the sample with frequency ω. The sample response S(t), as sensed by IR spectroscopy, contains the frequency ω and higher harmonics at wavelengths that are significant for those parts of the sample that have been affected by the stimulation. Selective detection of the periodic sample responses is performed by phase sensitive detection (PSD), resulting in A_n of fundamentals ω (n=1) and their harmonics nω (n=2,3,....), as well as the phase shifts in between the n-th harmonic and the stimulation. $\varphi_{n,PSD}$ is the operator-controlled PSD phase setting. Fig. from [5].

After starting of an ME experiment the investigated system leaves its equilibrium state and achieves a new steady-state. This process is finished after three times the largest

relaxation time of the system. Now data acquisition begins by recording spectra, whereas the stimulation period T is divided in equidistant time slices. Spectra representing the time slices are the so-called sample point spectra (SPS). Stimulation of the system accompanied by simultaneous measuring of SPS is repeated till the desired signal-to-noise ratio is achieved. Then corresponding SPS are averaged resulting in the response of the sample $A(\tilde{\nu}, t)$ according to eq. (18).

$$A(\tilde{\nu}, t) = A_0(\tilde{\nu}) + \sum_k A_k(\tilde{\nu}) \cdot \sin(k\omega t + \phi_k) \qquad (18)$$

$A(\tilde{\nu}, t)$ includes now the time-resolved information about the spectral response of the sample, which was periodically stimulated by the frequency ω. Generally, $A(\tilde{\nu}, t)$ represents the overlay of all responses to the fundamental frequency ω as well as to higher harmonics k·ω. $A_0(\tilde{\nu})$ is the mathmatical expression of the mean absorbance per modulation period and is given by

$$A_0(\tilde{\nu}) = \frac{1}{T} \int_0^T A(\tilde{\nu}, t)\, dt \qquad (19)$$

A digital phase sensitive detection (PSD) is performed on $A(\tilde{\nu}, t)$ producing phase-resolved or demodulated spectra according to eq. (20),

$$A_k^{\phi_k^{PSD}}(\tilde{\nu}) = \frac{2}{T} \int_0^T A(\tilde{\nu}, t) \cdot \sin(k \cdot \omega t + \phi_k^{PSD})\, dt \qquad (20)$$

Inserting eq. (18) into eq. (20) gives after integration

$$A_k^{\phi_k^{PSD}}(\tilde{\nu}) = A_k(\tilde{\nu}) \cdot \cos(\phi_k - \phi_k^{PSD}) \qquad (21)$$

The main qualities of PSD are described by eqs. (18) – (21). Demodulation of $A(\tilde{\nu}, t)$, which reflects the periodic response of the system, is carried out by multiplication with a so-called demodulation function, in most cases a harmonic function, like in eq. (20). If demodulation occurs at ω (k = 1), the response to the fundamental frequency

is evaluated. Responses to higher harmonics ($k > 1$) are accessible by demodulation at frequencies $k \cdot \omega$. Generally, the mathmatical operation of eq. (20) takes out the amplitude of the sample response, which was triggered by frequency $k \cdot \omega$, from the entire signal resulting in phase-resolved spectra described by eq. (21). ϕ_k^{PSD} denotes the operator-controlled phase angle. With its help the phase delay ϕ_k of the $k \cdot \omega$ response between the start of stimulation with frequency ω and the response of the system can be determined.

If the system is stimulated by a harmonic function, responses at $k \neq 1$ are a hint for non-linear events in reaction kinetics. Time-resolved information about the investigated process is in principle also available via the phase delays ϕ_k because they are influenced by rate constants and reaction kinetics. If the relaxation times τ_i of the excited process fulfill the condition $0.1 < \omega\tau_i < 10$, where ω is the angular frequency of the modulation and τ_i is the i-th relaxation time of the system, modulation spectroscopy with subsequent phase sensitive detection provides a Fourier analysis of the system response, which is typical of the reaction scheme to be evaluated. Traditional difference spectroscopy cannot offer this information.

If the modulation period is long compared to the relaxation times, like in concentration-modulated excitation, MES exhibits following advantages compared to usual difference spectroscopy. (i) Demodulated spectra feature a signal-to-noise ratio at least 10 times better than spectra obtained by traditional difference spectroscopy, since all noise, which has not the frequency ω of the stimulation, is eliminated by PSD. (ii) Demodulated spectra exhibit a stable baseline because only changes caused by excitation within a modulation period are identified by PSD. All other signals of the investigated system, which would contribute to usual difference spectra, are cancelled by this way. Detailed information about MES is available in [5,47].

For quantification of cholate bonded to HSA the following features of c-ME have to be considered: (1) The geometric mean of all intensity spectra of a modulation period was used as reference for calculating absorbance SPS, thus reflecting a concentration-modulated excitation of half the cholate concentration (c/2) around the mean. Therefore, amplitudes in phase-resolved absorbance spectra had to be multiplicated by a factor of 2 to represent the real concentration change of cholate. (2) Within one modulation period (T = 588 sec) the volume of the cholate solution and of PBS, respectively, was exchanged about 28 times in the sample cuvettes at the applied flow rate of 0.9 ml/min resulting in a nearly rectangular excitation function (see Fig. 41, p. 85).

A periodic rectangular function can be approximated by a sum of sinusoidal functions according to

$$f_{rect}(\omega t) = \frac{4a}{\pi} \cdot [\sin(\omega t) + \frac{\sin(3\omega t)}{3} + \frac{\sin(5\omega t)}{5} + ... + \frac{\sin(k\omega t)}{k}] \qquad (22)$$

The parameter a, in our case, corresponds to half of the cholate concentration used in the modulation experiments. t denotes the time. ω is the angular frequency of the modulation period T resulting in $1.07 \cdot 10^{-2}$ s^{-1} ($\omega = 2\pi/T$). Each summand of the Fourier series causes a stimulation of the HSA layer, but only the response to the fundamental frequency was used for quantification of bonded cholate. A graphic representation of one period of a rectangular function with an amplitude of 2.5 (reflecting the situation of the c-ME experiment with 5 mM cholate) and its first three Fourier components (k = 1, 3, 5) is shown in Fig. 9. The amplitude of the fundamental frequency is enhanced by a factor of $4/\pi$ compared to the rectangular function. Therefore, the amplitudes of phase-resolved spectra in experimental results had to be multiplied by $2 \times \pi/4 = \pi/2$ to reflect the absorbance change between zero and maximum concentration.

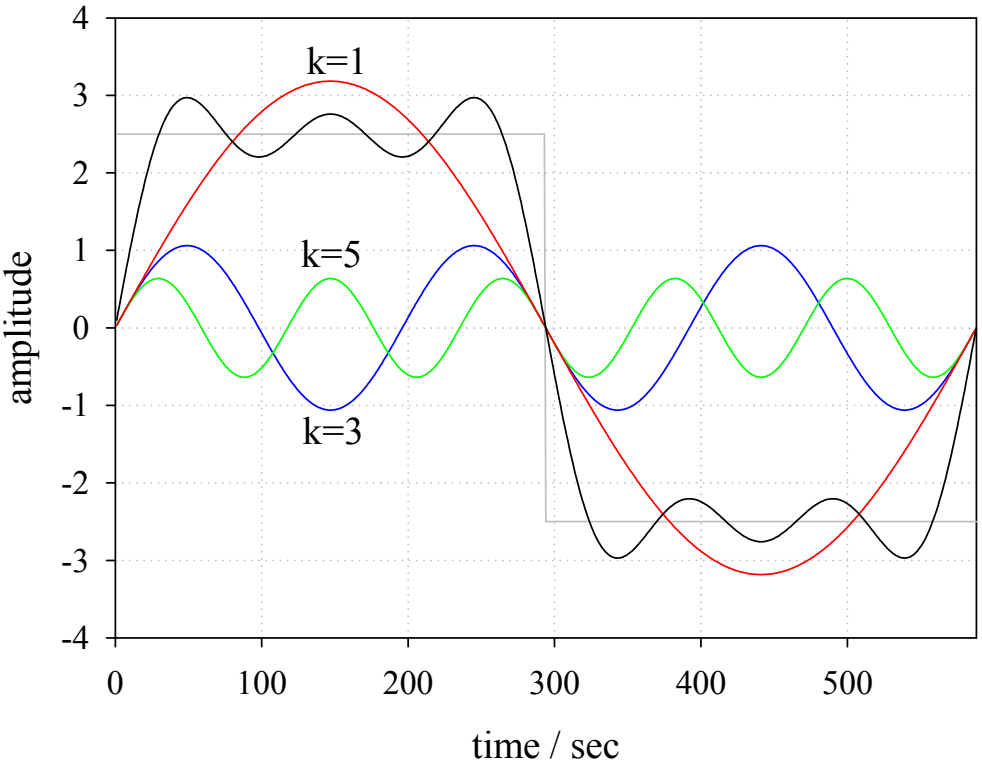

Fig. 9. Rectangular function (a = 2.5, $\omega = 1.07 \cdot 10^{-2}$ s^{-1}, T = 588 sec) according to eq. (22) and Fourier components (k = 1, 3, 5). The sum (black) of the first three summands (k = 1: red, k = 3: blue, k = 5: green) of the Fourier series represents a simple approximation of the rectangular function (gray). The amplitude of the fundamental frequency (k = 1) is enhanced by a factor of $4/\pi$ compared to the amplitude of the rectangular function, a fact, which had to be considered in evaluation of c-ME experiments.

2.4 Receptor-ligand interactions

2.4.1 Principles

The chemical equation for an association between a receptor (R) and a ligand (L) is given by

$$R + nL \underset{k_d}{\overset{k_a}{\leftrightarrow}} RL_n \qquad (23)$$

where k_a is the association rate constant and k_d is the dissociation rate constant of the receptor-ligand complex. n denotes the number of identical, but not cooperative bonding sites of the ligand. The association constant K_a (not to be mixed up with the association rate constant k_a) of the ligand bonding reaction is $K_a = k_a/k_d$, whereas the dissociation constant K_d is $K_d = 1/K_a = k_d/k_a$.

Data of bonding studies are analyzed by applying a modified type of the Langmuir adsorption isotherme given by [31]

$$y = \frac{B_{max} \cdot x}{K_d + x} \qquad (24)$$

where the number of bonded ligand molecules (y-axis) is plotted against the concentration of free ligand (x-axis). B_{max} denotes the maximum number of bonding sites of the ligand on the receptor.

In case of two independent types of bonding sites the equation results in

$$y = \frac{B_{max,1} \cdot x}{K_{d,1} + x} + \frac{B_{max,2} \cdot x}{K_{d,2} + x} \qquad (25)$$

where $B_{max,1}$ and $B_{max,2}$ are the maximum numbers of bonding sites characterized by $K_{d,1}$ and $K_{d,2}$, respectively.

2.4.2 Surface plasmon resonance (SPR)

A common technique used for the analysis of receptor-ligand interaction is surface plasmon resonance (SPR) [31]. It allows the determination of bonding curves by monitoring the association and dissociation of a receptor-ligand complex in real time. The interaction partners have not to be labeled. The principle of SPR measurements is based on an optical phenomenon (see Fig. 11). The core unit is a sensor chip consisting of a thin gold film with a modified surface fixed on one side. One reactant is attached to the

modified sensor surface, whereas the other reaction partner flows past this surface in solution. If the two interaction partners form a complex, the mass on the surface of the sensor chip increases. After dissociation of the complex the mass is reduced. These changes are accompanied by alterations in the refractive index in the aqueous layer near the surface of the sensor chip measured by an optical detection unit on the dry side of the chip. The signal is represented by arbitrary resonance units (RU), which are approximately proportional to the change in mass [31].

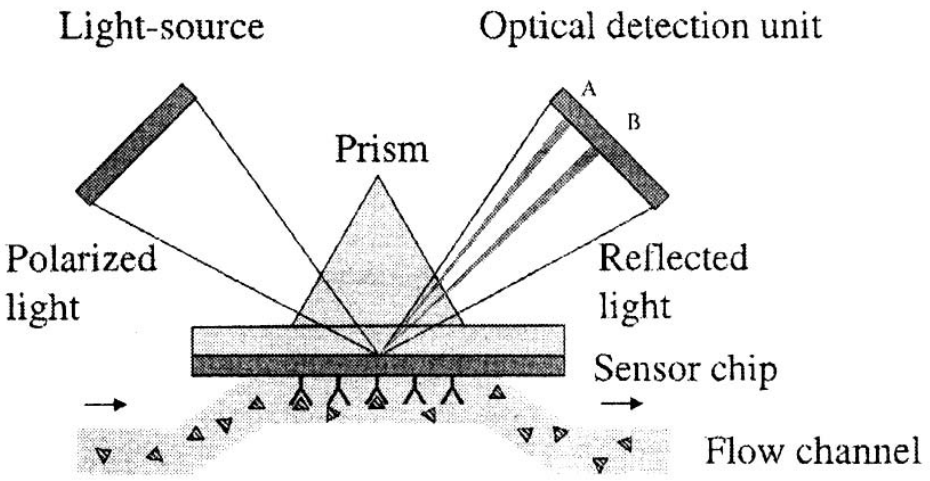

Fig. 11. Schematic setup of a surface plasmon resonance (SPR) detection unit [31]. One interaction partner is immobilized on a modified gold surface, whereas the other flows by in solution. On the other side of the sensor chip a beam of polarized light is reflected by the gold layer. The optical phenomenon of SPR leads to a reduction in the intensity of reflected light at a certain angle (A). This effect is dependent on the refractive index at the surface of the sensor and, thereby, on the mass bonded to the chip (B). The response is then displayed in resonance units (RU).

3 Materials and methods

3.1 Chemicals and biochemicals

Interaction of hTNFα with anti-hTNFα antibody

Human TNFα used in this work was a recombinant version produced in yeast and bought from Strathmann Biotec AG. The monoclonal antibody against hTNFα known as Infliximab (Remicade®) was obtained from Dieter Falkenhagen, Center for Biomedical Technology, Danube University Krems. BSA was used as purchased from Sigma (A7906). Phosphate buffered saline (PBS) consisted of 10 mM Na_2HPO_4/NaH_2PO_4 pH 7.6, 100 mM NaCl, and 0.02% (w/v) sodium azide NaN_3.

Interaction of HSA with cholate

Human serum albumin (HSA; Sigma code: A3782) and sodium cholate (C6445) were used as purchased from Sigma. PBS consisted of 10 mM Na_2HPO_4/NaH_2PO_4 pH 7.2, 150 mM NaCl, and 0.02% (w/v) NaN_3.

All solutions were prepared with ultrapure water (Elga, USA) offering a specific resistance of 18MΩ•cm (25°C). Before use all solutions were degased.

3.2 Experimental setup of FTIR ATR measurements

FTIR spectra were recorded with Bruker IFS 25 and IFS 66 spectrometers at 4 cm^{-1} resolution using Blackman-Harris 3-term apodization and a zero filling factor of 4. Phase correction of single-sided interferograms measured by IFS 25 was performed using Mertz procedure. Interferograms recorded by IFS 66 were measured using the double-sided mode allowing the calculation of the intensity spectrum as power spectrum. This mode should be used preferentially if the spectrum has extended ranges of low light intensity, e. g.

absorption of H_2O vibrational modes. The sample compartment of the spectrometer was purged with dry and carbon dioxide free air.

Both spectrometers were equipped with an attenuated total reflection (ATR) attachment (Optispec, Neerach, CH) providing a mercury-cadmium telluride (MCT) detector and an aluminium grid polarizer on a KRS-5 substrate (Specac, Orpington, U.K.) enabling measurements with parallel (pp) and perpendicular (vp) polarized IR light. A setup of the SBSR ATR attachment is presented in Fig. 12.

Multiple internal reflection elements (MIRE) were made of germanium in a trapezoidal shape with dimensions of 52 x 20 x 2.0 mm^3 and 51 x 20 x 1.5 mm^3, respectively. The entrance and exit areas for the IR beam were prepared for an angle of incidence θ of 45°. The outline of a MIRE used in all experiments is shown in Fig. 7.

Before use the reflection element was cleaned with aceton, water, and ethanol consecutively, until there were no visible impurities left. After removing of small particles originating from cleaning tissues with compressed air the reflection element was exposed 3 min to plasma (Harrick Sci. Corp.) to get rid of remaining traces of organic compounds. Cleaness of the Ge plate was checked by the appearance of $\nu(CH_2)$ bands at ~2920 and ~2850 cm^{-1}. If these bands vanished entirely in the FTIR ATR intensity spectrum measured by the single beam mode, the plate was regarded as to be clean. If this procedure did not lead to a clean surface, each side of the plate was polished 10 min by machine (Logitech PM5) with a pellon cloth rotating at 60 rpm or 3 min manually with a nylon cloth by means of a 0.25 μm diamond paste.

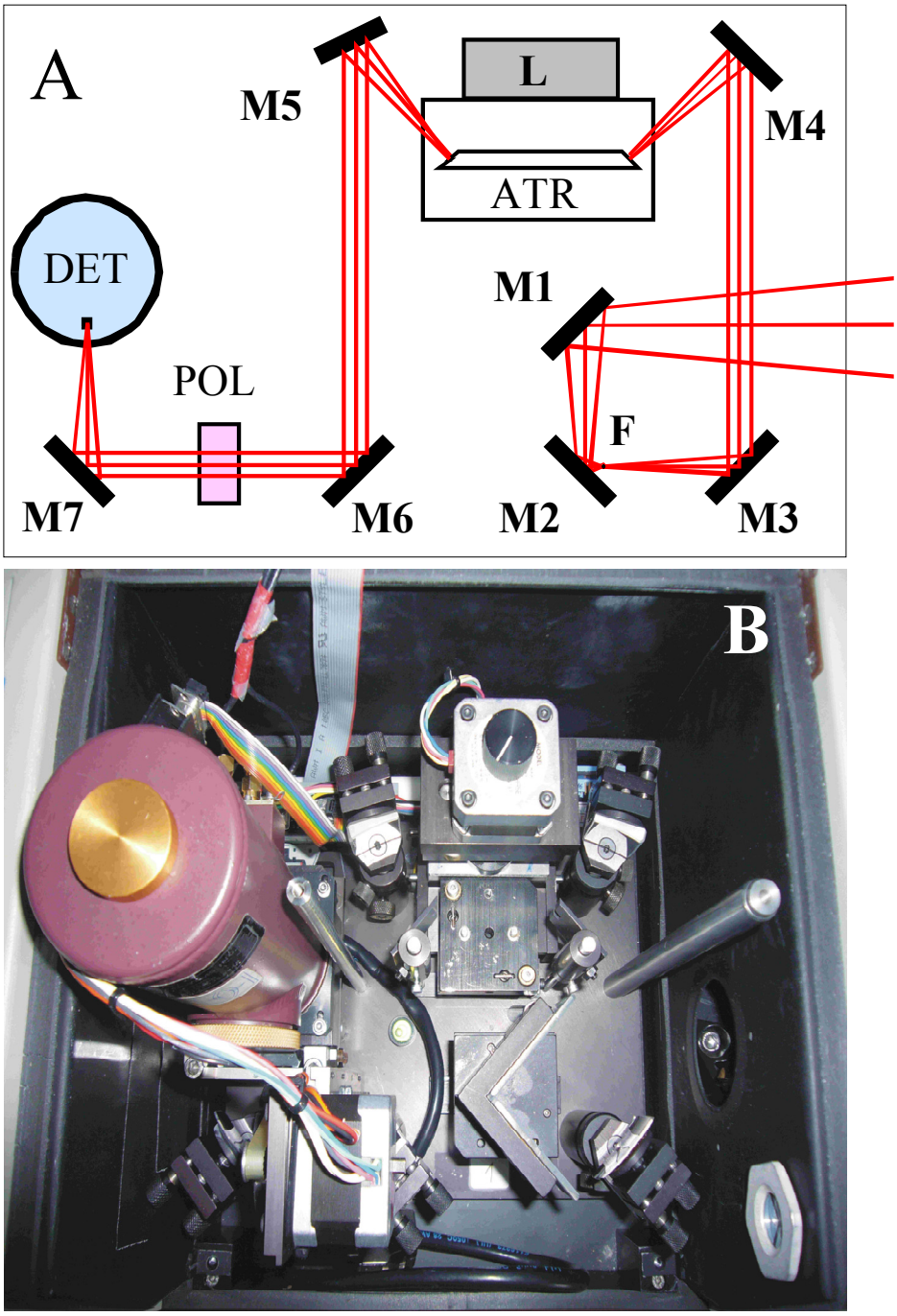

Fig. 12. Setup of ATR attachment. (A) The planar mirrors M1 and M2 cause a displacement of the focus in the sample compartment of the spectrometer to the position F. A parallel beam with a radius of half a centimeter is produced by the off-axis parabolic mirror M3. The cylindrical mirror M4 brings the beam into focus at the entrance area of the reflection element. M5 exhibiting the same qualities as M4 produces a parallel beam again. The planar mirror M6 redirects the light through the polarizer POL. The off-axis parabolic mirror M7 focuses the beam to the detector DET. L refers to the lift, which is used for changing the position of the flow-through cell in height. Fig. from [23]. (B) Photo of ATR attachment placed in the sample compartment of the spectrometer (Bruker IFS 25 or IFS 66).

The clean multiple internal reflection element (MIRE) was then mounted between the front and back side of a hydrodynamically optimized flow-through cell [32] made of Delrin®, as shown in Fig. 13. Front and back side of the cell were connected by four screws made of Nylon®. Each side of the cell consisted of two compartments independently accessible for liquids and gases. Each compartment offered a volume of 80µl and was sealed by a viton O-ring.

Peristaltic pumps (Ismatec, CH) were used for transportation of all solutions into the flow-through cell with the help of viton tubings. Flow rates of liquids were in the range of 50 µl/min to 1000 µl/min in all experiments corresponding to 0.6 – 12.5 exchanges of the compartment volume per minute. The temperature of the cell was kept constant at 25°C by water circulation in attached thermostatization plates (see Fig. 14).

The mean length of a compartment is a parameter determining the number of active internal reflections because the sample was only inside the cuvette in contact with the MIRE. The geometrical shape of one compartment can be seen as rectangle with length L connected to two semicircles with radius r (see Fig. 13). Therefore, the average length $\bar{l}$ of a sealed compartment resulted in [33]

$$\bar{l} = L + 2 \cdot \frac{1}{\pi} \int_0^{\pi} r \sin x dx = L - 2 \cdot \frac{1}{\pi} r \cos x \Big|_0^{\pi} = L + \frac{4r}{\pi} \qquad (26)$$

The number of active internal reflections is given by

$$N = \frac{\bar{l}}{k \cdot \tan \theta} \qquad (27)$$

where k and θ denote the thickness of the MIRE and the angle of incidence (45°), respectively. Thus, the length of one cuvette corresponded to a number of 26.8 (1.5 mm plate) and 19.6 (2.0 mm plate) active internal reflections, respectively.

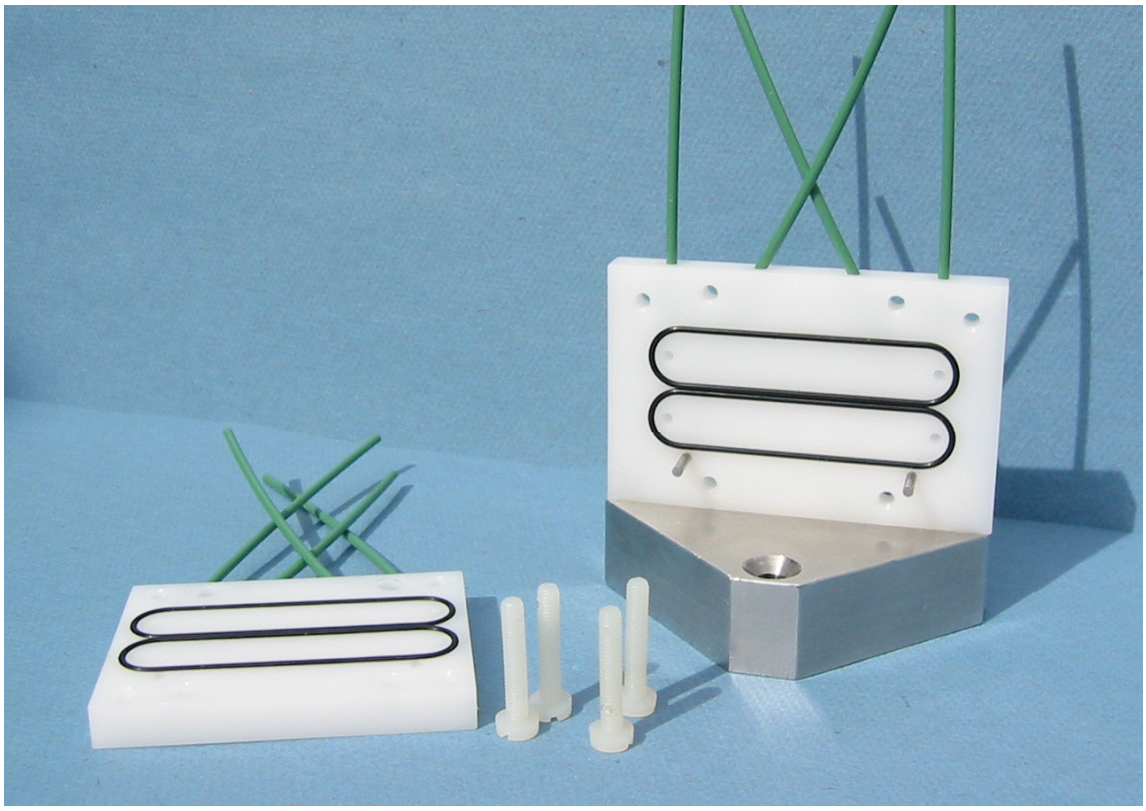

Fig. 13. Flow-through cell for FTIR ATR measurements used in this work. The cell was made of Delrin® and consisted of four compartments (two on each side) independently accessible for liquids and gases. Each compartment was sealed by a viton O-ring and had a volume of about 80 µl. The Ge MIRE was mounted between the front and back side of the cell, which were connected by four screws made of Nylon®. Metal plates for thermostatization can be attached at the outer wall of front and back side cover (see Fig. 14).

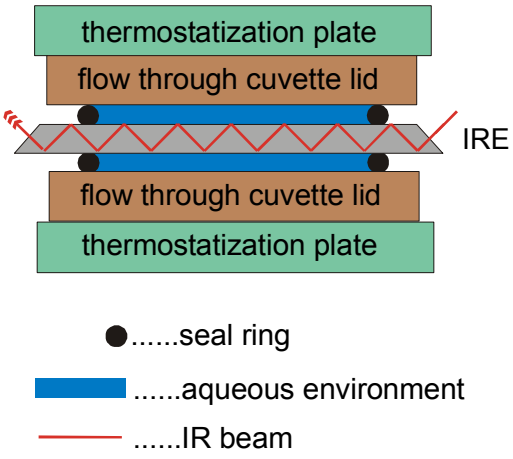

Fig. 14. Schematic top view of the flow-through cell with attached plates for thermo-statization after mounting of the MIRE and filling of the compartments with buffer.

3.3 Single beam sample reference (SBSR) method

Two compartments placed above each other on either side of the MIRE were used as sample (S) and reference (R), respectively. A computer-controlled lift, which was mounted on the ATR attachment, enabled measuring of the S and R channel in a short time delay by vertical displacement of the flow-through cell (Fig. 15).

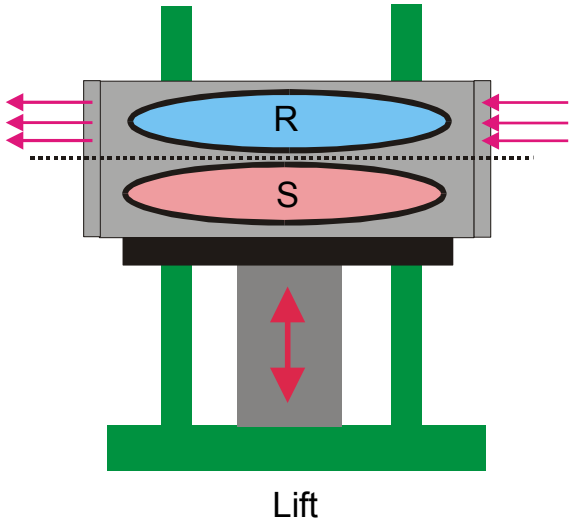

Fig. 15. Schematic representation of the lift on the ATR attachment. Two compartments placed above each other on either side of the MIRE were used as sample (S) and reference (R), respectively. A computer-controlled lift mounted on the ATR attachment enabled quasi simultaneously measuring of the upper and lower half of the MIRE by vertical displacement of the flow-through cell in a parallel IR beam. Since S and R are accessible by a single beam, this technique is referred to as single beam sample reference (SBSR) method.

Alternating collecting of intensity spectra of S and R compartments was performed till the desired signal-to-noise ratio was achieved. Since S and R are accessible by the single beam of the FTIR spectrometer, this technique is referred to as single beam sample reference (SBSR) method [18]. SBSR absorbance spectra were calculated from corresponding intensity spectra, i.e. -log (S/R). An advantage of such a setup is shown in Fig. 16. Spectra A and B are traditional single beam absorbance spectra of the R and S compartments of the reflection element, respectively. The corresponding reference spectra

of the R and S compartments were recorded at the beginning, whereas the sample spectra were measured 60 min later. Both spectra are influenced by atmospheric changes (i.e. fluctuations of water vapor and carbon dioxide). Spectrum C is the corresponding SBSR spectrum, which is not longer affected by such disturbances because they influence all compartments in the same way and, therefore, they are compensated in the difference spectrum. A second advantage is the enhanced baseline stability in longtime experiments because S and R compartments were of the same age and history as long as they were treated the same way. Also instabilities of the detector were eliminated by this method.

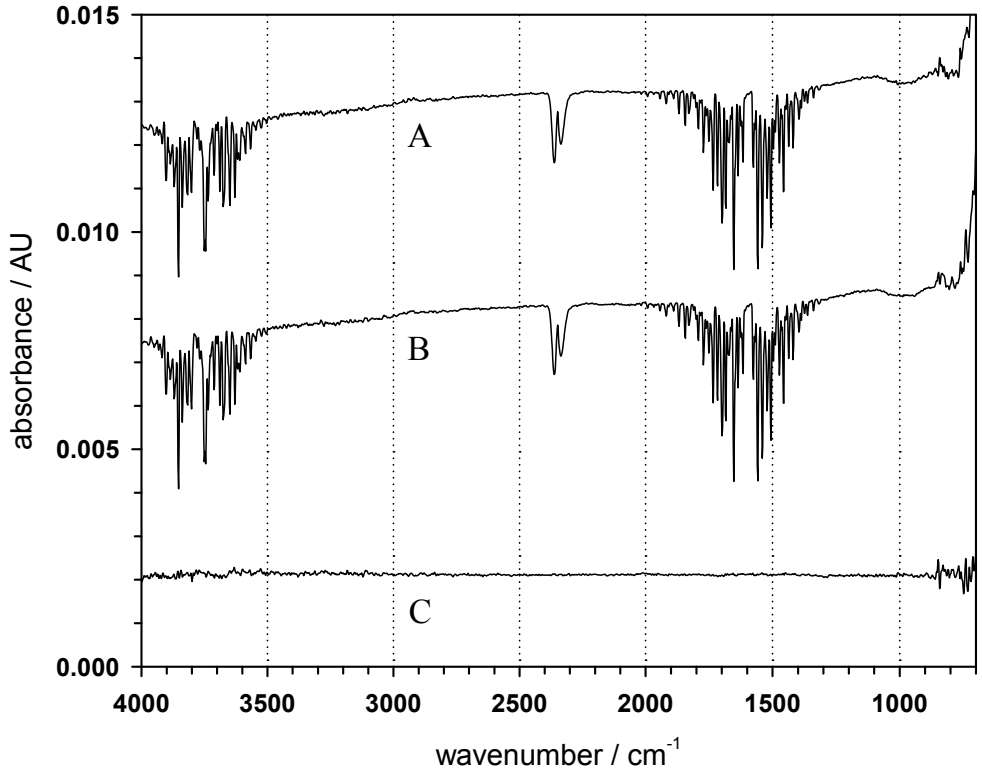

Fig. 16. FTIR ATR absorbance spectra of a Ge MIRE after the cleaning procedure according to Section 3.2 in dry air environment. (A) and (B) exhibit the changes in spectra resulting from different amounts of water vapor and CO_2 because the corresponding single channel spectra are recorded 60 min apart of each other in the R and S compartments, respectively. (C) Corresponding SBSR spectrum. It is characterized by a complete compensation of all water vapor and CO_2 absorption bands. Also changes of optical properties resulting from surface modifications after plasma cleaning vanished because of the quasi-simultaneous data acquisition in R and S compartments. Therefore, also a straight baseline was achieved. Fig. adapted from [34].

3.4 Interaction of hTNFα and anti-hTNFα-antibody: how the experiment was performed

A pictorial description of the course of the experiment in the R and S compartments is shown in Fig. 17. First, all compartments were filled and rinsed with PBS till the system was stable, which was controlled by recording of spectra. After measuring of reference spectra the S compartments (front and back side) were filled at a flow rate of 1ml/5min with a TNFα solution (66.7 µg/ml PBS) using a volume of 1.2 ml; then the pumps were stopped.

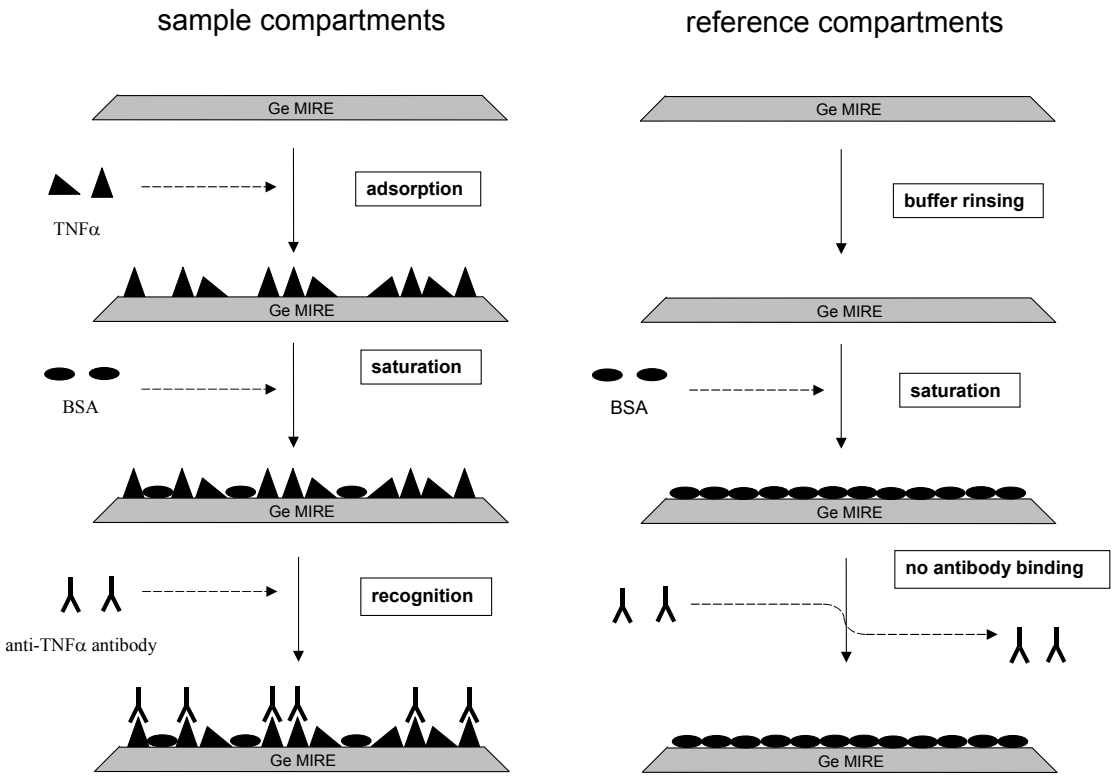

Fig. 17: Course of the experiment. In the S compartments TNFα adsorbed to the reflection element. BSA was used to saturate remaining bonding sites. The anti-TNFα antibody recognized the epitopes of immobilized TNFα resulting in a stable bond formation. In the R compartments a layer of BSA was produced to show that the presented antibody did not bond unspecificly to adsorbed BSA. Each of these steps was followed by recording of spectra. Procedures of buffer washing after adsorption of proteins and bonding of the antibody are omitted. Fig. from [2].

After adsorption of TNFα (1 h) the S compartments were rinsed with PBS for 76 min (1ml/10min) to remove loosely attached protein molecules. All the time the R compartments were treated in the same way with PBS. Then spectra of the adsorbed TNFα layer were recorded.

A solution of BSA (25 mg/ml PBS) was pumped through all compartments for 38 min (15 min at a flow rate of 1ml/5min and for additional 23 min at a flow rate of 1ml/20min). Remaining bonding sites of the Ge surface of the S compartments and all bonding sites of the R compartments were saturated by this procedure. Again, all compartments were rinsed, but this time with a low-concentrated BSA solution (100 µg/ml in PBS) for 38 min. Spectra of both compartments, S (immobilized TNFα and BSA) and R (immobilized BSA only), were measured. In the same way as dissolved BSA was used for saturation before, a solution of anti-TNFα antibody (AB) and BSA (both 100 µg/ml in PBS) was offered to all compartments for 38 min. This solution was removed by washing with BSA dissolved in PBS (100 µg/ml) for 38 min at a flow rate of 1ml/5min. Spectra of AB bonded to TNFα (S compartments) and of BSA without AB (R compartments) were recorded. Afterwards, all compartments were rinsed extensivly with BSA solution (100 µg/ml in PBS) at a flow rate of 1ml/20min for 10.5 h to evaluate the amount of protein, which was lost after such a washing procedure.

All rinsing and washing procedures were observed by simultaneously recording of spectra. Using 100 µg BSA/ml in PBS instead of PBS alone for washing purpose should reduce the loss of BSA that was already adsorbed to the reflection element and the tubings, as it was shown in preliminary experiments [9].

3.5 Preparing of human serum albumin (HSA) layers for c-ME experiments

First all compartments of the flow-through cell were filled with PBS. Then a solution of HSA (20.0 mg/ml in PBS) was pumped 2.2 min through the S cuvettes at a flow rate of 0.9 ml/min exchanging the volume of the cuvettes 12 times. Now the pump was stopped that adsorption of HSA could complete in a flow-free state. The remaining quantity of dissolved HSA in the S cuvettes was 4.82×10^{-11} mol corresponding to 1.5 times the final surface concentration of HSA. As realized by experiments with permanent flow of dissolved HSA, the dilution effect in the bulk solution under the applied conditions turned out to be irrelevant with respect to the achieved surface concentration. After 5 hours the adsorbed HSA layer was washed with PBS at a flow rate of 0.9 ml/min till stability of the surface concentration was attained. During the whole procedure PBS was also pumped through the R cuvettes at a flow rate of 50 µl/min. The washing step was controlled by recording SBSR spectra with pp and vp incident light.

3.6 Concentration-modulated excitation (c-ME)

3.6.1 c-ME by cholate

c-ME or concentration modulation was performed by periodic alteration of the concentration of cholate in the S compartments of the flow-through cell by two computer-controlled pumps. A schematic setup of the c-ME experiment is shown in Fig. 18. Before starting of modulation experiments, the flow-through cell and all supplying tubes were filled with PBS and rinsed as long as there were no changes in the spectra. Then the tubes providing the ligand were refilled with a solution of cholate in PBS.

During the first half of a modulation period the cholate solution was pumped through the S channels of the cell, while during the second half-period the channels were

flushed by pure PBS, both with the same flow rate of 0.9 ml/min. Within one modulation period of 9.8 min 32 intensity spectra referred to as sample point spectra (SPS) were recorded by collecting 88 scans per spectrum.

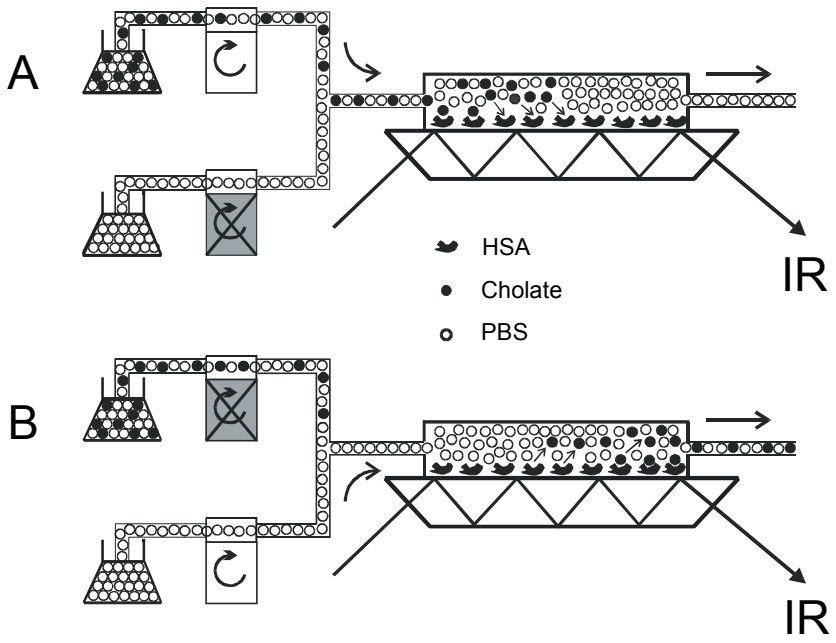

Fig. 18. Schematic setup for a concentration-modulated excitation (c-ME) experiment studying specific interactions between immobilized human serum albumin (HSA) and cholate. (A) During the first half of a modulation period (4.9 min) a solution of cholate in PBS was pumped through the S cuvettes of the flow-through cell containing an HSA monolayer adsorbed to the reflection element. (B) During the second half-period cholate was removed by PBS. In order to subtract the signal caused by the change of cholate in the bulk solution only, the experiment was also performed without HSA layer using the same parameters. Fig. from [34].

c-ME was carried out with parallel (pp) and perpendicular (vp) polarized incident light as follows: six modulation periods measured with pp light were in between of two series of six modulation periods recorded with vp light. An arrangement of modulation periods like this was referred to as vp-pp-vp modulation measurement. The two series of vp spectra were co-added and exhibited the same mean age as the corresponding pp spectrum. The reason for accumulating twice the number of scans in vp light is the reduced vp light intensity of the IR beam provided by the FTIR spectrometer leading to a worse

signal-to-noise ratio compared to pp light. Before demodulation, which was performed according to eq. (20), SPS were transformed into absorbance spectra using unity as reference. This unusual procedure is allowed because phase-resolved spectra resulting from the fundamental and higher harmonic responses reflect changes within the modulation period only and, therefore, they are independent from the choice of the reference spectrum [47]. For determination of cholate bonded to adsorbed HSA only the absorption amplitude of phase-resolved spectra demodulated at the fundamental frequency was used.

Applying different concentrations of cholate in PBS, modulation experiments were carried out as follows: After assembling and mounting of the flow-through cell in the spectrometer, first modulated excitation of the Ge plate without HSA layer was performed by alternately pumping cholate solution and PBS through the according compartments. This part served later as reference measurement to substract the signal caused only by the change of cholate in the bulk solution. After disassembling and cleaning of the plate and the flow-through cell, the protein layer was build up according to Section 3.5. Then the HSA layer was modulated with the cholate solution using the same parameters as in modulation without layer.

3.6.2 c-ME by ionic strength

According to [35] the ionic strength I of an aqueous solution is given by

$$I = \frac{1}{2} \cdot \sum_i z_i^2 \cdot c_i \qquad (28)$$

where z_i denotes the ionic valence of the ion i with the concentration c. The ionic strength of PBS used in this works resulted in 175 mM. c-ME by ionic strength was performed according to Section 3.6.1, but instead of a cholate solution a PBS with the ionic strength of 195 mM, adjusted by NaCl, was used.

4 Results and discussion – Part A: Interaction of hTNFα with an anti-hTNFα antibody

4.1 Adsorption of TNFα

TNFα adsorbed directly from aqueous solution to the reflection element according to the procedure described in Section 3.4 (p. 42). After completion of this process the immobilized protein was washed with PBS to remove loosely attached molecules. Stability of the amount of adsorbed protein was achieved after about 45 min, as it is shown in Fig. 19.

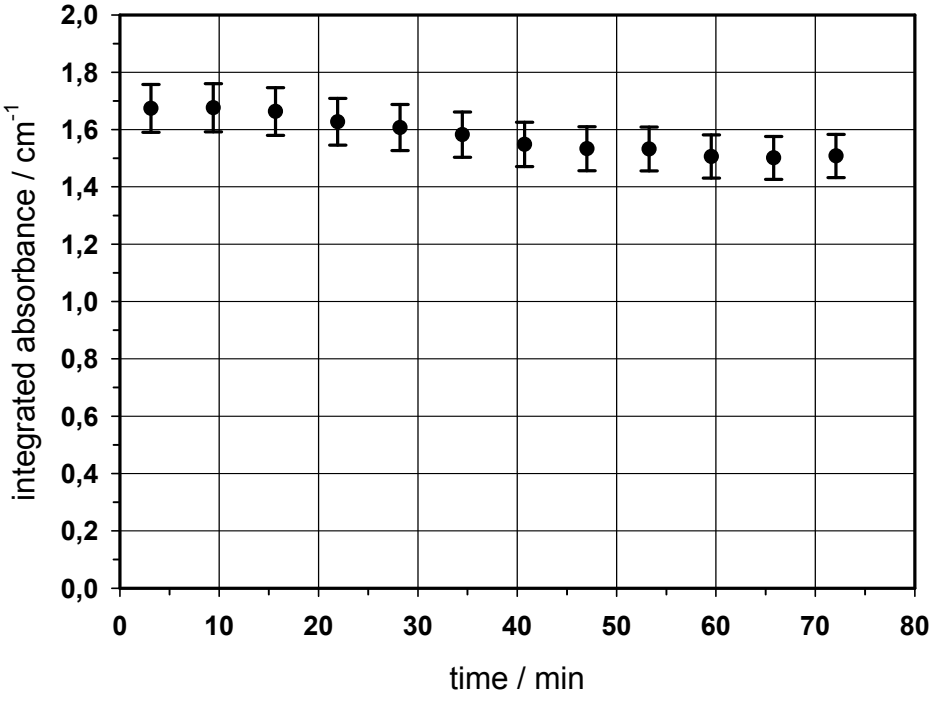

Fig. 19: Course of the integrated absorbance of the amide II band of adsorbed TNFα measured with pp incident light. After adsorption the immobilisate was washed with PBS to remove loosely attached molecules resulting in a decrease of TNFα of about 8 % compared to the beginning of the rinsing procedure. Fig. from [2].

Spectra of the TNFα layer measured in presence of PBS are shown in Fig. 20A. The maximum of the amide I band at 1636 cm^{-1}, the weak shoulder at 1690 cm^{-1} and the shoulders of the amide II band at 1521 cm^{-1} and at 1562 cm^{-1} exhibit the presence of

antiparallel β-sheet structures [36,37,38,39]. This shows that the main structural elements of TNFα (no α-helices, 45% antiparallel β-sheets) remained also after adsorption. Moreover, the amide III band at 1259 cm^{-1} featured a characteristic shape allowing the discrimination from BSA and the antibody in the case they are present at the same time on the surface of the MIRE (see Fig. 21).

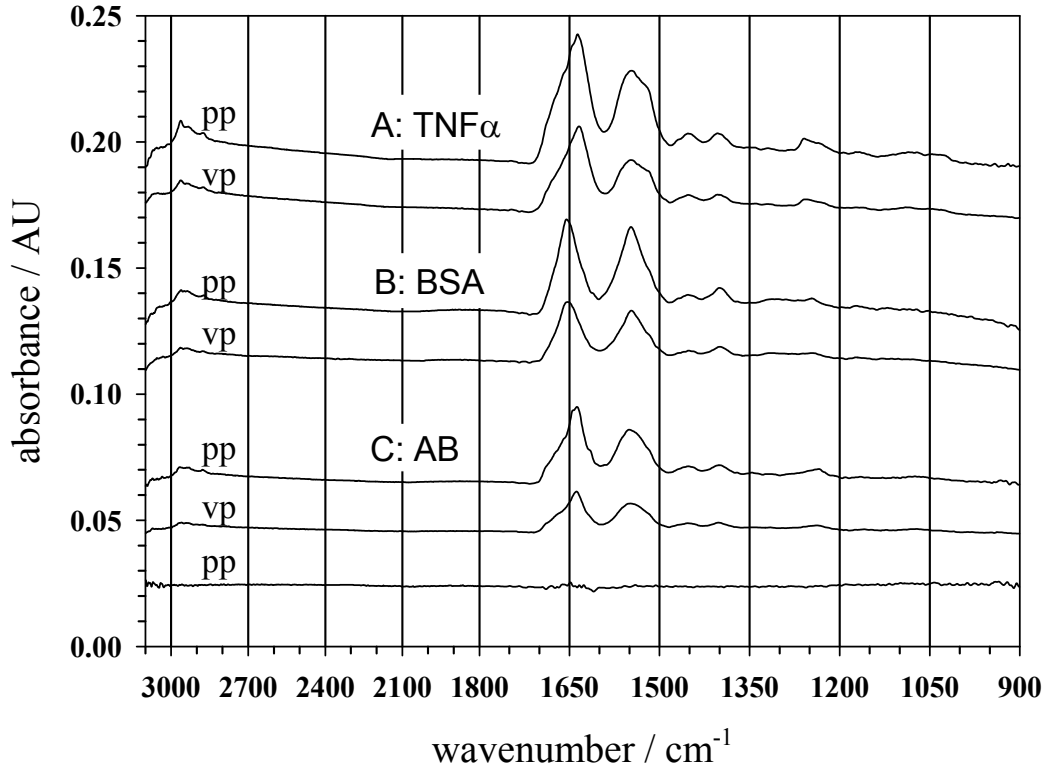

Fig. 20: FTIR ATR absorbance spectra of adsorbed TNFα, adsorbed BSA and anti-TNFα antibody bonded to TNFα. All spectra were recorded in aqueous solution with parallel (pp) and perpendicular polarized (vp) incident light. (A) TNFα layer immobilized to the reflection element of the sample compartments and measured after washing with PBS. Reference spectra: Ge plate in contact with PBS. (B) BSA layer immobilized to the reflection element of the reference compartments and measured after washing with 100 µg BSA/ml PBS. Reference spectra: Ge plate in contact with PBS. (C) Top, middle: Anti-TNFα antibody bonded to the TNFα layer of the S compartments. Reference spectra: TNFα layer after saturation with BSA. Bottom: Difference spectrum of the BSA layer before and after antibody treatment. There was no detectable bonding of the antibody to the BSA layer. Fig. from [2]. A magnified presentation of the amide III region is shown in Fig. 20.

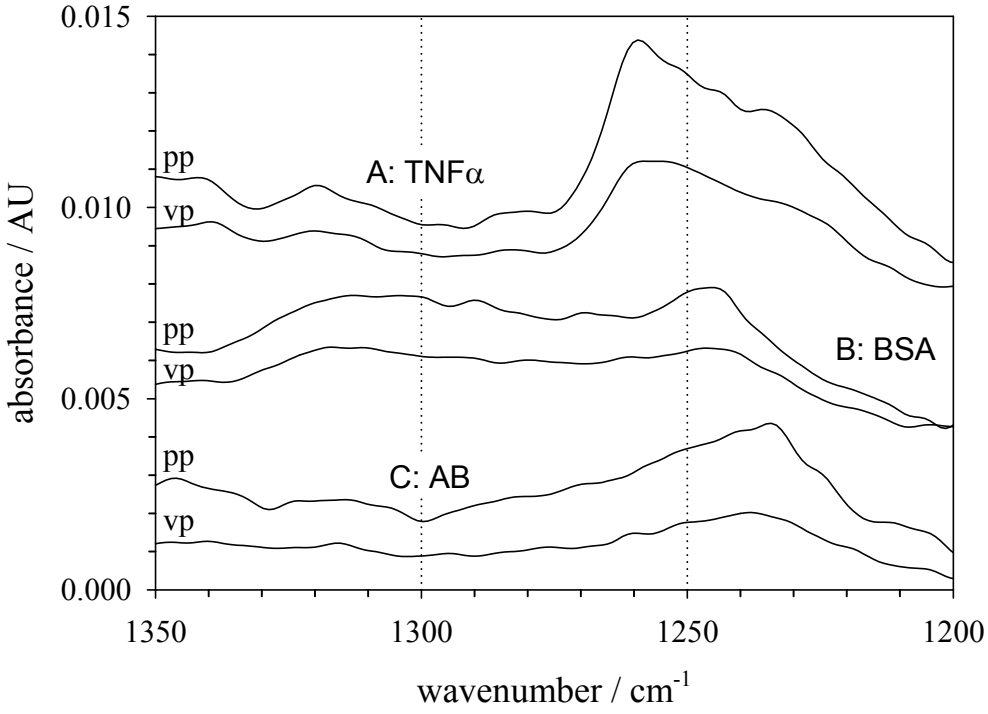

Fig. 21: Magnified presentation of the amide III region of adsorbed TNFα (A), adsorbed BSA (B), and anti-TNFα antibody bonded to immobilized TNFα (C) shown in Fig. 20. The proteins can be distinguished easily with the help of maximum and shape of the amide III bands.

The surface concentration of TNFα resulted in $\Gamma_{TNF\alpha} = (7.51 \pm 0.66) \times 10^{-12}$ mol cm^{-2} evaluated by the amide II band of Fig. 20A according to Section 2.2.3 (p. 22). As depicted in Section 1.2 the profile of a TNFα molecule can be seen as a cone with a basal plane of approximately 2400 Å^2 ($d \approx 55$Å) and a height of about 55Å. Two border cases of adsorption determining the limits for the average area per molecule on the reflection element were taken into account. (1) The molecules attach with the basal plane. In such a case the required area of one molecule is ~2400 Å^2 corresponding to a surface concentration of $\Gamma_{min} \approx 6.9 \times 10^{-12}$ mol cm^{-2}. (2) The molecules adsorb to the reflection element like thrown cones. In this case the required area of one molecule can be

approximated as a sector of a circle and results in ~1800 $Å^2$ corresponding to a surface concentration of $\Gamma_{max} \approx 9.2\times10^{-12}$ mol cm^{-2}.

The surface concentration of the TNFα layer, as it was experimentally determined, resulted in $\Gamma_{TNF\alpha} = 7.51\times10^{-12}$ mol cm^{-2}, which is in between Γ_{min} and Γ_{max}. Assuming 100% coverage of the reflection element with a monolayer and that the TNFα molecules keep their shape after adsorption, this would imply that ~73% of the protein molecules adsorbed as described in border case (1) and ~27% according to border case (2).

4.2 Saturation with BSA and evaluation of the BSA layer

After adsorption of TNFα to the S compartments a high-concentrated solution of BSA (25 mg/ml) in PBS was pumped through all compartments of the flow-through cell. This was done because of two reasons. (1) In [9] it was shown that the anti-TNFα antibody (AB) attaches also to the surfaces of the Ge MIRE. After adsorption of TNFα to the S compartments of MIRE free bonding sites of the Ge surface remained that could lead to unspecific adsorption. Without saturation it would not be possible to distinguish between specific bonding of the AB to TNFα and unspecific adsorption of the AB to the Ge plate. (2) Saturation of bonding sites in the R compartments was performed to show that a BSA layer protects against unspecific adsorption to Ge [9] and that there is no bonding of the AB to a BSA layer.

After saturation was completed and replacing of the high-concentrated BSA solution by PBS, spectra of the R and S compartments were measured. The absorbance of the BSA layer prepared in the R compartments is shown in Fig. 20B. Evaluation of the surface concentration was done using the amide II absorption band and resulted in $\Gamma_{BSA} = (5.70 \pm 0.49)\times10^{-12}$ mol cm^{-2}.

The shape of a BSA molecule can be seen as an oblate ellipsoid with the dimensions of 40Å x 40Å x 140Å, as it was determined by hydrodynamic measurements [40]. For estimation of the area required after adsorption the ellipsoid was approximated as a cuboid with the same dimensions. Again two border cases of adsorption were taken into account: (1) The molecules attach with a basal plane of 40Å x 140Å = 5600 $Å^2$ to the reflection element resulting in a surface concentration of $\Gamma_{min} \approx 3.0\times10^{-12}$ mol cm^{-2}. (2) The molecules adsorbe with the basal plane of 40Å x 40Å = 1600 $Å^2$. This case corresponds to a surface concentration of $\Gamma_{max} \approx 10.4\times10^{-12}$ mol cm^{-2}.

The surface concentration determined by experiments resulted in $\Gamma_{BSA} = 5.70\times10^{-12}$ mol cm^{-2}, which is settled between Γ_{min} and Γ_{max}. Assuming as in the case of TNFα, that there is 100% coverage of the reflection element with a monolayer and that the shape of the BSA molecules is not influenced by adsorption, this would imply that ~64% of the protein molecules adsorbed as described in border case (1) and ~36% according to border case (2).

The α-helix is the main secondary structural element of BSA with an amount of ~60%, whereas there is no hint for β-pleated sheet conformation [41]. The amide I and II band of the BSA layer adsorbed to the R compartments (see Fig. 20B) exhibit maxima at 1655 cm^{-1} and 1548cm^{-1}, respectively, as it was expected for α-helical structure [36, 42].

Spectral details of the amide I and II regions of the S compartments after saturation with BSA are represented by Fig. 22. The spectra reflect a replacement of already adsorbed TNFα by BSA in a small extent. This can be seen by the positive amide I and II peaks at 1655 cm^{-1} and 1548 cm^{-1}, respectively, due to an increase of α-helical structures. Corresponding negative peaks in the amide I (1690 cm^{-1}, 1633 cm^{-1}) and in the amide II region (1562 cm^{-1}, 1521 cm^{-1}) result from a decrease of β-sheet structures.

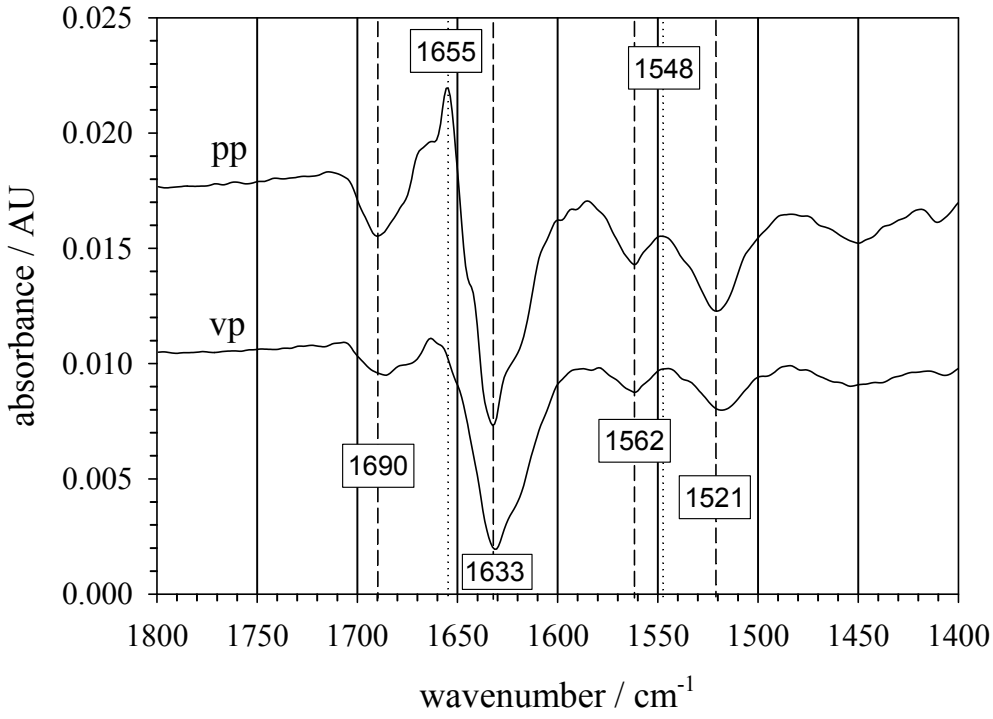

Fig. 22: Effect on the TNFα layer caused by saturation of remaining bonding sites on the MIRE with BSA, as seen by the amide I and II regions. The spectra were recorded after preparing of the TNFα layer and saturation of the S compartments with BSA. Reference spectra: TNFα layer before saturation. The spectra exhibit a replacement of already adsorbed TNFα (negative bands at 1690, 1633, 1562 and 1521 cm^{-1} corresponding to β-sheet structure) by BSA (positive bands at 1655 and 1548 cm^{-1} corresponding to α-helical structure) in a small extent. Fig. from [2].

4.3 Bonding of anti-TNFα antibody to TNFα

After pumping of a solution of anti-TNFα antibody (AB) and BSA into all compartments and washing with a BSA solution according to Section 3.4 (p. 42) spectra of the S and R compartments were recorded. For evaluation of absorbance spectra the condition before AB contact was taken as reference. As seen in Fig. 20C (top, middle), the protein spectra of the S compartments demonstrate an enrichment of the AB at the surface of the reflection element because the concentration of dissolved AB alone was too low to result in an evaluable signal. The corresponding spectrum of the R compartments measured with pp incident light (Fig. 20C, bottom) shows clearly the absence of bonded or adsorbed AB indicating that remaining bonding sites of the S compartments can be completely

saturated by offering a high-concentrated BSA solution. Thus, the antibody present at the S compartments must be a result of specific bonding to TNFα. The surface concentration of the AB was evaluated according to Section 2.2.3 (p. 22) and resulted in $\Gamma_{AB} = (1.41 \pm 0.12) \times 10^{-12}$ mol cm^{-2}. The ratio of surface concentrations $\Gamma_{TNF\alpha} / \Gamma_{AB}$ resulted in 5.33. Evaluated surface concentrations of all involved proteins are summarized in Table 3. Since TNFα and the antibody have the same main structural element, i.e. the β-sheet, the amide I and II bands exhibit a similiar shape. Nevertheless, they can be distinguished by their typical amide III bands (see Fig. 21).

Table 3: Input parameters, surface concentrations, dichroic ratios and wavenumbers of selected absorption peaks of involved proteins [2].

Parameter	TNFα	BSA	TNFα-antibody
Molecular weight (kDa)	52.05	66.40	146.0
Number of amide bondings per molecule	468	582	1316
Integrated absorbance A_{pp} of amide II band of parallel polarized spectra (cm^{-1}). Linear baseline.	1.536±0.077	1.439±0.072	0.792±0.040
Integr. absorbance A_{vp} of amide II band of perpendicular polarized spectra (cm^{-1}). Linear baseline.	0.843±0.042	0.808±0.040	0.468±0.023
Range of integration[(x)] (cm^{-1})	1482.0 - 1592.5	1485.1 - 1600.2	1482.0 - 1592.5
Results			
Surface conc. Γ calculated from A_{pp} and A_{vp} of amide II band (10^{-12} mol/cm^2)	7.51±0.66	5.70±0.49	1.41±0.12
Experimental dichroic ratio $R_{exp} = A_{pp} / A_{vp}$ of amide II (for comparison: $R_{iso,\ thin\ film} = 1.67 \pm 0.12$)	1.82±0.13	1.78±0.13	1.69±0.12
Concentration in solution (mg/ml)	0.067	25	0.100
Wavenumbers of selected peaks in the amide I region of parallel polarized spectra (cm^{-1})	1636 (max) 1690 (shoulder)	1655 (max)	1638 (max) 1690 (shoulder)
Wavenumbers of selected peaks in the amide II region of parallel polarized spectra (cm^{-1})	1521 (shoulder) 1546 (max) 1562 (shoulder)	1548 (max)	1517 (shoulder) 1550 (max)
$\tilde{\nu}_{max}$ (amide III) of pp spectra (cm^{-1})	1259 (sharp)	1246 (broad)	1235 (broad)

[(x)]Different ranges of integration are a result of the different composition of the proteins concerning their secondary structural elements.

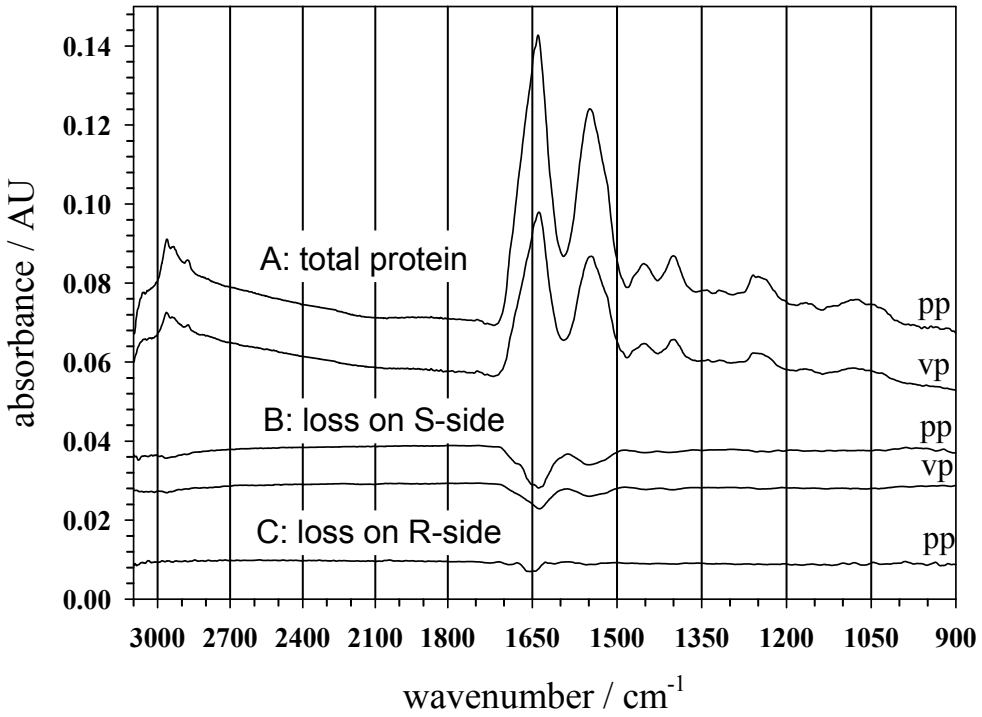

Fig. 23: FTIR ATR absorbance spectra of proteins present at the same time on the surface of the reflection element of the S compartments after antibody presentation and spectra of decrease of proteins of R and S compartments after washing with 100 µg BSA/ml PBS. (A) These spectra consist of the contribution of proteins, which were present on the reflection element of the S compartments after antibody presentation, i.e. TNFα and anti-TNFα antibody for the most part and BSA for the smallest part. Reference spectra: Ge plate in contact with PBS. (B) Decrease of proteins present on the reflection element of the S compartments after washing with 100 µg BSA/ml PBS for 10.5 h (1ml/20min). Reference spectra: The total amount of protein present at the beginning of the washing procedure (Spectra A of this Figure). As a result of the small decrease of 7.4% it was not possible to evaluate the individual loss of each protein. (C) Decrease of immobilized BSA present on the reflection element of the R compartments after washing with 100 µg BSA/ml PBS for 10.5 h (1ml/20min). Reference spectra: The BSA layer at the beginning of the washing procedure (Spectrum B, pp of Fig. 20). There was no evaluable loss of BSA. Fig. from [2].

As a last step of the experiment, the antigen-antibody complex of the S compartments and the BSA layer of the R compartments were investigated concerning

their steadiness against elution by rinsing with a low-concentrated BSA solution (100 μg/ml PBS). Absorbance spectra of the total amount of protein before washing are presented in Fig. 23A. After a rinsing time of 10.5 h spectra were recorded again. Absorbance spectra of Fig. 23B reflect a loss of protein of ~7.4 % in the S compartments; corresponding spectra of Fig. 23A were used as reference. Because of the small decrease it was not possible to evaluate the individual loss of each protein. The absorbance spectrum of the R compartments calculated from intensity spectra, which were measured before and after the rinsing procedure, shows no loss of protein (Fig. 23C). This indicates clearly that the BSA layer remained stable during the rinsing process.

4.4 Orientation of amide bonds in TNFα, BSA, and anti-TNFα antibody

Spectra measured with polarized incident light provide information about orientation of vibrational modes in adsorbed proteins, i.e. secondary structural elements or functional groups. The experimental dichroic ratio R, as defined by the ratio of integrated absorbances A_{pp} and A_{vp} evaluated from spectra recorded with pp and vp incident light (see Section 2.2.2, p. 20), gives access to this information.

A_{pp} and A_{vp} of the amide II band of each immobilized protein were evaluated to determine the average orientation of the transition dipole moment $\vec{M}$ of the amide II vibration ($\overline{\vec{M}}_{\text{amide II}}$) with respect to the Ge plate fixed-coordinate system (see Fig. 7). Results are summarized in Table 3. The calculated dichroic ratio of the amide II band in case of isotropicly distributed amide bonds in a thin film on the surface of a reflection element made of Germanium with the optical parameters $\theta = 45°$, $n_1 = 4.0$, $n_2 = 1.45$ and $n_3 = 1.33$ (see Table 2) results in $R_{\text{iso,thin film}}$ (amide II) = 1.67 ± 0.12 [23]. If the experimental dichroic ratio R is lower, the angle α_{exp} between the direction of $\overline{\vec{M}}_{\text{amide II}}$ and

the normal to the reflection element is located between the magic angle $\alpha_M \approx 54.7°$ and 90° ($\alpha_M < \alpha_{exp}$(amide II) <90°), if it is higher, the angle lies between 0° and the magic angle ($0° < \alpha_{exp}$(amide II) $< \alpha_M$). If α_{exp}(amide II) results in the magic angle it is not possible to discriminate whether there is an alignment or an isotropic distribution of the direction of $\vec{M}$ of the amide bonds.

The experimental dichroic ratios of the amide II band of TNFα and BSA resulted in $R_{exp,TNF\alpha}$(amide II) = 1.82 ± 0.13 and $R_{exp,BSA}$(amide II) = 1.78 ± 0.13, respectively, corresponding to $\alpha_{exp,TNF\alpha}$(amide II) = (52.2 ± 0.8)° and $\alpha_{exp,BSA}$(amide II) = (53.1 ± 0.9)°. Both results reflect a slight orientation of $\overline{\vec{M}}_{\text{amide II}}$, and thus, of the amide bonds, rather along the normal (z-axis) of the reflection element than parallel to the xy-plane.

The dichroic ratio of the anti-TNF-α antibody was found to be at $R_{exp,AB}$(amide II) = 1.69 ± 0.12. The uncertainty of this value is within the expected dichroic ratio for an isotropic layer $R_{iso,\ thin\ film}$ (see above) indicating no preferred orientation of amide bonds of the antibody bonded to TNFα. In such a case an alignment of certain domains cannot be excluded completely because of the size of the antibody molecule. If, e.g. in large molecules, secondary structural elements are arranged isotropically, the dichroic ratio always results in $R_{iso,\ thin\ film}$.

5 Results and discussion – Part B: Interaction of HSA with cholate

5.1 Critical micelle concentration (cmc) and absorbance spectra of cholate dissolved in phosphate buffered saline (PBS)

Cholate has qualities of a mild detergent (see Section 1.5, p. 12) and is known to form micelles of small size (2 – 3 molecules) above a cmc of 11 mM in 150 mM NaCl [43]. A correlation between the surface tension σ_L of the solution and the concentration of a detergent distributed between the mixed phase and the surface of the solvent is given by the Gibbs Thomson theorem [44].

$$\Gamma = -\frac{1}{RT} \cdot \frac{d\sigma_L}{d \ln c^M} \qquad (29)$$

c^M and Γ denote the concentration of the detergent in the mixed phase and in the interface between liquid and air, respectively. R and T are the gas constant and the temperature. Eq. (29) is only valid for a monomolecular layer of the detergent on the surface of the solution.

The cmc is dependent on composition and temperature of the solvent. Therefore, the surface tension of a concentration series of cholate in phosphate buffered saline (PBS) used in this work was measured by tensiometry (Kruess Digital Tensiometer K10ST) at a temperature of 25°C. Results are shown in Fig. 24. At very low concentrations (0 – 5 µM) the influence of cholate on the surface tension σ of PBS was so small that σ stayed constant within the error limits. In the range of 0.2 – 6.0 mM σ of the cholate solution exhibited a linear decrease dependent on the logarithm of cholate concentration. Since in this range the first derivative is constant, the surface concentration of cholate would be also constant. Such a result is in contradiction to eq. (29) because a declining surface tension is a sign of enrichment, i.e. of an increasing concentration, of cholate on the surface. A

reasonable explanation is that the formation of micelles already started at the beginning of the linear decrease, especially at the gas-liquid interface. Above 6.0 mM cholate, the surface tension was no longer reduced indicating that the micelles had reached their full size. This led to the conclusion that under our conditions cholate did not exhibit a precise cmc, but it was possible to determine the concentration range from starting to completion of micelle formation reaching from 0.1 to 6.0 mM cholate.

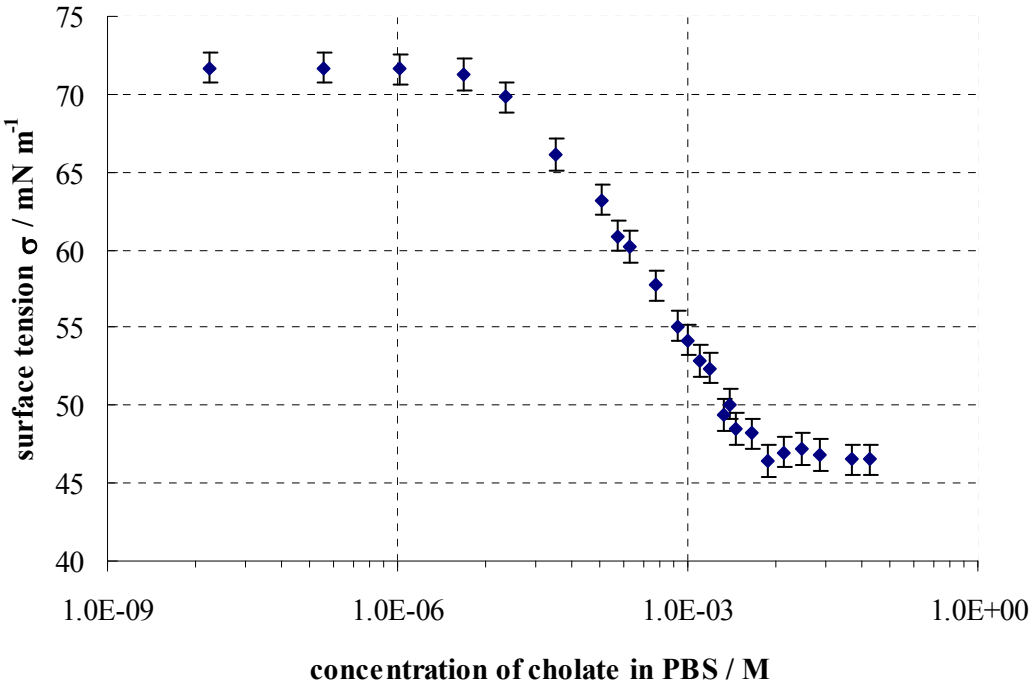

Fig. 24. Estimation of cmc of cholate dissolved in PBS. Surface tensions σ of cholate solutions in the concentration range of 0.011 µM - 75 mM were measured by tensiometry. The formation of micelles started at the beginning of the linear decrease of the surface tension, i.e. in the range of 0.1 – 0.3 mM, and was completed at 5.5 - 6.0 mM cholate.

FTIR ATR absorbance spectra of cholate at various concentrations in PBS measured with parallel (pp) and perpendicular (vp) polarized incident light are shown in Fig. 25. The most prominent bands are the asymmetric (ν_{as}) and symmetric (ν_s) stretching vibrations of the COO^- group at 1544 cm^{-1} and 1405 cm^{-1}, respectively. The slightly negative band of the water bending vibration at 1635 cm^{-1} results from water displacement

by dissolved cholate in the S compartments, while pure PBS was used as reference in the R compartments of the flow-through cell. Instead of $\nu_{as}(COO^-)$, which was influenced by the water bending vibration, the integrated absorbance of $\nu_s(COO^-)$ was evaluated to quantify cholate in all experiments.

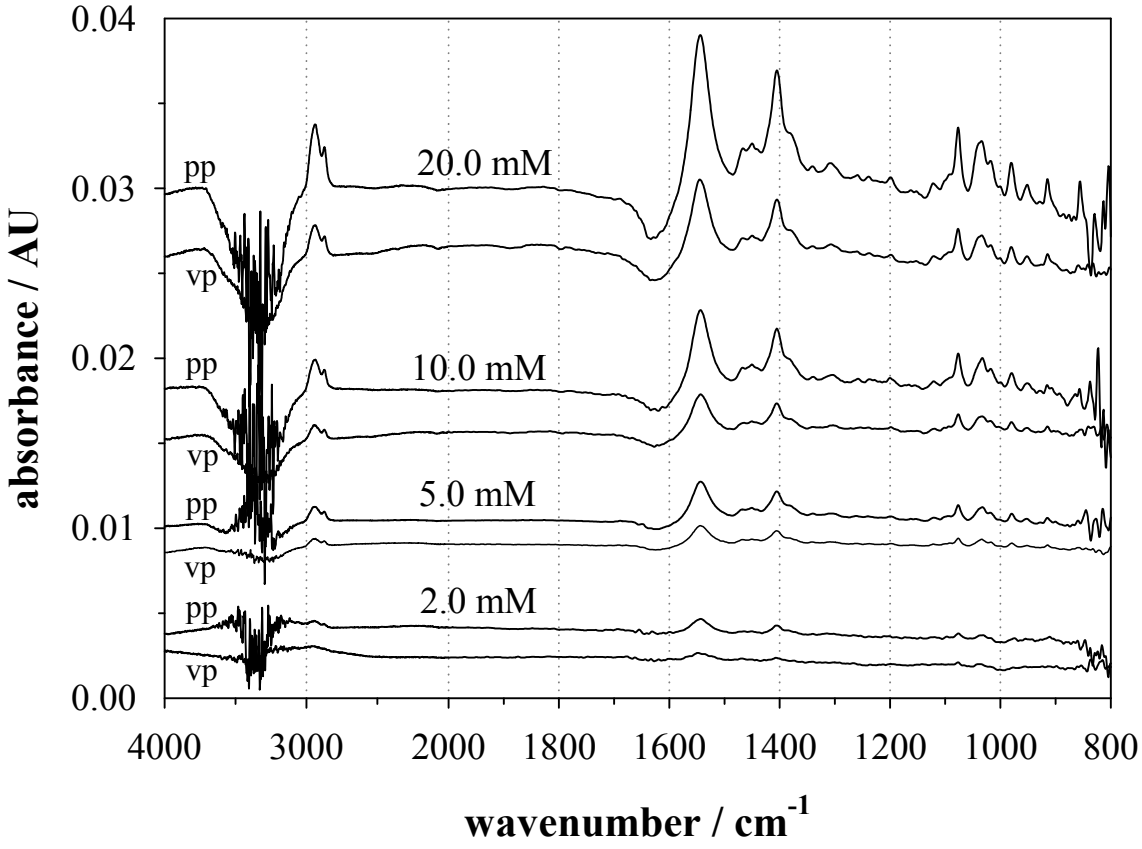

Fig. 25. FTIR ATR absorbance spectra of cholate at different concentrations in PBS measured with parallel (pp) and perpendicular (vp) polarized incident light. The most prominent bands are the asymmetric (ν_{as}) and symmetric (ν_s) stretching vibrations of the COO^- group at 1544 cm^{-1} and 1405 cm^{-1}, respectively. The slightly negative band of the water bending vibration at 1635 cm^{-1} results from water displacement by dissolved cholate because pure PBS was the reference in the R compartments of the flow-through cell. Since the water bending vibration interferes with $\nu_{as}(COO^-)$, the integrated absorbance of $\nu_s(COO^-)$ was used for quantitative analysis.

The integrated molar absorption coefficient of $\nu_s(COO^-)$ $\int \varepsilon_{(COO^-)}(\tilde{\nu})\, d\tilde{\nu}$ at 1405 cm^{-1} was determined by a concentrations series of cholate in PBS (1.0 - 6.0 mM)

measured with pp and vp polarized incident light in the flow-through cell and resulted in $(1.36 \pm 0.14) \times 10^7$ cm mol^{-1} (range of integration: $1484 \pm 2 - 1350 \pm 2$ cm^{-1}). A detailed evaluation is presented in Appendix 7.2.

The correlation between the integrated absorbance of $\nu_s(COO^-)$ and the cholate concentration in the range used in this work for determination of a bonding curve is presented in Fig. 26. $\int \varepsilon_{(COO^-)}(\tilde{\nu})\, d\tilde{\nu}$ stayed constant within the whole range, as it is shown by the coefficients of determination R^2 of best fit straight lines of pp and vp measurements, resulting in 0.998 and 0.997, respectively. This finding supported the result of tensiometry, since a distinct transition from monomers to formation of micelles would also be accompanied by a sudden change of $\int \varepsilon_{(COO^-)}(\tilde{\nu})\, d\tilde{\nu}$ [44], which is not seen in Fig. 26.

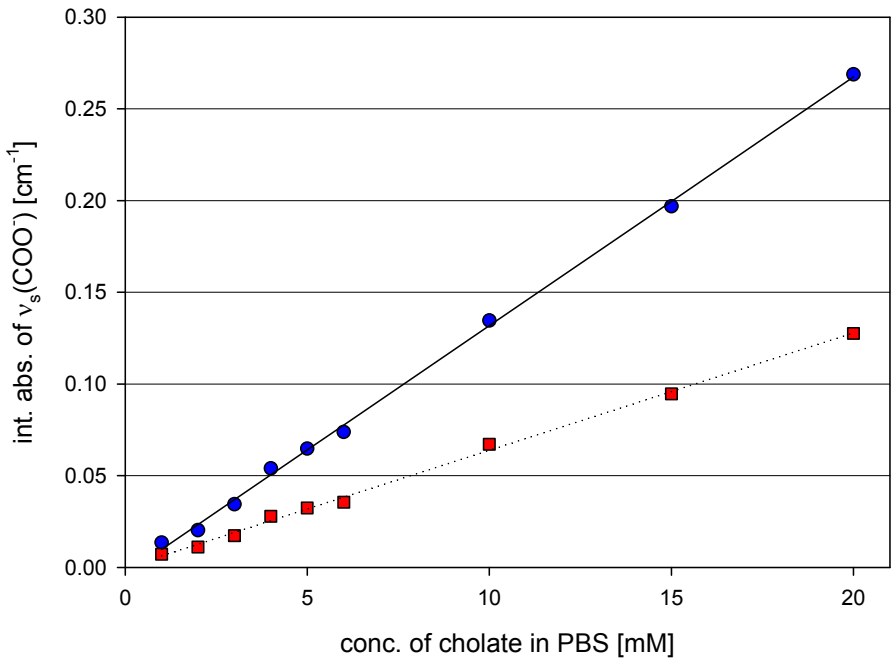

Fig. 26. Integrated absorbance of $\nu_s(COO^-)$ versus the cholate concentration in the range from 1 mM to 20 mM. The coefficients of determination R^2 of best fit straight lines of pp and vp measurements resulted in 0.998 and 0.997, respectively, proving that the integrated molar absorption coefficient $\int \varepsilon_{(COO^-)}(\tilde{\nu})\, d\tilde{\nu}$ stayed constant over the whole concentration range.

5.2 Characterization of immobilized human serum albumin (HSA) layers

For each concentration-modulated excitation (c-ME) experiment performed at different concentrations of cholate in PBS a new HSA layer was prepared according to Section 3.5 (p. 44) in order to have same conditions concerning the age of the layer. After completion of HSA adsorption to the reflection element the protein layer was rinsed with PBS for about (18 ± 1) h to remove loosely attached HSA molecules and to get a stable layer. A typical course of preparing HSA layers is shown in Fig. 19.

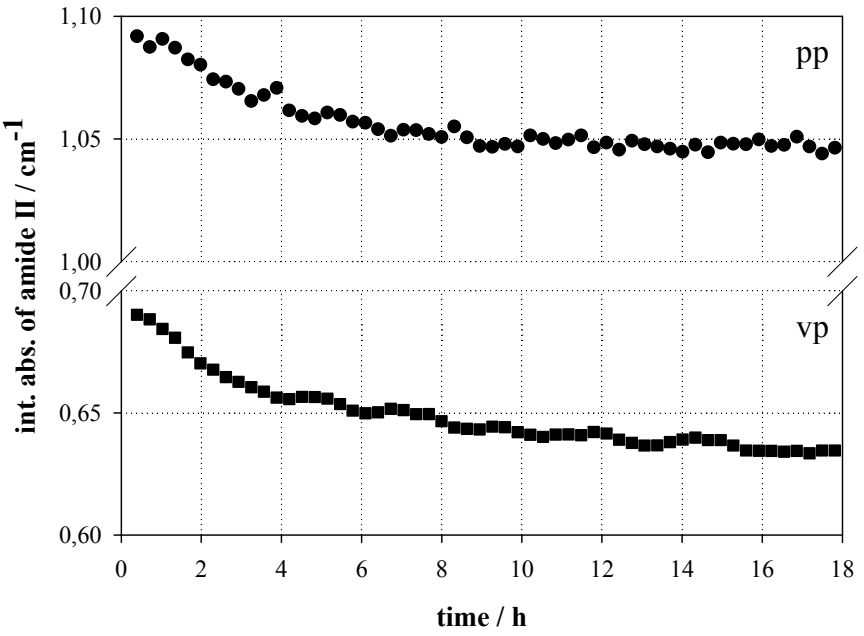

Fig. 27. Course of stabilization of a human serum albumin (HSA) layer. Integrated absorbances of the amide II vibration at 1547 cm^{-1} were used as indicator (Range of integration: 1600 ± 1 – 1485 ± 1 cm^{-1}). Circles (●) und squares (■) denote measurements with parallel (pp) and perpendicular (vp) polarized incident light, respectively. After spontaneous adsorption of HSA the layers were rinsed with PBS at a flow rate of 0.9 ml/min in order to remove loosely attached molecules. Quasi-stable layers were reached after (18 ± 1) hours resulting in surface concentrations slightly below a compact monolayer.

Absorbance spectra of an adsorbed HSA layer in PBS are shown in Fig. 28A. The maxima of the amide I and II vibrations are found at 1653 cm^{-1} and 1548 cm^{-1}, respectively, pointing to a predominantly helical structure [42]. This finding is in accordance with x-ray studies [12].

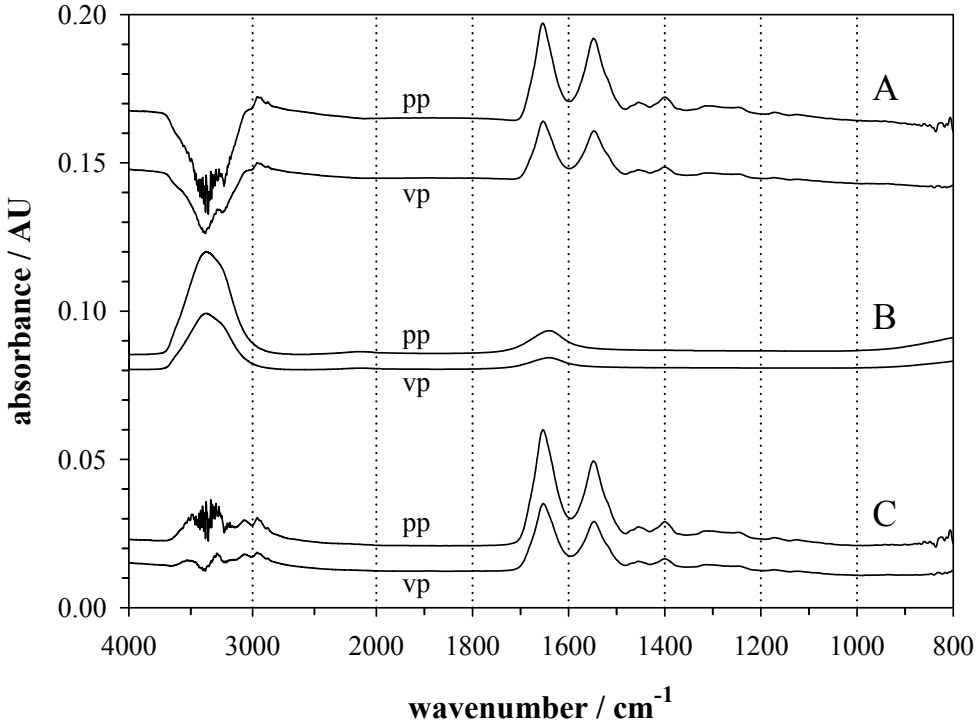

Fig. 28. FTIR ATR absorbance spectra of adsorbed HSA before (A) and after (C) solvent compensation, and of PBS (B) measured with pp and vp incident light. (A): Stable HSA layer in PBS before solvent compensation according to Section 2.2.4. Negative bands in regions of water absorption ($\nu(H_2O)$: 3350 cm^{-1}, $\delta(H_2O)$: 1640 cm^{-1}) resulted from PBS displacement by the layer in the S cuvettes of the flow-through cell, while in the R cuvettes PBS was in direct contact with the surface of the Ge MIRE, thus resulting in more intense absorbance spectra. (B): Absorbance spectra of PBS scaled by visual inspection to achieve optimum water compensation of (A). The corresponding layer thickness, as calculated according to Section 2.2.4, was 17 Å. In reality, the layer might be somewhat thicker, since PBS may penetrate the layer and exist as hydration water within it. Reference: air in empty R cuvette. (C): HSA after solvent compensation. A perfect compensation of bands resulting from OH stretching and bending vibrations was not possible because of the presence of water bonded to protein molecules and free OH groups of amino acid residues as a part of HSA.

Fig. 28A reveals negative bands in regions of water absorption ($\nu(H_2O)$: 3350 cm^{-1}, $\delta(H_2O)$: 1640 cm^{-1}). This overcompensation results from the fact that PBS was in direct contact with the Ge MIRE in the reference compartments, while in presence of HSA in the sample compartments, PBS was partly displaced by the layer. For correction of this feature the procedure of solvent compensation according to Section 2.2.4 (p. 24) was applied. Fig. 28B represents absorbance spectra of PBS, scaled to a layer thickness of 17 Å, which was found to result in optimum background compensation of the HSA layer shown in Fig. 28A. They are dominated by the water absorption bands because air in unfilled reference cuvettes was used as reference. Sum of the spectra of Fig. 28A and Fig. 28B resulted in the solvent compensated protein layer spectra, shown in Fig. 28C. The thickness of 17 Å reflects the lowest limit of the HSA layer because most propably the layer still enables some penetration of PBS. Moreover, water bonded by protein molecules as well as free OH groups of amino acid residues contributed to these spectral regions. As a consequence, a perfect compensation of OH stretching and bending vibrations is not possible. Thicknesses of PBS thin films resulting in best solvent compensation of adsorbed HSA layers used for all c-ME experiments are presented in Table 4.

Surface concentrations of HSA layers were calculated according to Section 2.2.3 and were in the range of $(4.98 \pm 0.39) \times 10^{-12}$ mol cm^{-2} to $(5.52 \pm 0.44) \times 10^{-12}$ mol cm^{-2}. These experimental values listed in Table 4 may now be compared with theoretical surface concentrations based on x-ray data. The threedimensional shape of HSA may be approximated as an equilateral triangle with sides of ~80 Å and a depth of ~30 Å [12]. Two extreme cases of adsorption are considered: (1) HSA molecules adsorb with the lateral surface, which results in 80×30 Å $= 2400$ $Å^2$ per molecule corresponding to a surface concentration of $\Gamma_{max} \sim 6.9 \times 10^{-12}$ mol cm^{-2}. (2) Molecules adsorb with the triangle base plane and occupy an area of about 2770 $Å^2$ per molecule corresponding to a surface concentration of $\Gamma_{min} \sim 6.0 \times 10^{-12}$ mol cm^{-2}. As a consequence, the experimentally

determined surface concentrations indicated that the coverage of the MIRE is close to a monolayer. Therefore, accessibility of HSA during a modulation experiment should not be limited by multilayer formation; however, lateral hindrance could still play a role.

Table 4. Data of HSA layers prepared for c-ME experiments at specified cholate concentrations. The index "0" of Γ_0 emphasizes the fact that the surface concentrations refer to the beginning of modulation experiments.

conc. of cholate in PBS [mM]	surface conc. Γ_0 of HSA [10^{-12} mol cm^{-2}]	dichroic ratio R (amide II) of HSA	rinsing time [h]	thickness of PBS layer used for solvent compensation [Å]
0.3	5.32 ± 0.42	1.71 ± 0.12	18	16
1.0	5.46 ± 0.43	1.61 ± 0.11	17	17
2.0	5.28 ± 0.42	1.65 ± 0.12	17	16
3.0	5.00 ± 0.40	1.65 ± 0.12	18	15
4.0	5.18 ± 0.41	1.67 ± 0.12	19	16
5.0	5.31 ± 0.42	1.63 ± 0.12	18	17
6.0	5.10 ± 0.40	1.69 ± 0.12	19	15
10.0	5.03 ± 0.40	1.70 ± 0.12	19	15
15.0	5.09 ± 0.40	1.63 ± 0.12	19	15
20.0	4.98 ± 0.39	1.64 ± 0.12	19	15

Concerning the mean orientation of α-helical segments, the analysis was based on the dichroic ratio of the amide II band according to Section 2.2.2 (p. 20) and was found to be in the range of 1.61 ± 0.11 to 1.71 ± 0.12 (see Table 4). The uncertainty of these values is within the expected dichroic ratio for an isotropic layer, i.e. $R_{iso,\ thin\ film} = 1.67 \pm 0.12$ (Ge MIRE, $\theta = 45°$, $n_1 = 4.0$, $n_2 = 1.45$, $n_3 = 1.33$) [23]. As a consequence, α-helical segments in the HSA layer are expected to be arranged isotropically, or in a manner that results in a mean orientation with respect to the z-axis corresponding to the magic angle of $\Theta_{mag} \sim 54.7°$. The latter, however, is unlikely. The isotropic arrangement of α-helices is maybe also favoured by long rinsing times because the amide bonds of the BSA layer prepared to protect the R compartments against unspecific adsorption in the experiment of

the first part of this work (see Section 4.2) exhibited a slight orientation (see Section 4.4) after a rinsing time of less than one hour.

5.3 Cholate bonding to immobilized HSA

Concentration-modulated excitations (c-MEs) of adsorbed HSA layers, as well as the reference experiments without layer, were performed by cholate solutions in the concentration range of 0.3 mM to 20 mM according to Section 3.6.1 (p. 44). Since no time resolved information can be expected at the applied low modulation frequency of 1.7 mHz, ϕ^{PSD} of the presented modulation spectra was adjusted in such a way that according to eq. (21) $\phi - \phi^{PSD} = 0$, thus resulting in maximum amplitude.

As a representative example of all c-ME, the evaluation of the experiment with the 5 mM cholate solution is presented in details [45]. Fig. 29A shows the response of the HSA layer to c-ME by 5 mM cholate, superimposed by the concentration modulation in the bulk phase. In order to get reference spectra for subtraction of the latter, c-ME was also performed without HSA layer (Fig. 29B). Fig. 29C is the difference of the spectra shown in Fig. 29A and Fig. 29B reflecting the response of the HSA layer to c-ME by 5 mM cholate. Responses to c-MEs by other concentrations of cholate are shown in Fig. 30. The displacement of cholate solution by the layer was taken into account according to Section 2.2.4 (p. 24).

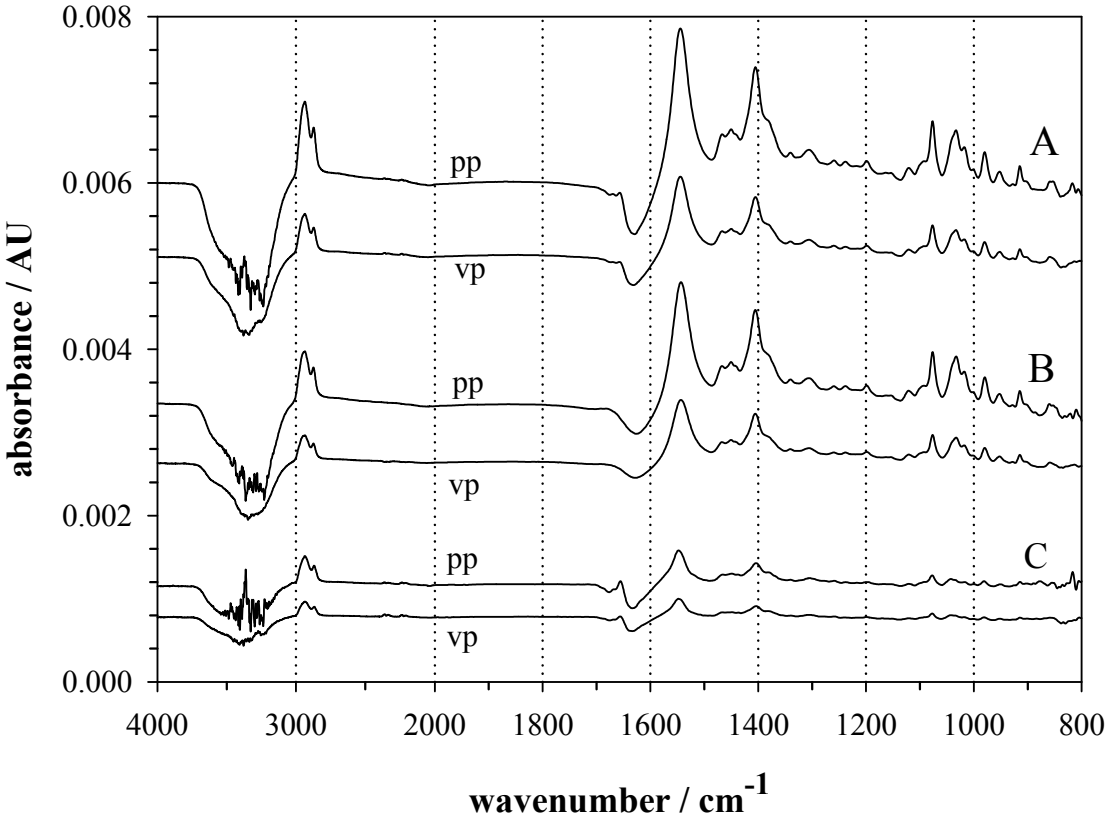

Fig. 29. Concentration-modulated excitation (c-ME) by 5.0 mM cholate measured with pp and vp incident light. (A) and (B): Demodulated FTIR ATR spectra in presence of a HSA layer (A) and in absence of the layer (B). According to eq. (21) ϕ^{PSD} was set in such a way that $(\phi - \phi^{PSD}) = 0$, in order to maximize one phase-resolved spectrum. Scaling of the integrated absorbance of $\nu_s(COO^-)$ at 1405 cm^{-1} to time zero, i.e. the beginning of the modulation experiments, was necessary to exclude the influence of an unknown impurity existing in variable amounts in every purchased cholate sample, as well as to eliminate disturbances by HSA detachment from the layer (see Section 5.4, p. 78). (C): Difference between spectra A and B reflecting reversible cholate bonding to HSA and structural responses of HSA upon interaction with cholate. An expanded scale presentation of the amide I and II region is given in Fig. 31.

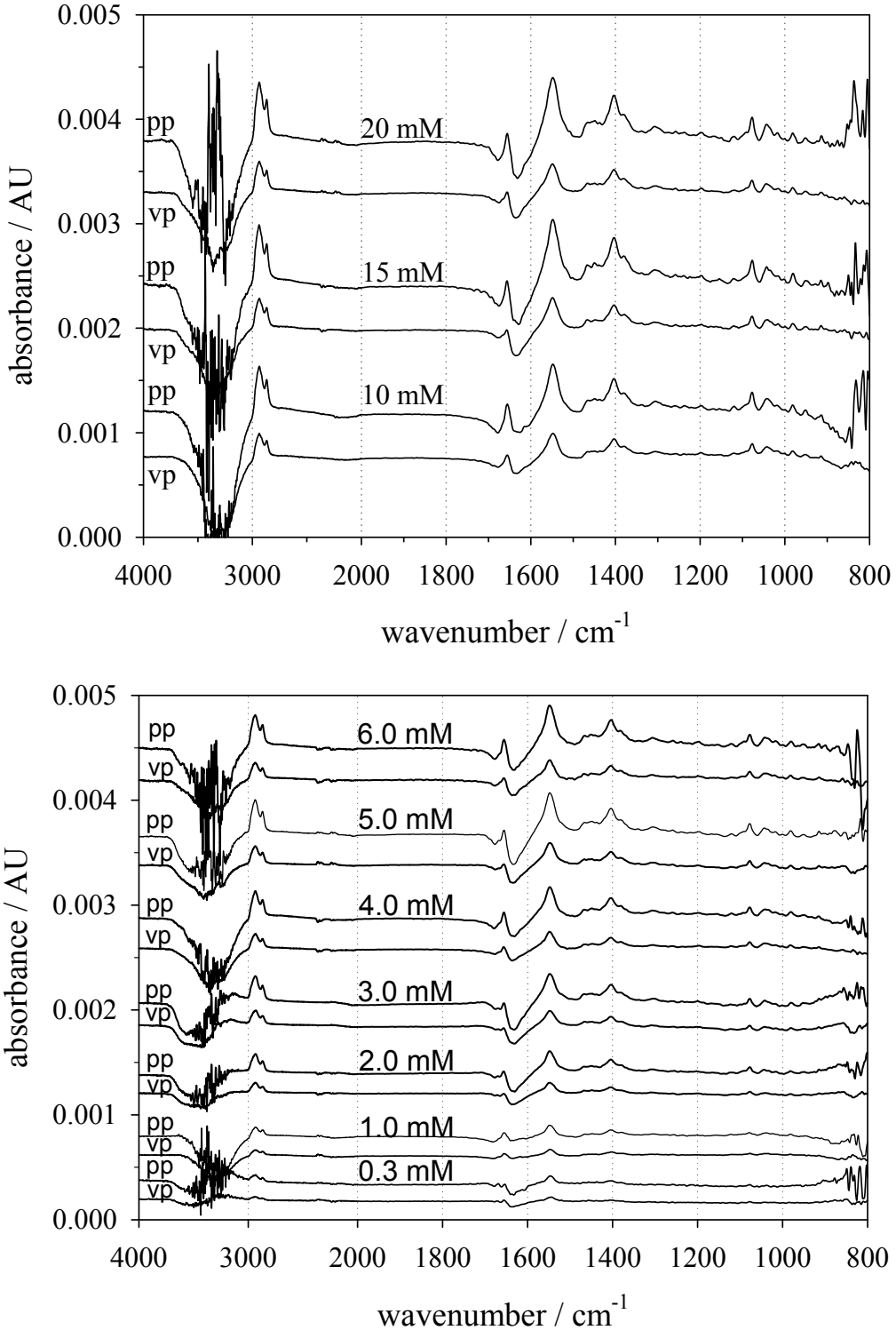

Fig. 30. Response of HSA layers to cholate interaction at indicated concentrations of cholate in PBS measured with pp and vp incident light. These spectra represent the difference of demodulated c-ME spectra in presence of the HSA layer and without layer, and, therefore, they reflect cholate bonded to HSA and structural responses of HSA upon cholate interaction.

5.3.1 Mean spatial orientation of bonded cholate

The dichroic ratios R of cholate (see Table 5) bonded at different concentrations to immobilized HSA were determined for $\nu_s(COO^-)$ according to Section 2.2.2 (p. 20). They were in the range of 1.78 ± 0.13 to 2.02 ± 0.15, except the one obtained from c-ME with 0.3 mM cholate. Under the same experimental conditions (Ge MIRE, $\theta = 45°$, $n_1 = 4.0$, $n_2 = 1.45$, $n_3 = 1.31$) a thin isotropic layer would result in $R_{iso,\ thin\ film} = 1.63 \pm 0.12$. Therefore, one may expect a slight mean ordering of bonded cholate, and that the mean direction of the transition dipole moment $\vec{M}$ of $\nu_s(COO^-)$, which has approximately the direction of the O-C-O bisectrice, forms angles Θ from 52.1° to 48.9° (± 0.9)° with the normal to the MIRE. The dichroic ratio and, thus, Θ obtained from the experiment with 0.3 mM cholate exhibit a big error limit compared to other results because corresponding integrated absorbances used for calculation were already influenced by high noise of evaluated spectra.

Table 5. Dichroic ratios of $\nu_s(COO^-)$ at 1405 cm^{-1} of cholate bonded to adsorbed HSA evaluated by c-ME experiments at indicated cholate concentrations in the bulk solution. Θ denotes the angle between the mean direction of the transition moment $\vec{M}$ of $\nu_s(COO^-)$ and the normal to the MIRE.

conc. of cholate in PBS [mM]	dichroic ratio R of $\nu_s(COO^-)$ of bonded cholate	Θ ($\vec{M}$ of $\nu_s(COO^-)$, $\perp$ to the MIRE) [deg]
0.3	1.68 ± 0.58	53.7 ± 5.7
1.0	1.93 ± 0.15	50.1 ± 0.9
2.0	1.79 ± 0.13	52.0 ± 0.9
3.0	1.80 ± 0.13	51.9 ± 0.9
4.0	1.79 ± 0.13	52.1 ± 0.9
5.0	1.78 ± 0.13	52.1 ± 0.9
6.0	1.92 ± 0.14	50.1 ± 0.9
10.0	1.85 ± 0.14	51.1 ± 0.9
15.0	2.01 ± 0.15	48.9 ± 0.9
20.0	1.99 ± 0.15	49.2 ± 0.9

5.3.2 Structural effects in HSA caused by cholate bonding

The response of adsorbed HSA to cholate interaction of all c-ME experiments is presented by spectra of Fig. 30. As an example, results of the c-ME experiment with 5.0 mM cholate are shown with an expanded presentation of the amide I and II regions in Fig. 31. The two dominant positive bands at 1544 cm^{-1} and at 1405 cm^{-1} reflect $\nu_{as}(COO^-)$ and $\nu_s(COO^-)$ of cholate bonded to HSA. The narrow band at 1656 cm^{-1} is assigned to the amide I vibration of adsorbed albumin. It appeared in-phase with the two carboxyl stretching vibrations, thus indicating unambiguously that it is a direct consequence of cholate bonding to HSA. A reasonable interpretation of this observation is an increase of α-helical structures induced upon cholate bonding. Quantification of this increase was disabled by the influence of the water bending vibration at 1640 cm^{-1}.

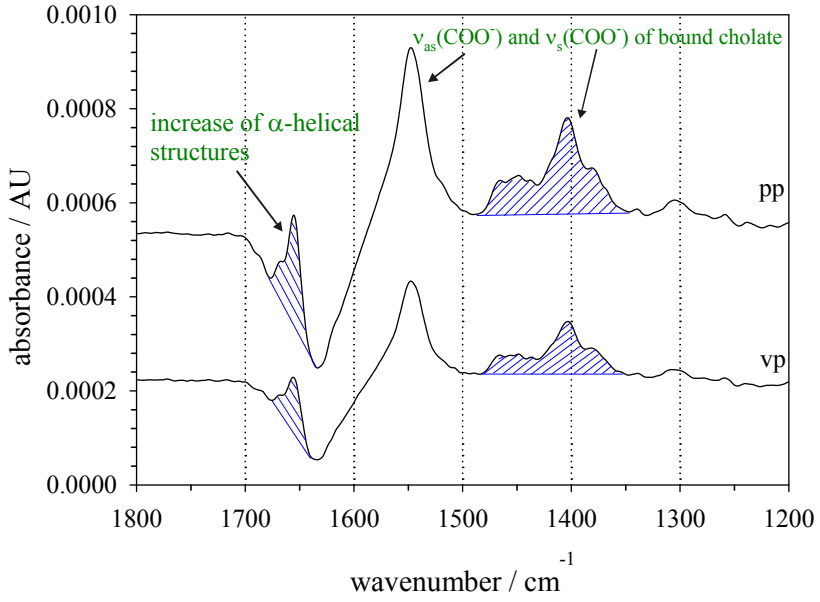

Fig. 31. Expanded scale of the amide I and II regions of spectrum C of Fig. 29. Modulating the concentration of cholate in PBS between 0 and 5 mM resulted in a reversible bonding of cholate represented by $\nu_{as}(COO^-)$ and $\nu_s(COO^-)$ at 1544 cm^{-1} and at 1405 cm^{-1}, respectively. In addition, a narrow band at 1656 cm^{-1}, i.e. in the amide I region appeared synchronously with cholate bonding to HSA. A tentative interpretation is that α-helical structures of HSA were increased upon cholate bonding. Range of integration of $\nu_s(COO^-)$: 1484 ± 2 – 1350 ± 2 cm^{-1}.

5.3.3 Results of ionic strength modulation

A ionic strength modulation of an HSA layer was performed according to Section 3.6.2 (p. 46). The aim of this experiment was to find out whether modulated changes of ionic strength of PBS alone also cause periodic alterations of secondary structural elements of HSA.

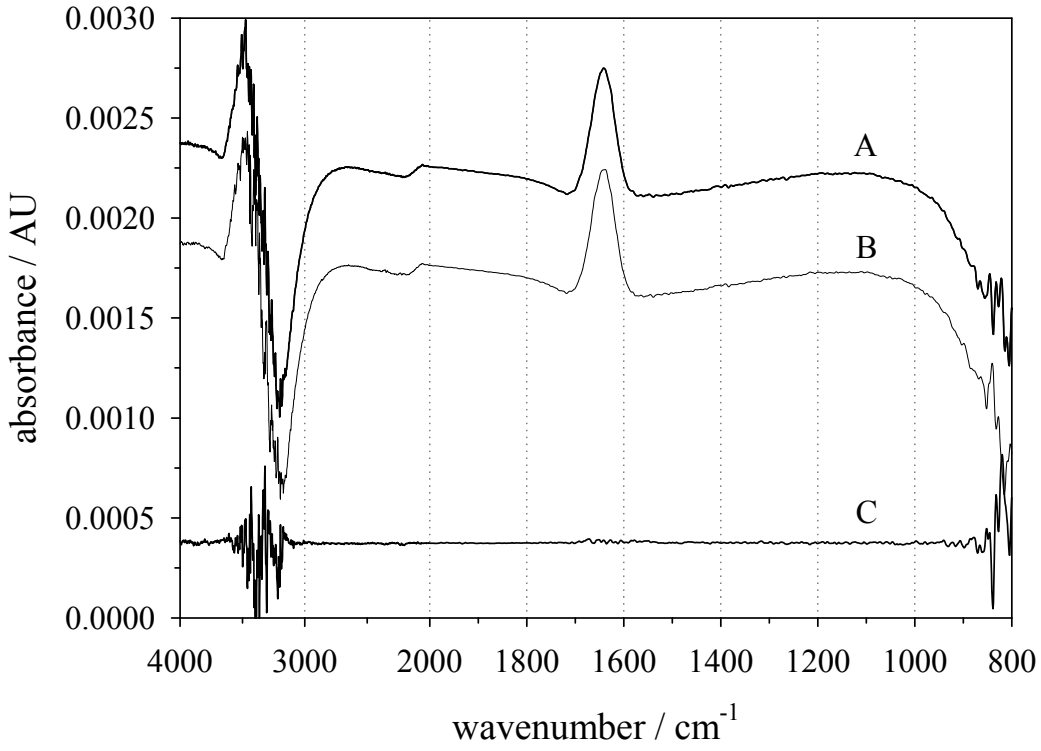

Fig. 32. Ionic strength modulation. Demodulated and averaged pp spectra of 18 successive vp-pp-vp modulation measurements without (A) and in presence (B) of an HSA layer are dominated by the water bending vibration at 1640 cm^{-1} and the stretching vibration at 3400 cm^{-1}. (C) is the difference of spectra A and B representing the response of the HSA layer to the ionic strength modulation. It shows clearly that the shift of ionic strength in the amount of 20 mM had no visible effect on secondary structures of adsorbed HSA. Since there was no evaluable signal in pp spectra, vp spectra are not shown.

Demodulated and averaged pp spectra of 18 successive vp-pp-vp modulation measurements without and in presence of an HSA layer are shown in Fig. 32A and Fig. 32B, respectively. Both spectra are dominated by the water bending vibration at

1640 cm^{-1} and the stretching vibration at 3400 cm^{-1}. The sigmoidal shape of the latter reflects different qualities of water structure caused by varying ionic strength of PBS. Fig. 32C is the difference of spectra in Fig. 32A and Fig. 32B representing the response of the HSA layer to the ionic strength modulation. The spectrum shows clearly that the shift of ionic strength in the amount of 20 mM had no visible effect on secondary structures of adsorbed HSA. Demodulated vp spectra are not shown because they also exhibited no evaluable signal.

5.3.4 Stoichiometric ratio of HSA-cholate interaction

Whereas the way of evaluation in this paragraph is valid for all c-ME experiments, the results refer again to c-ME by 5 mM cholate. Although quasi-stability of the protein layer was achieved by washing with PBS, as shown in Fig. 27, the ability of cholate to act as detergent, caused still a very slow linear decrease of the surface concentration of HSA in the amount of 1.1 % per 10 hours. In order to evaluate the course of the surface concentration of HSA, pp and vp SBSR spectra were recorded after each vp-pp-vp modulation measurement. The course of the concentration of bonded cholate was determined by evaluation of demodulated spectra of successive vp-pp-vp modulation measurements. Data analysis was made according to Section 2.2.3 and 2.2.4. The results are presented in Fig. 33A for HSA and Fig. 33B for cholate bonded to adsorbed HSA. The stoichiometric ratio at the beginning of c-ME was then determined by extrapolation of both curves to time zero by means of linear regression. The resulting surface concentrations were found to be $\Gamma_{0,HSA} = (5.31 \pm 0.49) \times 10^{-12}$ mol cm^{-2} and $\Gamma_{0,cholate} = (3.21 \pm 0.42) \times 10^{-11}$ mol cm^{-2} leading to a ratio of 6.1 ± 0.9 cholate molecules per adsorbed HSA at 5.0 mM cholate in PBS. The resulting course of stoichiometry is shown in Fig. 33C. As a consequence, the bonding affinity of an immobilized HSA

molecule was reduced from 6 to 5 cholate molecules within 95 hours. This fact may be explained by denaturation of HSA due to aging and hydrodynamic stress by ME.

Results and measuring times of all other c-ME experiments are shown in Table 6. The stoichiometric ratios were used to evaluate a bonding curve in Section 5.6 (p. 88). The lower the concentration of cholate in PBS the more vp-pp-vp modulation measurements were performed in order to achieve an optimal signal response of the HSA layer to c-ME. One vp-pp-vp measurement lasted three hours. Since in case of c-ME of HSA layers after each vp-pp-vp modulation cycle SBSR spectra were recorded to determine the surface concentration of HSA, the measuring time was extended by half an hour per vp-pp-vp measurement compared to c-ME without layer.

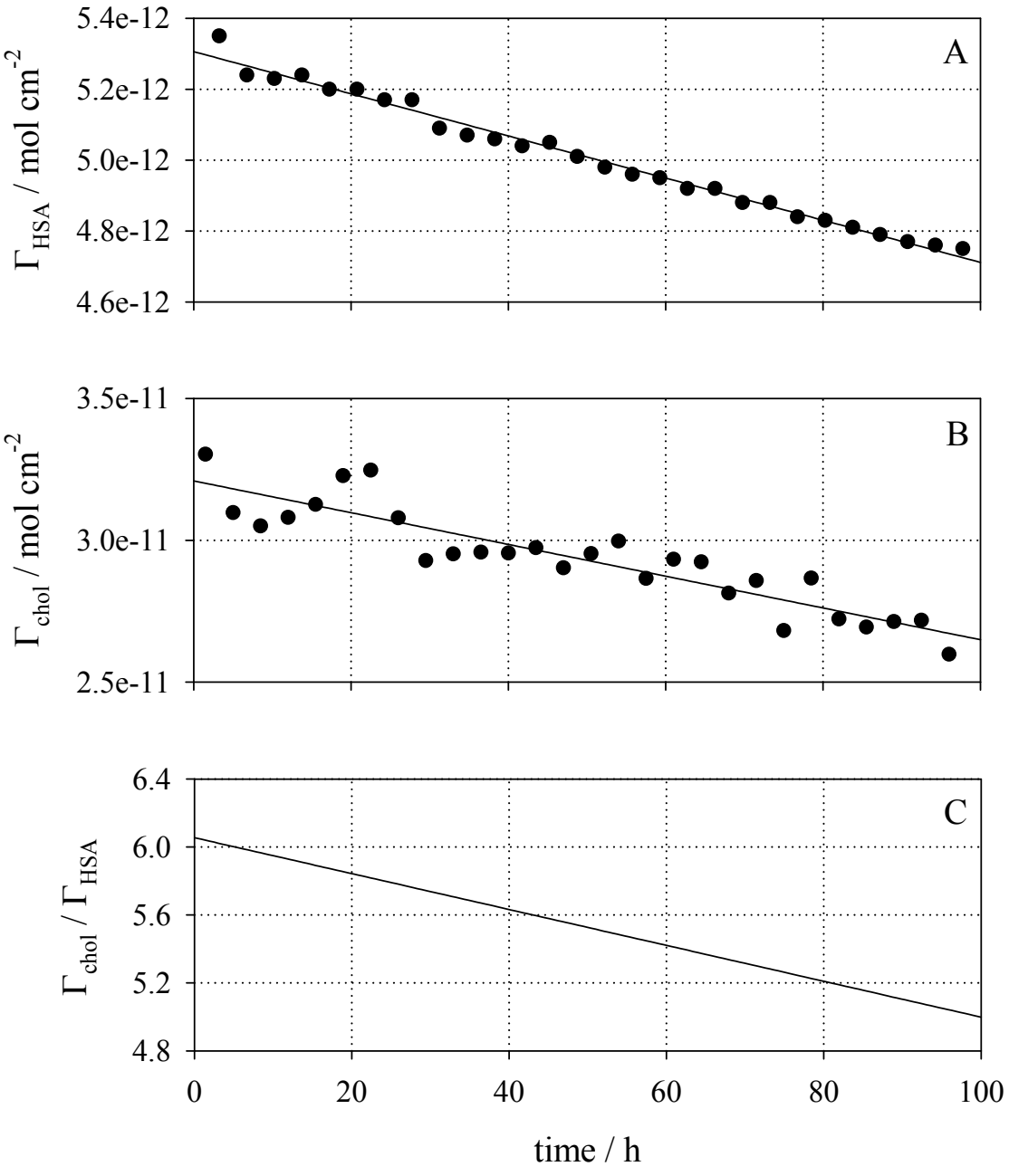

Fig. 33. Time dependent decrease of surface concentrations of immobilized HSA Γ_{HSA} (A) and of cholate Γ_{chol} reversibly bonded to adsorbed HSA (B), as well as of the bonding affinity of HSA during c-ME by 5 mM cholate (C). (A): The surface concentration of immobilized HSA decreased by about 1.1 % per 10 hours due to detachment from the Ge MIRE. The ability of cholate to act as detergent and mechanical stress by c-ME might be the main reasons. (B): The maximum surface concentration of reversibly bonded cholate decreased by about 1.8 % per 10 hours. Detachment and denaturation of HSA might be the main reasons for that. Surface concentrations were evaluated according to Section 2.2.3 and 2.2.4. Best fit straight lines were calculated by linear regression. (C): Decrease of the bonding affinity of HSA due to the effects depicted by (A) and (B).

Table 6. Results and measuring times of c-ME experiments.

conc. of cholate in PBS [mM]	surface conc. Γ_0 of bonded cholate [10^{-12} mol cm^{-2}]	stoichiometric ratio ($\Gamma_{0,cholate}$ / $\Gamma_{0,HSA}$)	number of vp-pp-vp modulation measurements without/with HSA layer	measuring time [h] without/with HSA layer
0.3	3.48 ± 1.08	0.65 ± 0.21	30/30	90/105
1.0	8.87 ± 1.21	1.62 ± 0.26	28/28	84/98
2.0	15.7 ± 2.08	2.97 ± 0.46	30/28	90/98
3.0	22.1 ± 3.14	4.42 ± 0.51	25/25	75/88
4.0	25.0 ± 2.83	4.83 ± 0.66	30/27	90/95
5.0	32.1 ± 3.90	6.05 ± 0.88	28/28	84/98
6.0	33.0 ± 4.50	6.47 ± 1.02	16/16	48/56
10.0	46.1 ± 5.85	9.17 ± 1.37	14/14	42/49
15.0	53.8 ± 6.79	10.57 ± 1.57	10/10	30/35
20.0	57.7 ± 7.07	11.59 ± 1.69	10/12	30/42

As a next step, we can consider the consequence of a reduced measuring time on results. Stoichiometric ratios and their errors evaluated by using all and the first half of vp-pp-vp modulation measurements are presented in Table 7 showing evidently that they do not differ significantly except the error of the ratio resulting from c-ME by the 0.3 mM cholate solution.

This finding led to the conclusion that only the accuracy of the stoichiometric ratio obtained from c-ME by 0.3 mM cholate is enhanced by using the whole measuring time for evaluation, whereas the errors of all other stoichiometric ratios have already reached their optimum after half of measuring time. This is due to the fact that errors are not only determined by the accuracy of integrated absorbances of $\nu_s(COO^-)$, which is enhanced by long measuring times, but also by the accuracy of all parameters of eq. (13). After half of measuring time the error of integrated absorbances of $\nu_s(COO^-)$ is already so small that the constant errors of the remaining parameters, e.g. the number of active internal reflections and other (see Table 2), dominate the overall error.

Table 7. Stoichiometric ratios of bonded cholate and adsorbed HSA after full and half of measuring time.

concentration of cholate in PBS [mM]	stoichiometric ratio ($\Gamma_{0,cholate}$ / $\Gamma_{0,HSA}$)	stoichiometric ratio after half of measuring time
0.3	0.65 ± 0.21	0.60 ± 0.56
1.0	1.62 ± 0.26	1.70 ± 0.28
2.0	2.97 ± 0.46	2.91 ± 0.47
3.0	4.42 ± 0.51	4.28 ± 0.66
4.0	4.83 ± 0.66	4.74 ± 0.70
5.0	6.05 ± 0.88	5.98 ± 0.87
6.0	6.47 ± 1.02	6.50 ± 1.00
10.0	9.17 ± 1.37	9.09 ± 1.38
15.0	10.57 ± 1.57	10.47 ± 1.64
20.0	11.59 ± 1.69	11.55 ± 1.69

On the other hand, for detection and analysis of structural changes in adsorbed HSA layers induced by interaction with cholate, spectra with a signal-to-noise ratio in the mikro-absorbance region were needed. For that reason, long measuring times had to be accepted, whereas for evaluation of stoichiometric ratios and thus, the bonding curve, half of the measuring time was already sufficient.

So far, for determination of stoichiometric ratios the solvent compensation according to Section 2.2.4 (p. 24) was taken into account. c-ME experiments were also evaluated without consideration of solvent compensation to demonstrate the effect of this procedure (see Table 8). The contribution of the replaced solvent layer to the corrected spectrum is determined by the concentration of dissolved cholate and the thickness of the layer. Since the latter was in the range of (16 ± 1) Å in all experiments (see Table 4, p. 64), the influence on stoichiometric ratios was mainly dependent on the concentration of dissolved cholate, as it is also shown by a graphic representation of stoichiometric ratios with and without solvent compensation in Fig. 34. The ratios differed only a few percent, however, ignoring the solvent correction would cause a systematic error in evaluation of the bonding curve.

Table 8. Stoichiometric ratios of bonded cholate and adsorbed HSA with and without taking solvent correction into account.

concentration of cholate in PBS [mM]	stoichiometric ratio ($\Gamma_{0,cholate}$ / $\Gamma_{0,HSA}$)	stoichiometric ratio without solvent correction	difference of stoichiometric ratios in %
0.3	0.65 ± 0.21	0.64 ± 0.22	1.9
1.0	1.62 ± 0.26	1.61 ± 0.25	1.2
2.0	2.97 ± 0.46	2.92 ± 0.45	2.0
3.0	4.42 ± 0.51	4.34 ± 0.50	1.8
4.0	4.83 ± 0.66	4.68 ± 0.65	2.5
5.0	6.05 ± 0.88	5.89 ± 0.85	2.6
6.0	6.47 ± 1.02	6.25 ± 0.99	3.3
10.0	9.17 ± 1.37	8.83 ± 1.33	3.7
15.0	10.57 ± 1.57	10.05 ± 1.50	4.8
20.0	11.59 ± 1.69	10.93 ± 1.60	5.7

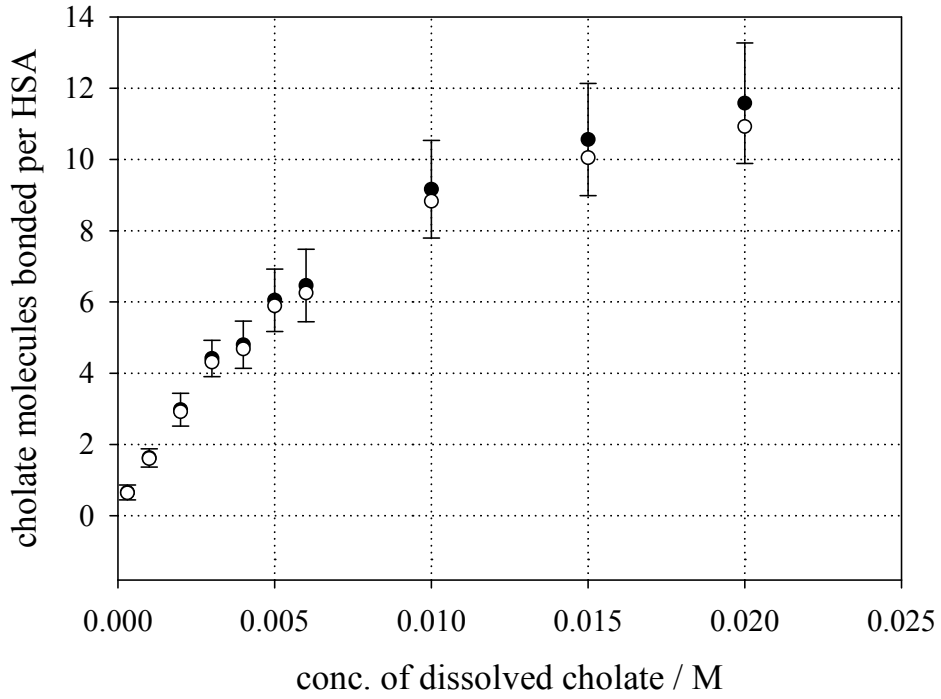

Fig. 34. Stoichiometric ratios of cholate and adsorbed HSA with (●) and without (○) consideration of solvent compensation. Ignoring the procedure of solvent compensation according to Section 2.2.4 resulted in lower stoichiometric ratios, which would lead to a systematic error in evaluation of the bonding curve. For better clarity error bars of stoichiometric ratios without solvent compensation are not shown.

5.3.5 Estimation of sensitivity

Following considerations give an estimation of the sensitivity of the method.

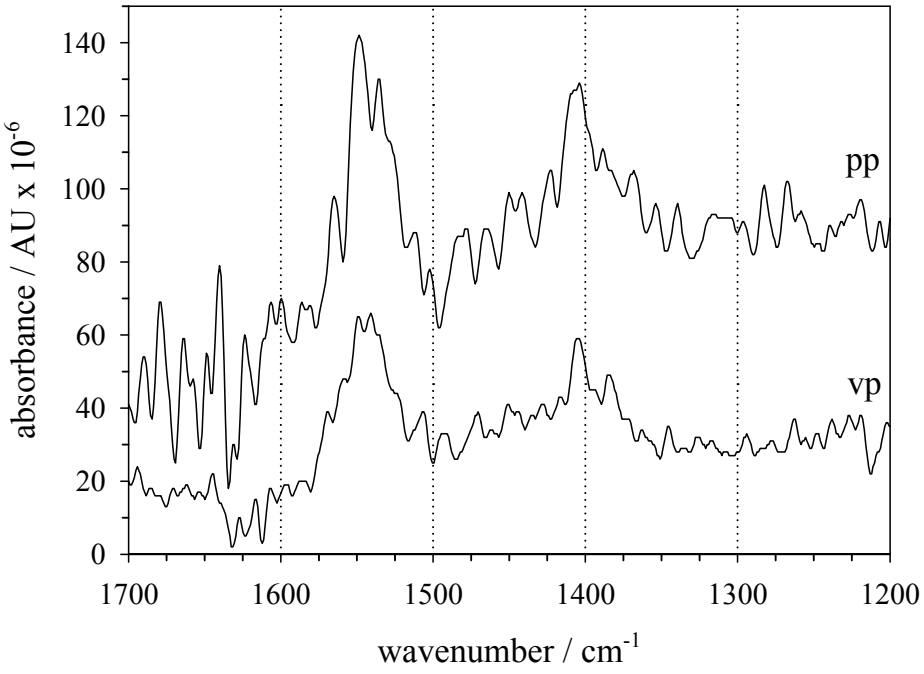

Fig. 35. Phase-resolved spectra at maximum of amplitude resulting from one vp-pp-vp modulation measurement of c-ME by 0.3 mM cholate. A measuring time of 3 h consisting of one hour using pp and two hours using vp incident IR light resulted in a peak-to-peak noise level of ~20 μAU (pp) and ~15 μAU (vp), respectively, in the spectral region of $\nu_s(COO^-)$.

As it is seen by Fig. 35, demodulated spectra of c-ME experiments resulting from one vp-pp-vp modulation measurement exhibited a peak-to-peak noise level of ~20 μAU (pp) and ~15 μAU (vp), respectively, in the spectral region of $\nu_s(COO^-)$. A measuring time of 3 h consisting of one hour using pp and two hours using vp incident IR light was necessary to achieve this noise level enabling the detection of surface concentrations of bonded cholate $\Gamma_{chol} \approx 10^{-11}$ mol cm^{-2}. For the detection of smaller surface concentrations multiple successive vp-pp-vp measurements were averaged to analyze the course within the experiment (see Fig. 45B and Fig. 46B).

Regarding the total time needed for the final result one has to take into account that there is also time needed for the measurement of reference spectra. This time should be at least the same as needed for sample measurements to keep the signal-to-noise ratio at the same level. Moreover, in this work the final integrated absorbance of $\nu_s(COO^-)$ used as reference absorbance was determined by regression of successive vp-pp-vp modulation measurements (see next Section). Such sequences took a multiple of time compared to a single modulation measurement, but resulted in an accuracy a few times better than in any single vp-pp-vp measurement.

5.4 Interference by impurities and detachment of HSA

5.4.1 Cholate bonding impurity

The integrated absorbancies of $\nu_s(COO^-)$ obtained by 28 successive vp-pp-vp modulation measurements of c-ME by 5 mM cholate in absence of the HSA layer are plotted against time in Fig. 36. In contradiction to an expected stable response, the signal increased linearly by 0.5 % per 10 hours indicating that small amounts of an unknown cholate bonding impurity adsorbed to the surface of the reflection element, thus increasing continuously the demodulated signal of cholate due to periodic accumulation at the surface of the MIRE. This impurity was present in different amounts in all purchased cholate samples and caused an increase of the signal in all c-ME experiments without HSA layer independently of the cholate concentration.

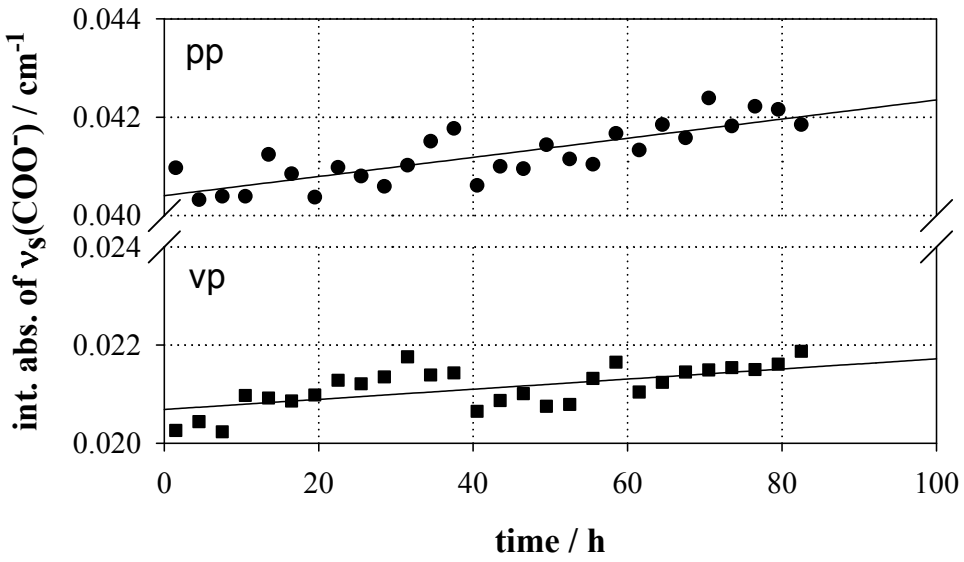

Fig. 36. Course of the maximum integrated absorbance of $\nu_s(COO^-)$ of cholate at 1405 cm^{-1} evaluated by vp-pp-vp modulation measurements of c-ME by 5 mM cholate without HSA layer (clean Ge MIRE). Unexpectedly, the signal increased linearly by about 0.5 % per 10 hours indicating that small amounts of an unknown cholate bonding impurity adsorbed to the clean surface of the Ge MIRE, thus enhancing continuously the modulation amplitude. To get rid of such a disturbance, data had to be extrapolated to time zero, i.e. the beginning of a modulation experiment. Best fit straight lines were calculated by linear regression.

Spectra of the impurity measured after c-ME are shown in Fig. 37. The presence of aliphatic CH_2 groups is proved by the antisymmetric and symmetric C-H stretching vibration at 2923 cm^{-1} and 2853 cm^{-1}, respectively, and also by the C-H bending vibration at 1465 cm^{-1}. The band at 1735 cm^{-1} can be assigned to C=O groups, whereas the broad band in the range of 1100 – 1300 cm^{-1} is a hint for C-O groups. Amide groups are characterized by the presence of amide I (1630 – 1660 cm^{-1}) and amide II (1530 – 1560 cm^{-1}) bands. These regions were influenced by the negative water bending vibration at 1640 cm^{-1} caused by replaced buffer and by overlapping with side chain vibrations of amino acids. For that reason, a separation and quantification of these bands was impeded.

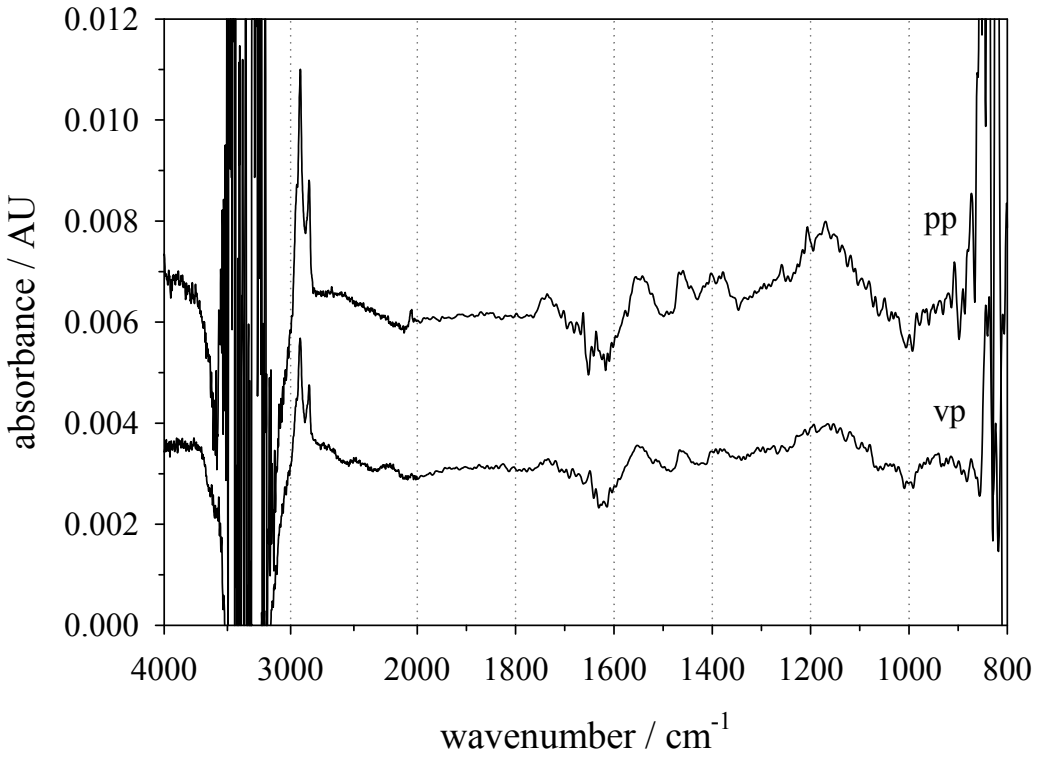

Fig. 37. FTIR ATR SBSR spectra of the impurity adsorbed to the MIRE. Spectra of the impurity were measured after c-ME without HSA layer with pp and vp incident light. Reference was the clean reflection element before starting of c-ME. The presence of aliphatic CH_2 groups was proved by the antisymmetric and symmetric C-H stretching vibration at 2923 cm^{-1} and 2853 cm^{-1}, respectively, and also by the bending vibration at 1465 cm^{-1}. For assignment of remaining bands the reader is referred to the text. An unambiguous assignment of the impurity to distinct chemical compounds was not possible.

Since cholate is extracted from gall bladders of sheep and cattle, most probably the impurity consists of different substances. However, the chemical class of lipoproteins would fulfill most of the conditions above, especially the unusual high amount of CH_2 groups, but an unambiguous assignment to distinct chemical compounds was not possible.

5.4.2 Detachment of HSA from the adsorbed layer

The course of the integrated absorbances of $\nu_s(COO^-)$ evaluated by the vp-pp-vp modulation measurements of c-ME using 5 mM cholate in presence of the HSA layer

showed a small decrease of the signal in the amount of 0.4 % per 10 hours (Fig. 38), reflecting a slow loss of cholate bonding sites and immobilized protein itself during the modulation experiment. A loss in a similar extent was also detected in other c-ME experiments except the experiment with 20 mM cholate (see Fig. 54 in Appendix 7.3, p. 114).

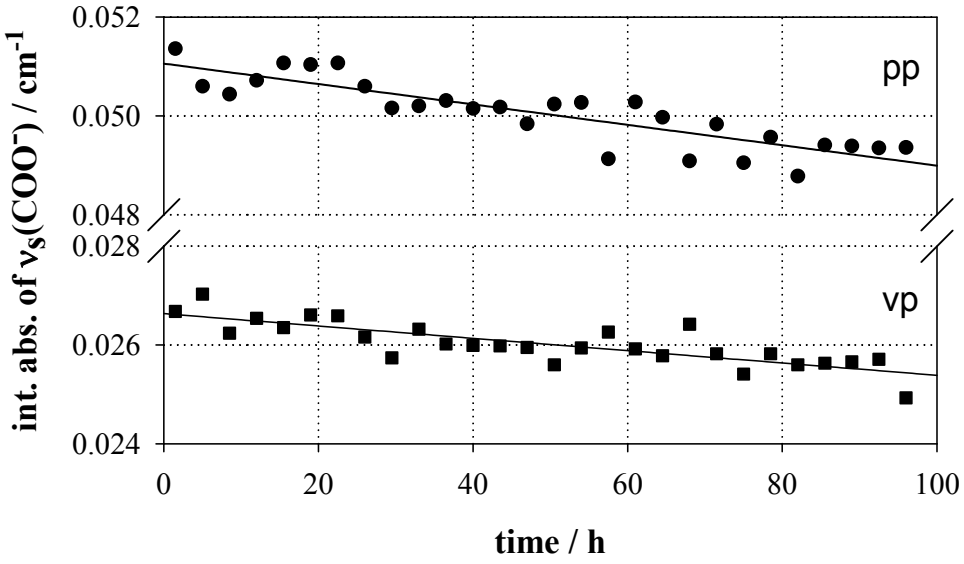

Fig. 38. Course of the maximum integrated absorbance of $\nu_s(COO^-)$ of cholate at 1405 cm^{-1} evaluated by vp-pp-vp modulation measurements of c-ME by 5 mM cholate in presence of the HSA layer adsorbed to the Ge MIRE. The small decrease of the signal in the amount of about 0.4 % per 10 hours reflects loss and denaturation of the immobilized protein.

An attachment of a small part of the unknown impurity, discovered in cholate, on free places of the Ge MIRE or on the adsorbed HSA itself was noticed at the end of all modulation experiments. For an example, spectra of the HSA layer measured after finishing the c-ME by 6 mM cholate are shown in Fig. 39, where the condition of the layer immidiately before start of cholate modulations was taken as reference. Negative amide bands were expected due to the loss of the HSA layer during c-ME. On the other hand, positive bands in the regions of CH_2 and C-O stretching vibrations indicated an increase of

substance on the reflection element, most probably by adsorption of the impurity found in cholate.

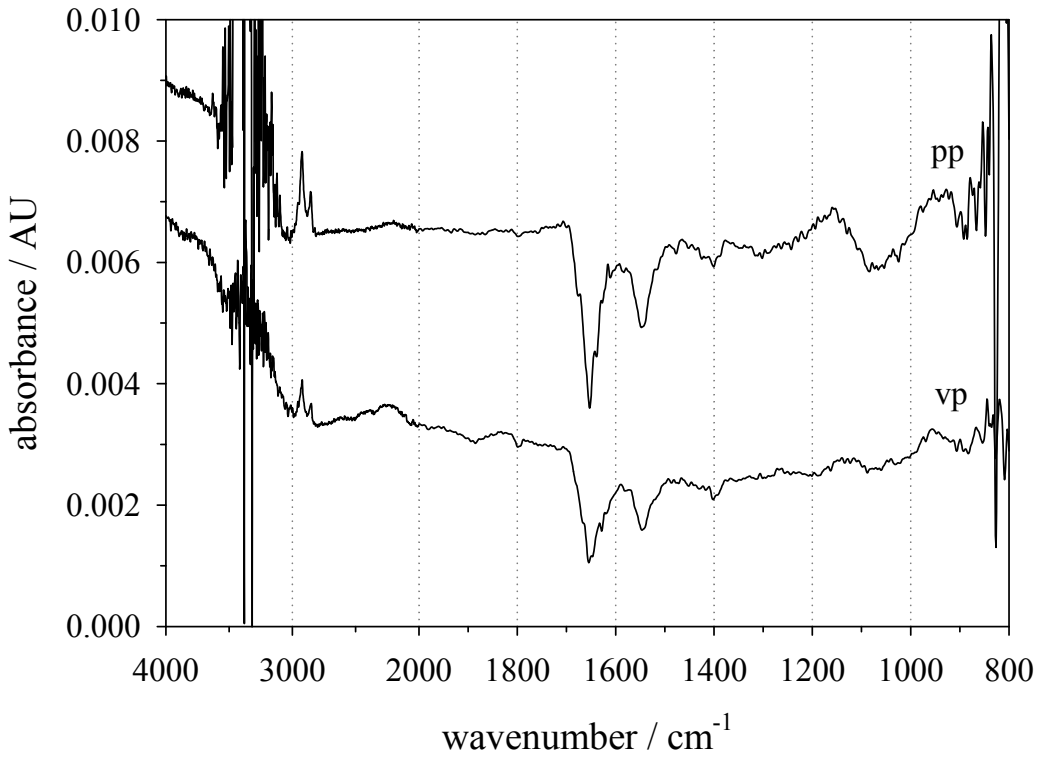

Fig. 39. FTIR ATR SBSR spectra demonstrating the effect of c-ME by cholate on the HSA layer. These spectra were measured at the end of the c-ME experiment with 6 mM cholate taking the spectrum of the layer immidiately before start of cholate modulations as reference. Negative amide bands were expected due to the loss of the HSA layer during c-ME. On the other hand, positive CH_2 stretching bands and bands at 1150 cm^{-1} and 950 cm^{-1} indicated most probably the adsorption of the impurity present in cholate.

5.4.3 Correction of interference by impurities and by loss of HSA

In order to get rid of effects as described in Section 5.4.1 and 5.4.2, time-resolved data of all experiments were extrapolated to time zero, i.e. the beginning of the c-ME experiment. Results of c-ME by 10 mM cholate shown in Fig. 40 demonstrate the importance of this correction.

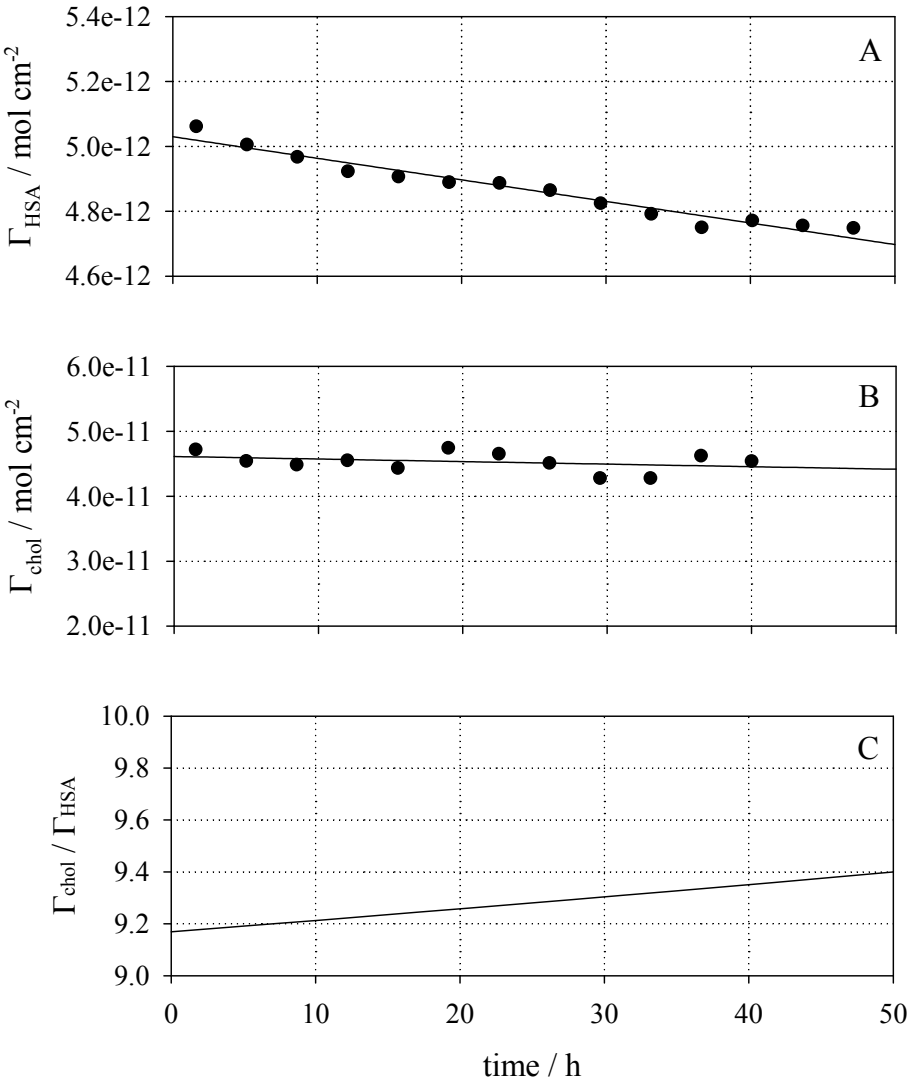

Fig. 40. Course of the surface concentration of immobilized HSA Γ_{HSA} (A), of cholate Γ_{chol} bonded to adsorbed HSA (B), and of the HSA ability to bond cholate (C) during c-ME by 10 mM cholate. (A) The surface concentration of immobilized HSA decreased in the amount of 1.5 % per 10 hours due to the ability of cholate to act as detergent. (B) The surface concentration of cholate bonded to adsorbed HSA decreased in the amount of 0.9 % per 10 hours as a result of a small loss of cholate bonding sites of adsorbed HSA and of immobilized HSA itself. (C) The HSA ability to bond cholate obtained by calculating the ratio of corresponding points of A and B shows an increase, although the surface concentration of HSA decreased. This result can only be explained by the fact that the cholate bonding impurity attached on free places of the reflection element or on HSA itself and overcompensated by this way the loss of bonding sites of HSA. Best fit straight lines were calculated by linear regression.

The courses of surface concentrations of HSA and bonded cholate are presented in Fig. 40A and Fig. 40B, respectively. Both show a decrease of the signal due to loss of HSA and bonded cholate. The stoichiometric ratio achieved at the beginning of c-ME resulted in 9.17 ± 1.33. The cholate bonding ability, as shown in Fig. 40C, increased, although the surface concentration of HSA decreased. This result can only be explained by the fact that the impurity, which adsorbed on free places of the reflection element or on HSA itself, also bonded cholate and overcompensated by this way the loss of bonding sites of HSA. As a consequence, the course of the cholate bonding ability reflects the sum of two opposing effects, i.e. the loss of bonding sites by detachment and denaturation of HSA and the increase of bonding sites by the attachment of the impurity present in different amounts in all purchased cholate samples. In such a case extrapolating of data to time zero led to a correct result. Evaluations of all c-ME experiments are presented in Appendix 7.3.

5.5 Analysis of excitation function

The stimulation period of modulation experiments was chosen in such way that no signal damping has to be expected due to too fast exchange of cholate and buffer solutions in the flow-through cell. It turned out that a modulation period of T = 588 s, corresponding to an angular frequency of $\omega = 1.07 \cdot 10^{-2}\ s^{-1}$, was adequate. Analysis of accumulated modulation periods of c-ME by 5 mM cholate measured with pp incident light may serve as an example. The symmetric stretching vibration of the carboxyl group $\nu_s(COO^-)$ of cholate at 1405 cm^{-1} was used as markerband. The time dependency of the concentration of cholate in the flow-through cell during stimulation periods, as shown in Fig. 41A, led to an excitation function close to rectangular with a Fourier series consisting of odd higher harmonics. Fig. 41B presents the response of the HSA layer to the stimulation by cholate. It was calculated as difference between the time resolved responses of cholate modulation

in presence and in absence of the HSA layer, respectively. The HSA layer seems to introduce a slight damping of higher harmonics of the HSA response; however, the response to the fundamental frequency, which was exclusively evaluated for determination of bonded cholate, could still reach its maximum amplitude.

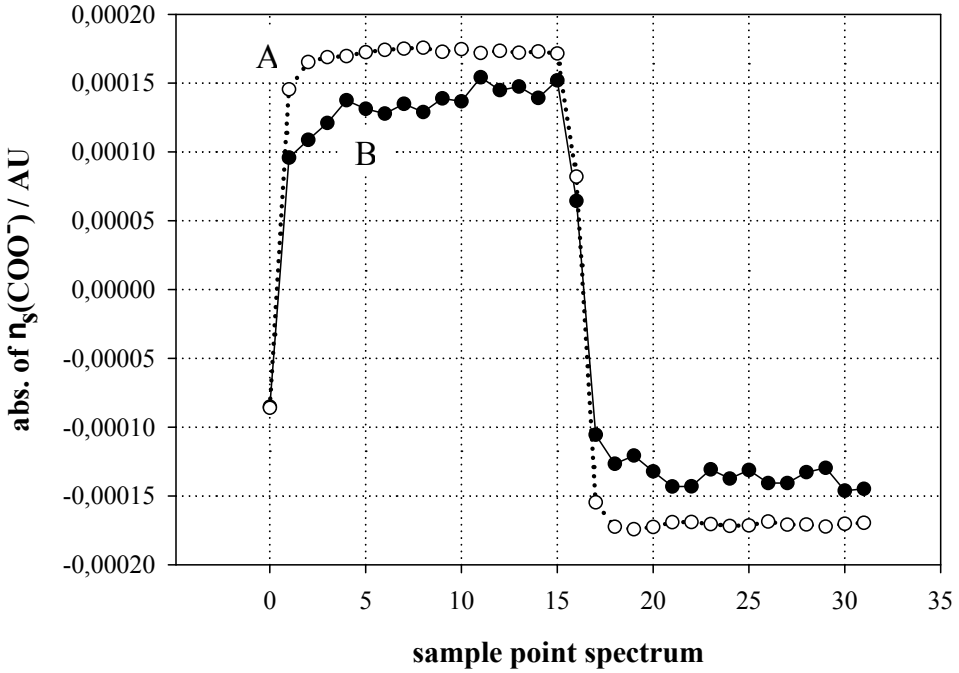

Fig. 41. Course of the amount of cholate within accumulated modulation periods of c-ME by 5 mM cholate measured with pp light. Trace (A) reflects the time dependency of the concentration of cholate in the flow-through cell in absence of the HSA layer scaled down by a factor of 5. Trace (B) is the response of the HSA layer to the stimulation of (A) after subtraction of background absorption. It reflects the amount of cholate bonded to HSA with original scaling. The stimulation characterized by (A) was close to rectangular, while the HSA layer seems to introduce a slight delay in the response, which was not analyzed with respect to its origin within this work. One sample point spectrum corresponds to $\Delta T = 18.4$ sec resulting in a stimulation period of $T = 32 \times \Delta T = 9.8$ min. Peak absorbances of $\nu_s(COO^-)$ at 1405 cm^{-1} were evaluated using the mean spectrum of averaged sample point spectra as reference. Corresponding data of A (○) and B (●) are connected for better clarity.

Demodulated responses to the fundamental frequency (sin(ωt); k = 1) and to higher harmonics (sin(kωt)/k; k = 2 to k = 8) of c-ME by 5 mM cholate without HSA layer at maximum amplitude measured with pp incident light are shown in Fig. 42. According to eq. (22) (see p. 31) the fundamental and higher harmonics with odd k cause responses with an amplitude exhibiting an intensity of 1/k of the fundamental response, whereas harmonics with even k produce no evaluable signals as long as a sinusoidal function is used for demodulation. Integrated absorbances of $\nu_s(COO^-)$, $\int A^{pp}_{(COO^-)}(\tilde{\nu})\,d\tilde{\nu}$, of the response to the fundamental and to odd higher harmonics and the ratios of $\int A^{pp}_{(COO^-)}(\tilde{\nu})\,d\tilde{\nu}$ are summarized in Table 9. The deviation of ratios between $\int A^{pp}_{(COO^-)}(\tilde{\nu})\,d\tilde{\nu}$ of the fundamental response and $\int A^{pp}_{(COO^-)}(\tilde{\nu})\,d\tilde{\nu}$ of the response to the 5th and 7th harmonic from theoretical values is due to the fact that the excitation function is not perfectly rectangular.

A non-linear response of the system, which would be seen by amplitudes in phase-resolved spectra of higher harmonics, is very unlikely because it should also lead to signals in phase-resolved spectra of even harmonics.

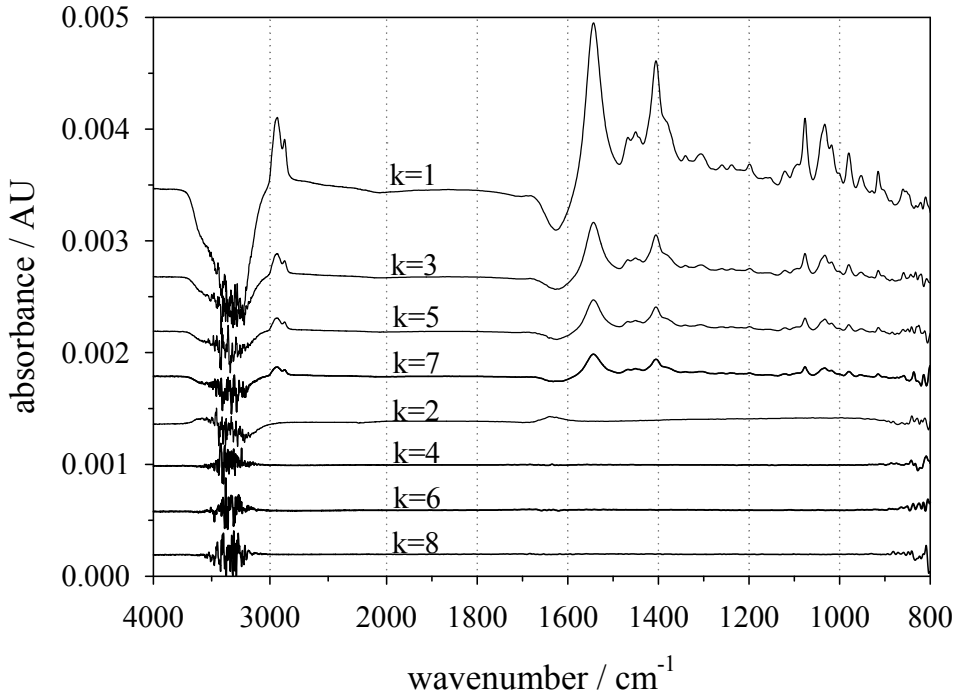

Fig. 42. Responses to the fundamental frequency (sin(ωt); k = 1) and to higher harmonics (sin(kωt)/k; k = 2 to k = 8) of c-ME by 5 mM cholate without HSA layer with maximum amplitude measured with pp incident light. Each summand of the excitation function of eq. (22) (see p. 31) causes an stimulation of the HSA layer and for that reason, only the fundamental and harmonics with odd k cause responses with an amplitude exhibiting an intensity of 1/k of the fundamental response, whereas harmonics with even k produce no signals as long as a sinusoidal function is used for demodulation.

Table 9. Integrated absorbances of $\nu_s(COO^-)$, $\int A^{pp}_{(COO^-)}(\tilde{\nu})\,d\tilde{\nu}$, of the response to the fundamental (k = 1) and to higher harmonics (k = 3, 5, 7), shown in Fig. 42, and ratios between $\int A^{pp}_{(COO^-)}(\tilde{\nu})\,d\tilde{\nu}$ of the fundamental response and $\int A^{pp}_{(COO^-)}(\tilde{\nu})\,d\tilde{\nu}$ of higher harmonic responses (k = 3, 5, 7).

k	$\int A^{pp}_{(COO^-)}(\tilde{\nu})\,d\tilde{\nu}$ / $[10^{-3}\ cm^{-1}]$	$\frac{\int A^{pp}_{(COO^-)}(\tilde{\nu})\,d\tilde{\nu}\quad (k)}{\int A^{pp}_{(COO^-)}(\tilde{\nu})\,d\tilde{\nu}\quad (k=1)}$	theoretical ratio
1	40.8 ± 2.0	1	
3	13.4 ± 0.7	3.0 ± 0.2	3
5	7.8 ± 0.4	5.2 ± 0.4	5
7	5.4 ± 0.3	7.6 ± 0.6	7

5.6 Bonding curve

The stoichiometric ratios characterizing the bonding behavior between cholate and adsorbed HSA were achieved by c-ME experiments at different concentrations of cholate in PBS (see Table 6, p. 74). These ratios are shown versus the concentration of dissolved cholate in Fig. 43 and may now be compared with the bonding curve of the system 'cholate bonded to HSA in solution' obtained by calculation according to eq. (25) of page 33 using the maximum number of bonding sites B_{max} and the dissociation constants $K_d = 1/K_a$ reported in [17], i.e. $B_{max,1} = 2.8$, $B_{max,2} = 12$, $K_{d,1} = 3.03\times10^{-4}$ mol l^{-1}, $K_{d,2} = 3.33\times10^{-3}$ mol l^{-1}. Results obtained by c-ME experiments and by calculation are summarized in Table 10 and represented in Fig. 43 by circles with error bars and the solid curve, respectively.

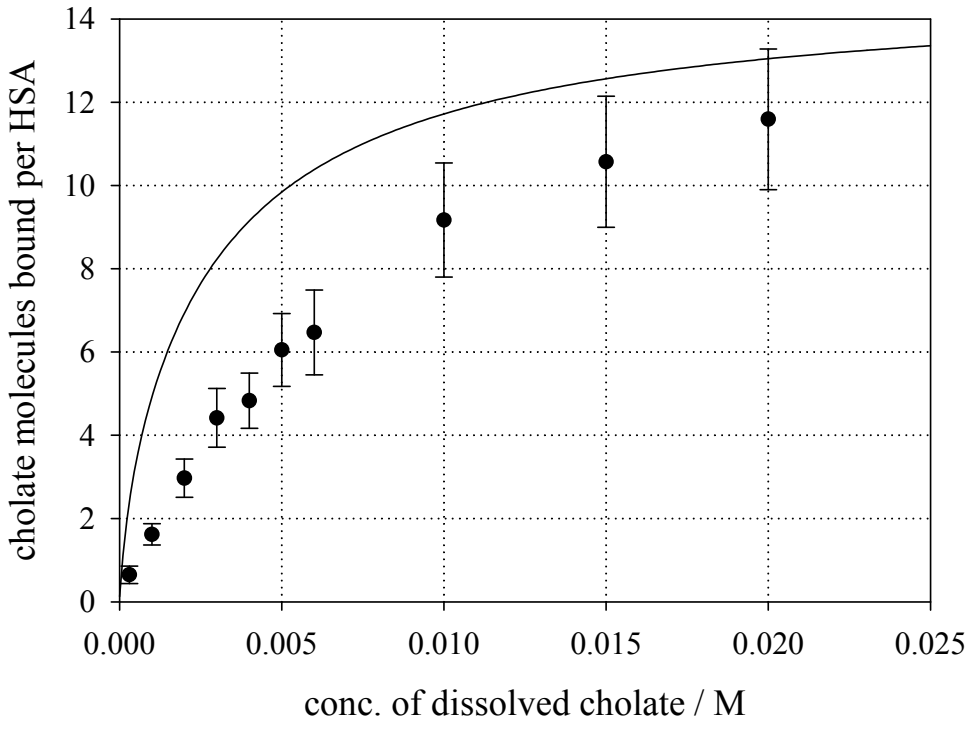

Fig. 43. Comparison of the number of cholate molecules bonded to adsorbed and dissolved HSA. Stoichiometric ratios achieved by c-ME experiments are represented by circles with error bars. The bonding curve of cholate and HSA in solution was obtained by calculation using the parameters of [17]. In the observed concentration range less cholate has bonded to adsorbed HSA than to HSA in solution.

Table 10. Number of cholate molecules bonded to HSA at different concentrations of cholate in PBS.

concentration of cholate in PBS [mM]	number of cholate molecules bonded to HSA		
	calculated according to eq. (25) using the parameters of [17]	evaluated by c-ME experiments	difference to calculated in %
0.3	2.4	0.65 ± 0.21	27.4
1.0	4.9	1.62 ± 0.26	33.0
2.0	6.9	2.97 ± 0.46	43.0
3.0	8.2	4.42 ± 0.51	50.9
4.0	9.1	4.83 ± 0.66	52.5
5.0	9.8	6.05 ± 0.88	61.5
6.0	10.4	6.47 ± 1.02	62.3
10.0	11.7	9.17 ± 1.37	78.2
15.0	12.6	10.57 ± 1.57	84.1
20.0	13.0	11.59 ± 1.69	88.8

As it was expected, less cholate has bonded to adsorbed HSA than to HSA in solution because as a result of adsorption the access to bonding sites was assumed to be limited. But on the other hand, the percentage of reduced bonded cholate, as shown in Table 10, stayed not constant over the whole concentration range indicating a bonding behavior completly different. Therefore, stoichiometric ratios were fitted according eqs. (24) and (25) using the constraints depicted in Table 11.

In fitting (a) the dissociation constants reported in [17] were used, i.e. $K_{d,1} = 3.03 \times 10^{-4}$ mol l^{-1} and $K_{d,2} = 3.33 \times 10^{-3}$ mol l^{-1}. The fitting resulted in $B_{max,1} = 0$ and $B_{max,2} = 11.3 \pm 1.7$ indicating a complete loss of the high affinity bonding sites. Therefore, in fitting (b) the model of one site saturation with $K_d = 3.33 \times 10^{-3}$ mol l^{-1} was applied resulting in $B_{max} = 11.4 \pm 1.7$. Since the fitting procedures with fixed K_d did not produce a satisfying result, in example (c) the model of one site saturation with no constraints was used resulting in a bonding curve with $B_{max} = 17.2 \pm 2.5$ and $K_d = (9.39 \pm 0.60) \times 10^{-3}$ mol l^{-1}, thus $K_a = 1/K_d = (107 \pm 7)$ l mol^{-1}. Bonding curves calculated from fitting results are shown in Fig. 44.

The fitting procedure itself was checked by applying the two site saturation model to the computed stoichiometric ratios (see Table 10) without any constraints resulting in the confirming values of $B_{max,1} = 2.8$, $B_{max,2} = 12$, $K_{d,1} = 3.03 \times 10^{-4}$ mol l^{-1}, $K_{d,2} = 3.33 \times 10^{-3}$ mol l^{-1}.

Table 11. Summary of fitting parameters and results applied to stoichiometric ratios got from c-ME experiments.

Fit	Equation used for fitting	Constraints	Fitting results
(a)	$y = \frac{B_{max,1} \cdot x}{K_{d,1} + x} + \frac{B_{max,2} \cdot x}{K_{d,2} + x}$	$K_{d,1} = 3.03 \times 10^{-4}$ mol l^{-1} $K_{d,2} = 3.33 \times 10^{-3}$ mol l^{-1}	$B_{max,1} = 0$ $B_{max,2} = 11.3 \pm 1.7$
(b)	$y = \frac{B_{max} \cdot x}{K_d + x}$	$K_d = 3.33 \times 10^{-3}$ mol l^{-1}	$B_{max} = 11.4 \pm 1.7$
(c)	$y = \frac{B_{max} \cdot x}{K_d + x}$	None	$K_d = (9.41 \pm 0.60) \times 10^{-3}$ mol l^{-1} $B_{max} = 17.2 \pm 2.5$

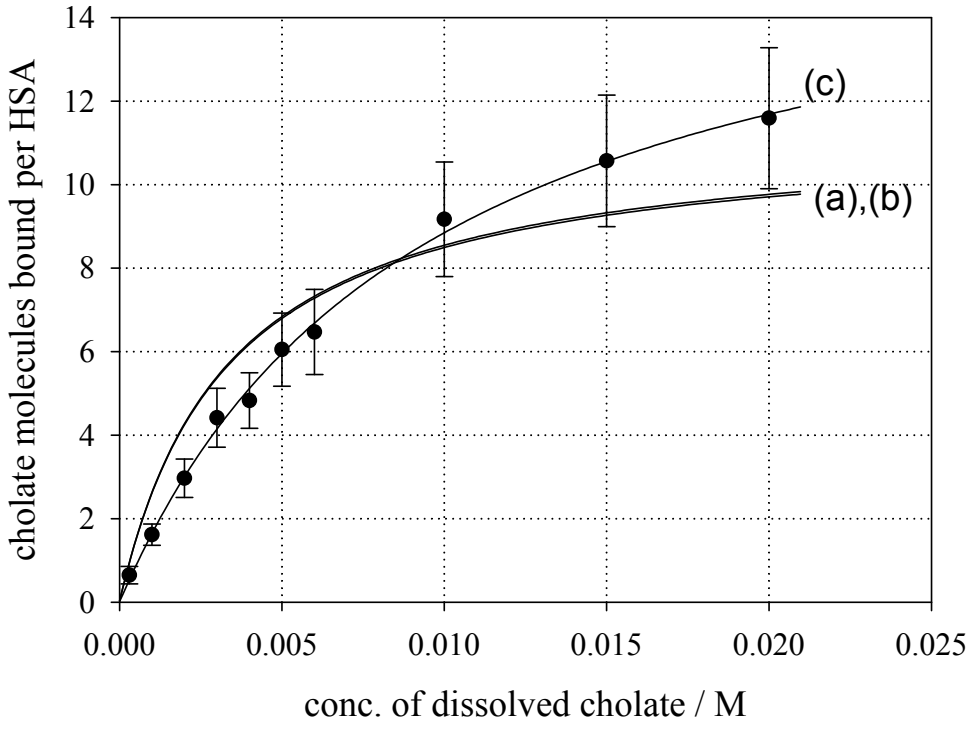

Fig. 44. Stoichiometric ratios characterizing the bonding between cholate and adsorbed HSA together with bonding curves resulting from fittings of Table 11. Stoichiometric ratios achieved by c-ME experiments are represented by circles with error bars. Since fittings (a) and (b) with fixed dissociation constants, known from [17], did not produce a satisfying output, in (c) no constraints for the fitting procedure were used resulting in a maximum number of bonding sites $B_{max} = 17.2 \pm 2.5$ and an association constant $K_a = 1/K_d = (107 \pm 7)$ l mol^{-1}.

These findings led to the following conclusions: Adsorbed HSA layers did not exhibit high affinity bonding sites. Maybe these sites were not accessible or even destroyed. Only one type of sites was found with a K_a about three times smaller than $K_{a,2}$ of the low affinity bonding sites reported in [17], whereas B_{max} was increased by 5.2. In fact, a decrease of B_{max} was expected because of lower accessibility of bonding sites in adsorbed HSA. Differences in K_a and B_{max} may be explained by following reasons: (i) The process of adsorption and the following washing procedure to get a stable HSA layer caused extensive changes in properties of HSA concerning the bonding of cholate. (ii) In both investigations a phosphate buffer with same pH and similiar ionic strength was used, but in [17] a temperature of 37 ± 0.2°C was applied compared to 25 ± 0.5°C in this work. (iii) Without specification of error limits the authors of [17] admit that the exact number of weak bonding sites could not be accurately defined due to the limitation of their analytical procedure, i.e. equilibrium dialysis. As a consequence, comparison of the number of low affinity bonding sites is restricted by this fact.

6 Conclusions

6.1 Interaction of hTNFα with anti-hTNFα antibody

In the first part of this PhD thesis the specific interaction of the cytokine TNFα with an anti-TNFα antibody was investigated by SBSR ATR FTIR spectroscopy. This work served as a basis for the establishment of a model system to examine receptor-ligand interactions. Adsorbed TNFα played the part of the receptor and the anti-TNFα antibody of the ligand. Two points had to be considered: (i) The protein acting as receptor should mantain its structure as much as possible also after immobilization and (ii) unspecific bonding of the ligand to the reflection element has to be avoided because it was shown in [9] that the anti-TNFα antibody adsorbs to the untreated surface of the Ge MIRE. Preceding saturation of the reflection element with a layer of bovine serum albumin (BSA) inhibited the unspecific attachment of the antibody. The adsorbed TNFα layer was also treated with a solution of BSA to cover free bonding sites. By this way, only specific bonding of the antibody to TNFα was possible. This procedure is also used in enzyme linked immunosorbent assays (ELISA) to avoid unspecific bonding. The evidence that the epitopes of immobilized TNFα were still recognized is given by the fact that the antibody was bonded by a ratio of one antibody per 5.33 TNFα molecules.

The surface concentration of immobilized TNFα, which was evaluated by FTIR ATR spectra measured with pp and vp incident light, supported the fact that TNFα adsorbed in a quite complete monolayer to the surface of the reflection element. 73 % of the molecules shaped like cones were fixed by the basal plane, the remaining 27 % by the envelope of the cone as shown schematically in Fig. 17. It should be noted that this theoretical consideration is valid only as long as the structure of the adsorbed protein keeps the same after immobilization. The antigen-antibody complex exhibited quite a stable

behavior even under conditions of permanent flow-through; the overall loss of protein resulted in 7.4 % after washing with 100 µg BSA/ml PBS for 10.5 h.

As a matter of fact, the use of a low-concentrated solution of BSA (100 µg/ml PBS) for washing stabilized the BSA layers, which protected against unspecific adsorption. Applying this solution had no disadvantageous influence on the antigen-antibody complex as it was seen by the stable appearance of the amide bands.

The realization of this long term experiment was enabled by the use of the SBSR ATR method, which provided an enhanced compensation of background signals and access to a reference aged in the same way as the sample. Additionally, single channel spectra of reference and sample compartments can be analyzed also independently of each other.

6.2 Interaction of HSA with cholate

The second part of this work had two goals: (i) Demonstrating the capability of special ATR spectroscopic techniques, such as concentration-modulated excitation (c-ME) and single-beam-sample-reference (SBSR) spectroscopy, to investigate specific interactions between a ligand and a receptor on a molecular level, and (ii) performing this analysis on an well investigated system of general interest, such as human serum albumin (HSA), in order to enable comparison of ATR results with published knowledge on HSA.

ATR spectroscopy reaches optimum efficiency when applied to thin films and surfaces. Therefore, HSA was immobilized by adsorption to the germanium multiple internal reflection element (Ge MIRE), being aware that this step is somewhat unnatural. Nevertheless, this system was very easy to handle, since HSA formed spontaneously a very stable monolayer at the Ge MIRE surface. This is a prerequisite for c-ME, which is based on a periodic exchange of the bulk solution in contact with the HSA layer. Cholate dissolved in PBS at concentrations of 0.3 mM to 20 mM was used as specifically

interacting ligand. Thus, c-ME was performed by exposing the HSA layer repeatedly to cholate solutions during one half-period of T/2 = 4.9 min, followed by a computer-controlled exchange of the cholate solution by pure PBS in the second half-period.

It turned out that a stable baseline is of utmost importance, since measuring times in the range of 90 hours were necessary to achieve sensitivities in the micro-absorbance region (see Fig. 31). This high sensitivity is required for the study of structural changes in monolayers, which are induced by interaction with a ligand dissolved in the bulk environment. Measurements with parallel and perpendicular polarized light, as well as repeated checks of the stability of the whole system are included in the indicated measuring time. c-ME in combination with SBSR spectroscopy is significantly superior to conventional difference spectroscopy. ME techniques may relatively easily be adapted to any FTIR spectrometer. Possible applications are described in details in [46]. Quantitative analysis of ME data is reported in [47].

The peak-to-peak noise level of one vp-pp-vp modulation measurement consisting of a measuring time of one hour using pp and two hours using vp incident IR light was ~20 μAU (pp) and ~15 μAU (vp), respectively. Working in such a range of sensitivity, some effects, which normally do not play a significant role, have to be considered. Among them one should note: (i) displacement of bulk solution by the layer adsorbed to the MIRE. This point is of significant importance for the determination of the number of cholate bonding sites per HSA because c-ME spectra are dominated by absorbance bands resulting from periodic exchange of the bulk solution. Bonded cholate has to be evaluated by a scaled subtraction of the bulk solution; (ii) instabilities in the progression of the experiment, such as detachment and denaturation of HSA; and (iii) midget traces of impurities in a used chemical product, which may adsorb to the sample or reference part of the MIRE and become visible in the spectrum due to the high sensitivity with respect to surface layers, as well as due to concentration enrichment at the surface. Procedures have

been developed in order to correct the experimental data quantitatively for disturbances as just mentioned.

Comparing our results with published data and getting insight into structural changes of HSA induced by cholate bonding, may be commented as follows: Stationary spectra of adsorbed HSA were recorded in the SBSR mode, which turned out to result in improved compensation of buffer bands and laboratory atmosphere in the background. Quantification of the protein layer and comparison with a theoretical surface concentration, derived by geometrical considerations, gave strong evidence that the covering was close to a monolayer. During modulation measurements a loss of immobilized HSA was observed due to mechanical stress by c-ME, and due to the fact that cholate has qualities of a mild detergent.

Evaluation of surface concentrations of immobilized HSA and of cholate bonded to adsorbed HSA was performed using experimental data corrected by interpolation to the beginning of each c-ME experiment. Under equilibrium conditions regarding the HSA layer and the cholate solution, the number of bonded cholate molecules per HSA molecule, i.e. the stoichiometric ratio, was calculated by the proportion of the surface concentrations $\Gamma_{0,cholate} / \Gamma_{0,HSA}$. Results of modulation experiments using cholate solutions in the range of 0.3 mM to 20 mM in PBS were fitted by applying the one site saturation model of receptor-ligand bonding resulting in a bonding curve with a maximum number of bonding sites $B_{max} = 17.2 \pm 2.5$ and an association konstant $K_a = (107 \pm 7)\,l\,mol^{-1}$. In published data [17] obtained by equilibrium dialysis two bonding constants were reported, namely $K_1 = 3300$ with 2.8 high affinity bonding sites, and $K_2 = 300$ with 12 low affinity bonding sites. Since findings achieved by equilibrium dialysis reflect the properties of dissolved HSA, comparison of results showed that adsorbed HSA exhibited only one type of bonding sites with a lower affinity than K_2, but with a higher B_{max}. High affinity bonding sites were not found because they were maybe not accessible or even destroyed in the adsorbed HSA

layer leading to the conlusion that adsorption and the following washing procedure to get a stable HSA layer caused extensive changes in properties of HSA concerning the bonding of cholate.

As another finding, our c-ME experiments revealed a conformational change of HSA upon cholate bonding, i.e. an increase of the α-helical content. Such a stabilizing effect of cholate and deoxycholate on α-helical structures was reported so far in the case of synthetic peptides like poly-L-Lysine only [48], but not for a protein of natural origin.

7 Appendix

7.1 MATLAB-Program for solvent compensation

Following program used for calculation of solvent compensation of albumin layers and of responses of HSA layers to cholate modulation was made by means of standard MATLAB software.

```
S1=load(['path' 'filename']); % spectrum to be compensated
S2=load(['path' 'filename']); % reference spectrum


% Refractive indices
n1=4;                       %(Ge)
n2=1.45;                    %(Layer)
n3=1.31;                    %(Bulk: buffer)

% Angle of incidence
theta=45;                   % degrees
% theta must be converted into radians, thus
theta=theta/180*pi;

% Estimated layer thickness: d
d=17.0;                       % Angström
% conversion to cm
d=d*1.e-8;

% Production of wavenumber and absorbance vectors
nu1=S1(:,1);
nu2=S2(:,1);
A1=S1(:,2);
A2=S2(:,2);


% checking if spectra can be compared
if size(S1)~=size(S2)
    error('spectra must have the same number of data points!!!')
end
if nu1~=nu2
    error('spectra must have the same range of wavenumbers!!!')
end


% calculation of dp
[m,n]=size(nu2);    % determination of number of data points

for i=1:m
    dp(i)=1/(2*pi*(n1^2*sin(theta)^2-n3^2)^(1/2)*nu2(i));
end
```

```
% calculation of the corrected reference spectrum
for i=1:m
    R_bulk_minus_layer(i)=A2(i)*exp(-2*d/dp(i));
end


R_bulk_minus_layer_transpos=R_bulk_minus_layer';
% transposition of row into column

R_correction=A2-R_bulk_minus_layer_transpos;
% calculation of absorbances to be added

Corrected_spectrum=A1+R_correction;
% calculation of absorbances of corrected spectrum

Corrected_spectrum_for_export=[nu2 Corrected_spectrum];
% spectrum as matrix

% save in format, which can be read by OPUS (software for spectroscopy)
dlmwrite('filename with full path',Corrected_spectrum_for_export,'\t')
```

7.2 Determination of the integrated molar absorption coefficient $\int \varepsilon(\tilde{\nu})\, d\tilde{\nu}$ of $\nu_s(COO^-)$ of cholate

FTIR ATR spectra of cholate dissolved in PBS were measured in the concentration range of 1 – 6 mM using pure PBS as reference. The integrated molar absorption coefficient $\int \varepsilon_{(COO^-)}(\tilde{\nu})\, d\tilde{\nu}$ was determined according to

$$\int \varepsilon_{(COO^-)}(\tilde{\nu})\, d\tilde{\nu} = \frac{\int A^{pp,vp}_{(COO^-)}(\tilde{\nu})\, d\tilde{\nu}}{c\, N\, \nu\, d^{bulk}_{e,pp,vp}} \qquad (30)$$

where $\int A^{pp,vp}_{(COO^-)}(\tilde{\nu})\, d\tilde{\nu}$ denotes the integrated absorbance of $\nu_s(COO^-)$ evaluated from spectra measured with pp and vp incident light, respectively. $d^{bulk}_{e,pp,vp}$ is the corresponding effective thickness of the bulk solution at the peak maximum of $\nu_s(COO^-)$ in pp and vp incident light, respectively, as given by eq. (7). It should be noted that at the same wavenumber $d^{bulk}_{e,pp}$ and $d^{bulk}_{e,vp}$ differ by a factor of 2. N is the mean number of active internal reflections. ν and c are the number of carboxylic groups and the concentration of cholate. All relevant parameters are summarized in Table 12. Results of pp and vp measurements were averaged and resulted in $\int \varepsilon_{(COO^-)}(\tilde{\nu})\, d\tilde{\nu} = (1.36 \pm 0.14) \times 10^7$ cm mol^{-1}.

Table 12. Parameters of eq. (30) used for evaluation of the integrated molar absorption coefficient $\int \varepsilon_{(COO^-)}(\tilde{\nu})\, d\tilde{\nu}$ of cholate.

(A) pp incident IR light

conc. of cholate in PBS [mM]	$\int A^{pp}_{(COO^-)}(\tilde{\nu})\, d\tilde{\nu}$ [10^{-2} cm^{-1}]	number of active reflections	ν of COO^-	$d^{bulk}_{e,pp}$ [10^{-5} cm]	$\int \varepsilon_{(COO^-)}(\tilde{\nu})\, d\tilde{\nu}$ [10^{7} cm mol^{-1}]
1.0	1.35	19.6	1	4.69	1.47
2.0	2.03	19.6	1	4.69	1.10
3.0	3.45	19.6	1	4.69	1.25
4.0	5.40	19.6	1	4.69	1.47
5.0	6.47	19.6	1	4.69	1.41
6.0	7.38	19.6	1	4.69	1.34

(B) vp incident IR light

conc. of cholate in PBS [mM]	$\int A^{vp}_{(COO^-)}(\tilde{\nu})\, d\tilde{\nu}$ [10^{-2} cm^{-1}]	number of active reflections	ν of COO^-	$d^{bulk}_{e,vp}$ [10^{-5} cm]	$\int \varepsilon_{(COO^-)}(\tilde{\nu})\, d\tilde{\nu}$ [10^{7} cm mol^{-1}]
1.0	0.71	19.6	1	2.34	1.55
2.0	1.11	19.6	1	2.34	1.21
3.0	1.73	19.6	1	2.34	1.26
4.0	2.79	19.6	1	2.34	1.52
5.0	3.24	19.6	1	2.34	1.41
6.0	3.55	19.6	1	2.34	1.29

7.3 Supplementary results of specific interaction studies of HSA with cholate

Following pages include an overview of the course of c-ME experiments performed with adsorbed HSA and cholate dissolved in PBS at concentrations from 0.3 mM to 20 mM. The evaluation of experimentally determined data is based on linear regression analysis according to Sect. 5.3.4 (see p. 71). For the convenience of the reader Table 13(A) summarizes the results of previous chapters, i.e. the surface concentrations of adsorbed HSA and bonded cholate as well as the resulting stoichiometric ratios of HSA-cholate interaction interpolated to time zero of each modulation experiment. Table 13(B) presents the percentage of change of these parameters within a measuring time of 10 h. A graphic representation of the evaluation is shown in Fig. 45 – Fig. 54. For comparison of slopes of corresponding graphs they are presented in the same scale. The letters A, B, and C denote:

A: time dependent decrease of the surface concentration of HSA Γ_{HSA} during the modulation experiment

B: course of the concentration of cholate Γ_{chol} reversibly bonded to the adsorbed HSA layer during the modulation experiment

C: time dependency of the stoichiometric ratio, i.e. the cholate bonding affinity of HSA, evaluated by division of B and A, i.e. $\Gamma_{chol} / \Gamma_{HSA}$

In all experiments a small loss of HSA was detected ranging from 0.4% to 1.3% per 10 h (see Section 5.2, p. 61). As a result of such a decrease of the receptor a reduction of bonded cholate at least in the same amount has to be expected. That was not the case in c-ME by 6 mM and 10 mM cholate solution, and the experiment with the 20 mM cholate solution showed even an increase of 0.9%/10 h of bonded cholate. Such unexpected results were caused by the presence of a cholate bonding impurity, which also adsorbed to the reflection element (see Section 5.4.1, p. 78). The influence of the impurity is clearly visible

in the representations of the cholate bonding ability (see Graph C of Fig. 51, Fig. 52, and Fig. 54), which show an increase despite of HSA loss. As a result of these findings we can conclude that all experiments were affected by the impurity, but not in the same extent because it was present in different amounts in all cholate charges. Interpolation of results to the beginning of each modulation experiment excluded the influence of the impurity.

Table 13. (A) Surface concentrations of adsorbed HSA Γ_{HSA} and reversibly bonded cholate Γ_{chol} as well as the resulting stoichiometric ratios of HSA-cholate interaction at the applied concentrations of cholate in PBS interpolated to time zero, i.e. the beginning of modulation experiments. (B) Decrease/Increase of Γ_{HSA}, Γ_{chol}, and of the stoichiometric ratios, i.e. the bonding affinities, within a measuring time of 10 h.

(A)

conc. of cholate in PBS [mM]	surface conc. $\Gamma_{0,HSA}$ [10^{-12} mol cm^{-2}]	surface conc. $\Gamma_{0,chol}$ [10^{-12} mol cm^{-2}]	stoichiometric ratio ($\Gamma_{0,cholate}$ / $\Gamma_{0,HSA}$)
0.3	5.32 ± 0.42	3.48 ± 1.08	0.65 ± 0.21
1.0	5.46 ± 0.43	8.87 ± 1.21	1.62 ± 0.26
2.0	5.28 ± 0.42	15.7 ± 2.08	2.97 ± 0.46
3.0	5.00 ± 0.40	22.1 ± 3.14	4.42 ± 0.51
4.0	5.18 ± 0.41	25.0 ± 2.83	4.83 ± 0.66
5.0	5.31 ± 0.42	32.1 ± 3.90	6.05 ± 0.88
6.0	5.10 ± 0.40	33.0 ± 4.50	6.47 ± 1.02
10.0	5.03 ± 0.40	46.1 ± 5.85	9.17 ± 1.37
15.0	5.09 ± 0.40	53.8 ± 6.79	10.57 ± 1.57
20.0	4.98 ± 0.39	57.7 ± 7.07	11.59 ± 1.69

(B)

conc. of cholate in PBS [mM]	$\Delta\ \Gamma_{HSA}$/10 h expressed as percentage of $\Gamma_{0,HSA}$	$\Delta\ \Gamma_{chol}$/10 h expressed as percentage of $\Gamma_{0,chol}$	Δ stoichiometric ratio/10 h expressed as percentage of $\Gamma_{0,cholate}$ / $\Gamma_{0,HSA}$
0.3	-0.9	-4.7	-3.8
1.0	-0.5	-2.6	-2.2
2.0	-1.0	-2.3	-1.3
3.0	-0.7	-1.5	-0.9
4.0	-1.0	-1.3	-0.4
5.0	-1.1	-1.7	-0.6
6.0	-0.9	-0.3	0.7
10.0	-1.3	-0.9	0.5
15.0	-0.4	-0.6	-0.2
20.0	-0.6	0.9	1.5

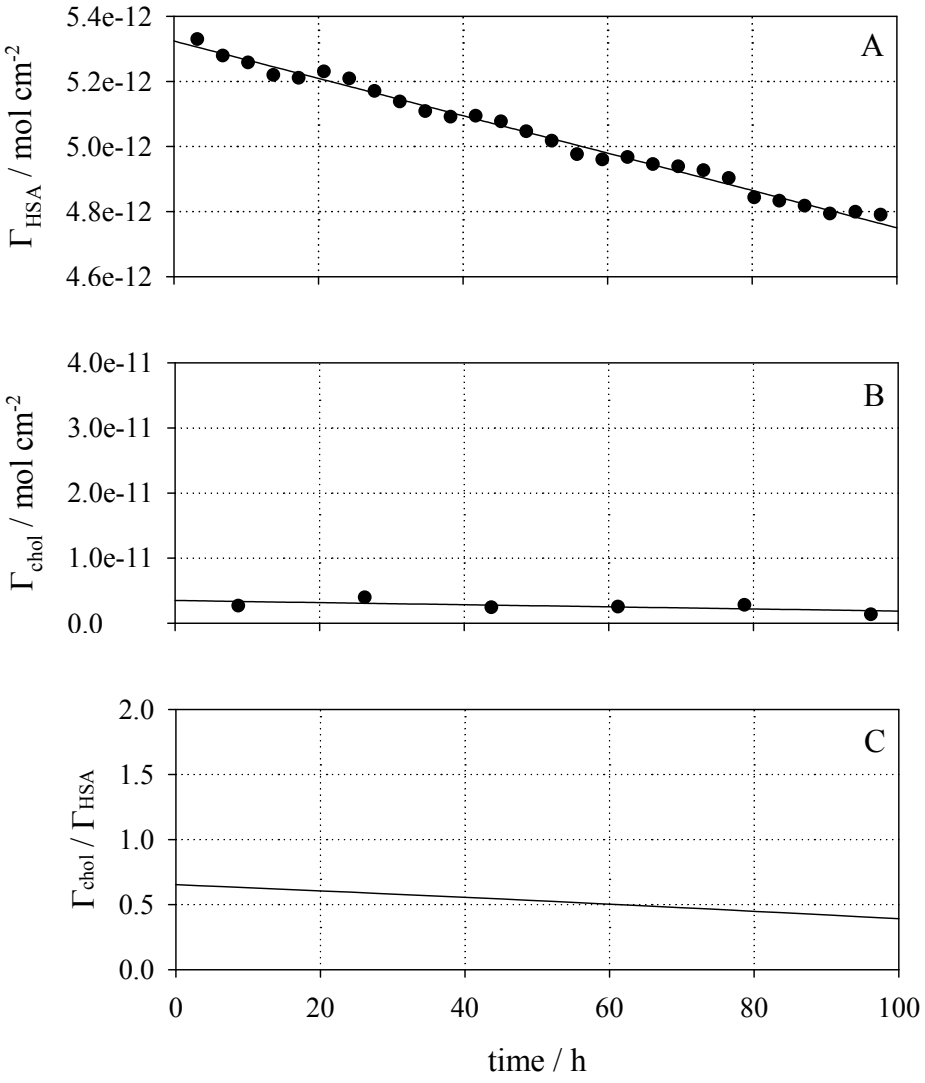

Fig. 45. Graphic representation of the evaluation of c-ME by 0.3 mM cholate solution. (A): The surface concentration of immobilized HSA decreased by about 0.9 % per 10 hours due to detachment from the Ge MIRE. (B): The surface concentration of reversibly bonded cholate Γ_{chol} decreased by about 4.7 % per 10 hours because of detachment and denaturation of HSA. Results of 5 successive vp-pp-vp modulation measurements were averaged to achieve a sufficient signal to noise ratio for determination of the course of Γ_{chol}. (C): Decrease of the bonding affinity of HSA $\Gamma_{cholate}$ / Γ_{HSA} due to the effects depicted by (A) and (B).

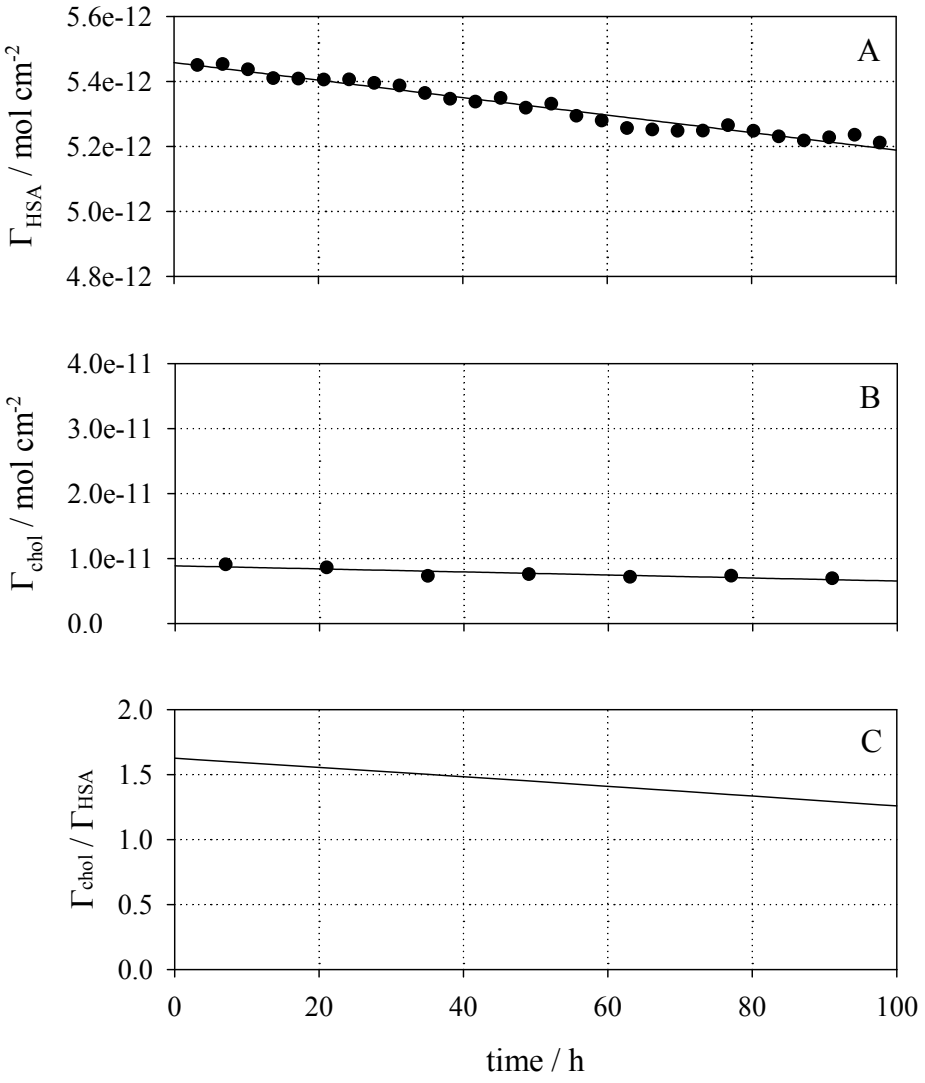

Fig. 46. Graphic representation of the evaluation of c-ME by 1.0 mM cholate solution. (A): The surface concentration of immobilized HSA decreased by about 0.5 % per 10 hours due to detachment from the Ge MIRE. (B): The surface concentration of reversibly bonded cholate Γ_{chol} decreased by about 2.6 % per 10 hours because of detachment and denaturation of HSA. Results of 4 successive vp-pp-vp modulation measurements were averaged to achieve a sufficient signal to noise ratio for determination of the course of Γ_{chol}. (C): Decrease of the bonding affinity of HSA $\Gamma_{cholate}$ / Γ_{HSA} due to the effects depicted by (A) and (B).

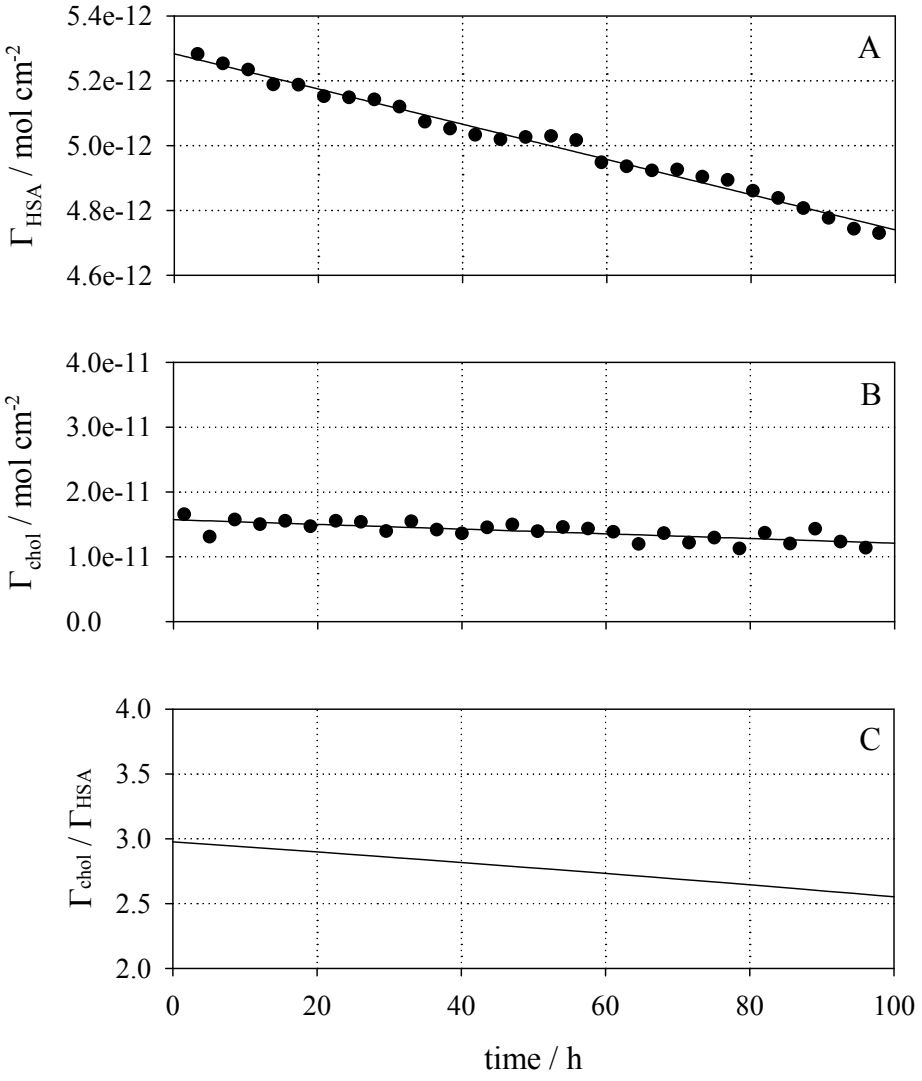

Fig. 47. Graphic representation of the evaluation of c-ME by 2.0 mM cholate solution. (A): The surface concentration of immobilized HSA decreased by about 1.0 % per 10 hours due to detachment from the Ge MIRE. (B): The surface concentration of reversibly bonded cholate Γ_{chol} decreased by about 2.3 % per 10 hours because of detachment and denaturation of HSA. (C): Decrease of the bonding affinity of HSA $\Gamma_{cholate}$ / Γ_{HSA} due to the effects depicted by (A) and (B).

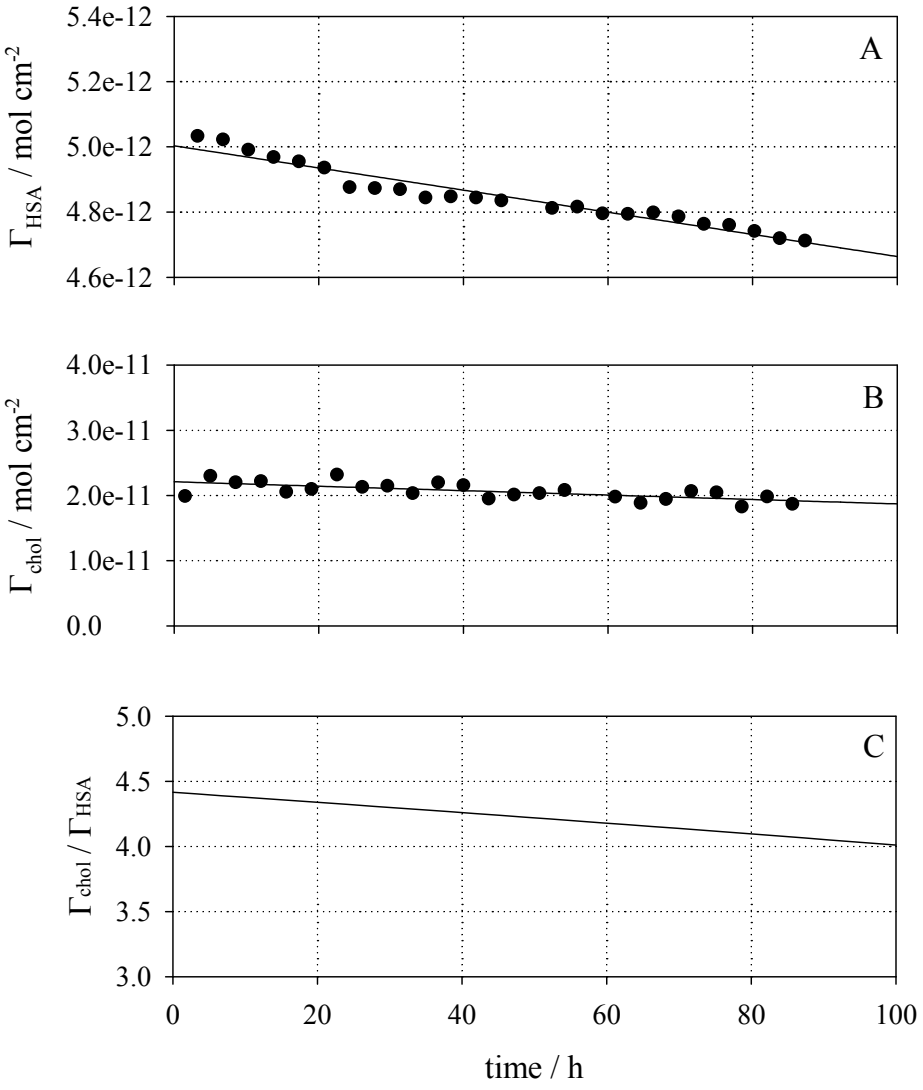

Fig. 48. Graphic representation of the evaluation of c-ME by 3.0 mM cholate solution. (A): The surface concentration of immobilized HSA decreased by about 0.7 % per 10 hours due to detachment from the Ge MIRE. (B): The surface concentration of reversibly bonded cholate Γ_{chol} decreased by about 1.5 % per 10 hours because of detachment and denaturation of HSA. (C): Decrease of the bonding affinity of HSA $\Gamma_{cholate}$ / Γ_{HSA} due to the effects depicted by (A) and (B).

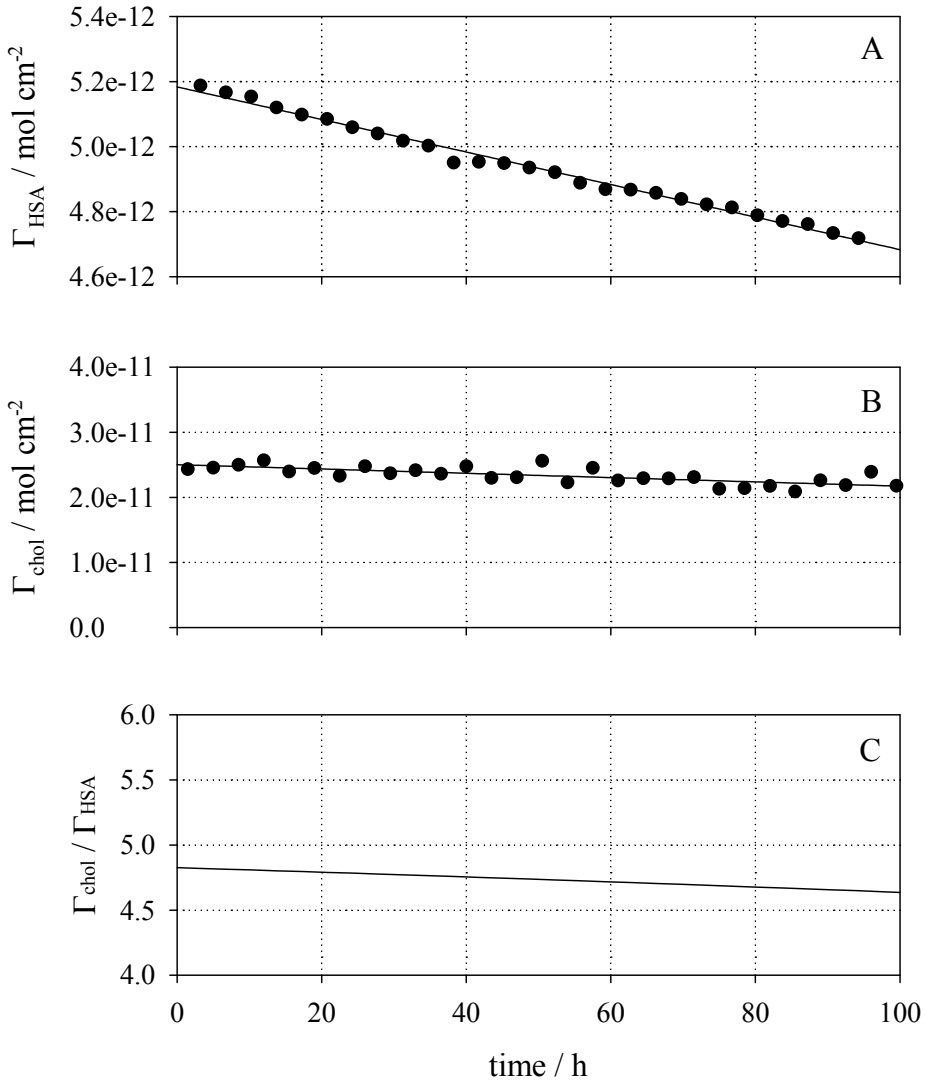

Fig. 49. Graphic representation of the evaluation of c-ME by 4.0 mM cholate solution. (A): The surface concentration of immobilized HSA decreased by about 1.0 % per 10 hours due to detachment from the Ge MIRE. (B): The surface concentration of reversibly bonded cholate Γ_{chol} decreased by about 1.3 % per 10 hours because of detachment and denaturation of HSA. (C): Decrease of the bonding affinity of HSA $\Gamma_{cholate}$ / Γ_{HSA} due to the effects depicted by (A) and (B).

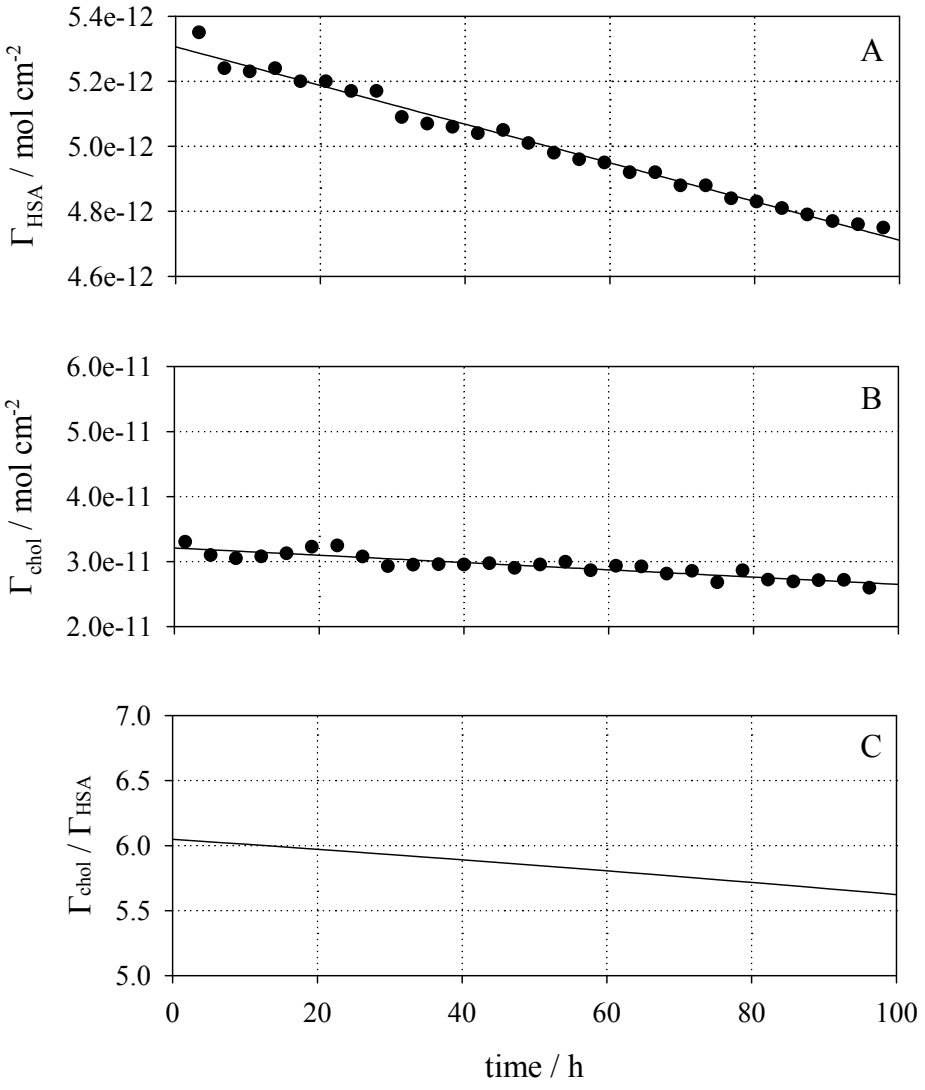

Fig. 50. Graphic representation of the evaluation of c-ME by 5.0 mM cholate solution. (A): The surface concentration of immobilized HSA decreased by about 1.1 % per 10 hours due to detachment from the Ge MIRE. (B): The surface concentration of reversibly bonded cholate Γ_{chol} decreased by about 1.7 % per 10 hours because of detachment and denaturation of HSA. (C): Decrease of the bonding affinity of HSA $\Gamma_{cholate}$ / Γ_{HSA} due to the effects depicted by (A) and (B).

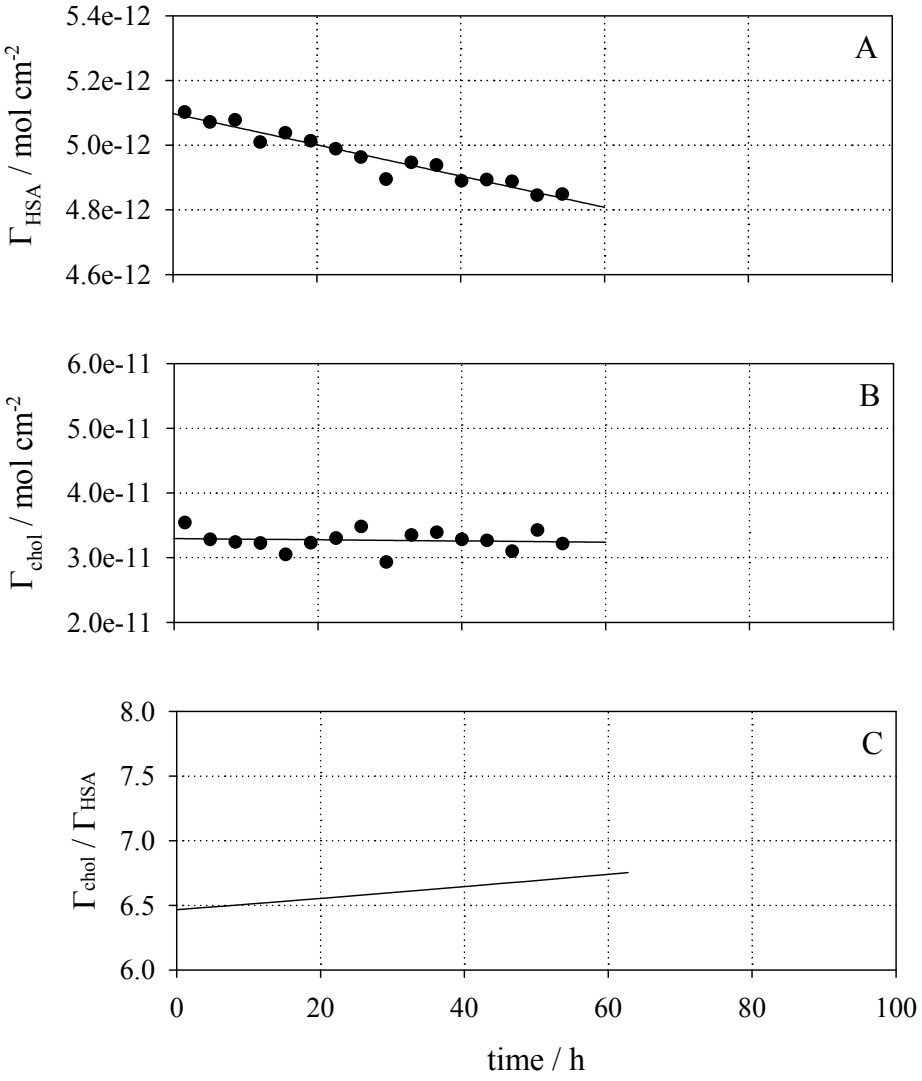

Fig. 51. Graphic representation of the evaluation of c-ME by 6.0 mM cholate solution. (A): The surface concentration of immobilized HSA decreased by about 0.9 % per 10 hours due to detachment from the Ge MIRE. (B): The surface concentration of reversibly bonded cholate Γ_{chol} decreased only by about 0.3 % per 10 hours. (C): The effect of detachment and denaturation of HSA was overcompensated by adsorption of the cholate bonding impurity resulting in an increase of the bonding affinity of about 0.7 % per 10 hours.

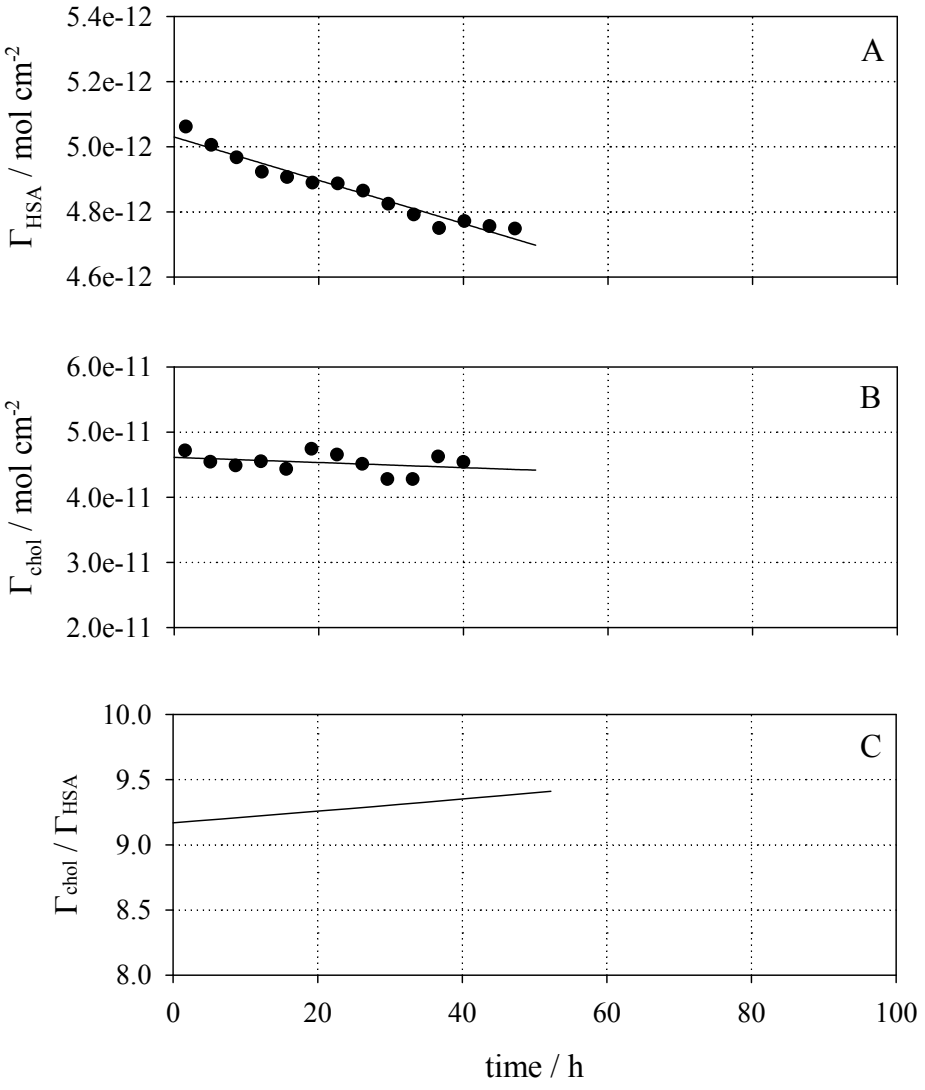

Fig. 52. Graphic representation of the evaluation of c-ME by 10.0 mM cholate solution. (A): The surface concentration of immobilized HSA decreased by about 1.3 % per 10 hours due to detachment from the Ge MIRE. (B): Compared to (A), the surface concentration of reversibly bonded cholate Γ_{chol} decreased only by about 0.9 % per 10 hours. (C): The effect of detachment and denaturation of HSA was overcompensated by adsorption of the cholate bonding impurity resulting in an increase of the bonding affinity of about 0.5 % per 10 hours.

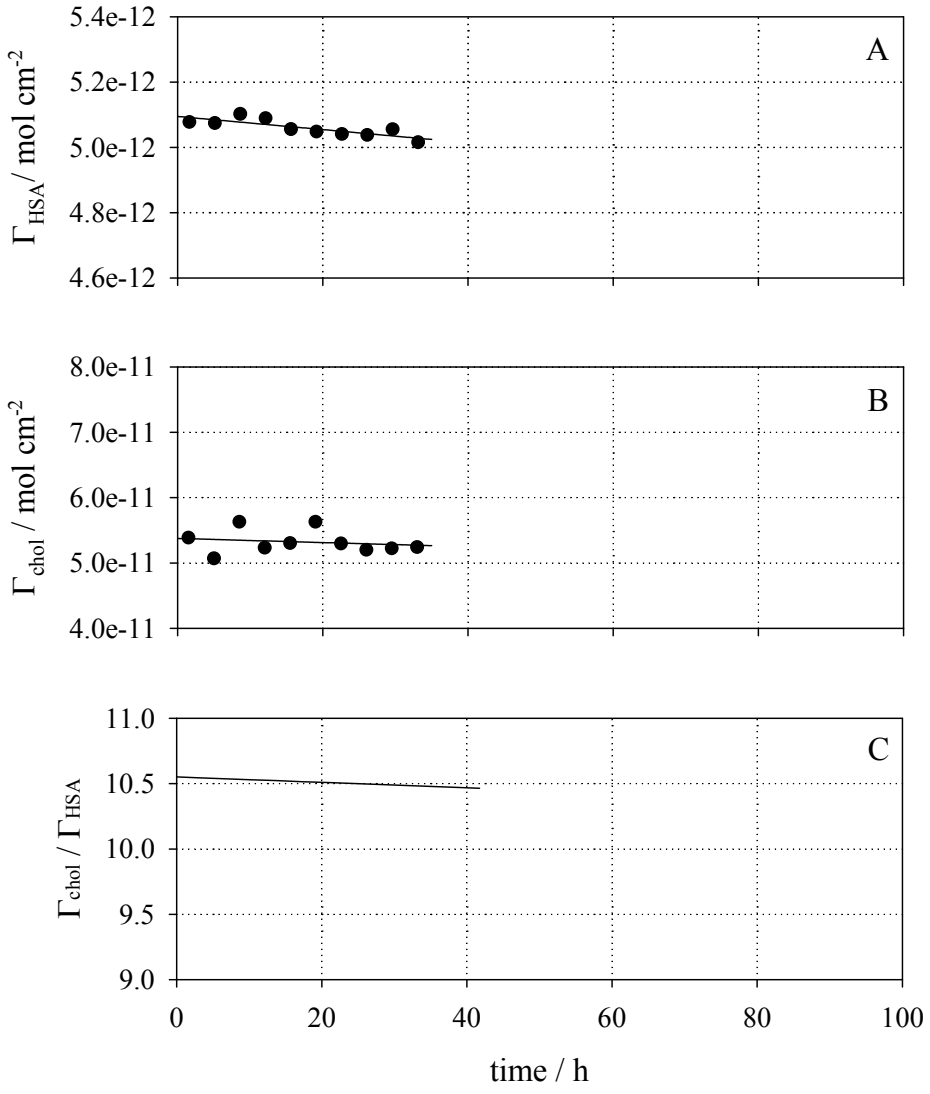

Fig. 53. Graphic representation of the evaluation of c-ME by 15.0 mM cholate solution. (A): The surface concentration of immobilized HSA decreased by about 0.4 % per 10 hours due to detachment from the Ge MIRE. (B): The surface concentration of reversibly bonded cholate Γ_{chol} decreased by about 0.6 % per 10 hours because of detachment and denaturation of HSA. (C): Decrease of the bonding affinity of HSA $\Gamma_{cholate} / \Gamma_{HSA}$ due to the effects depicted by (A) and (B).

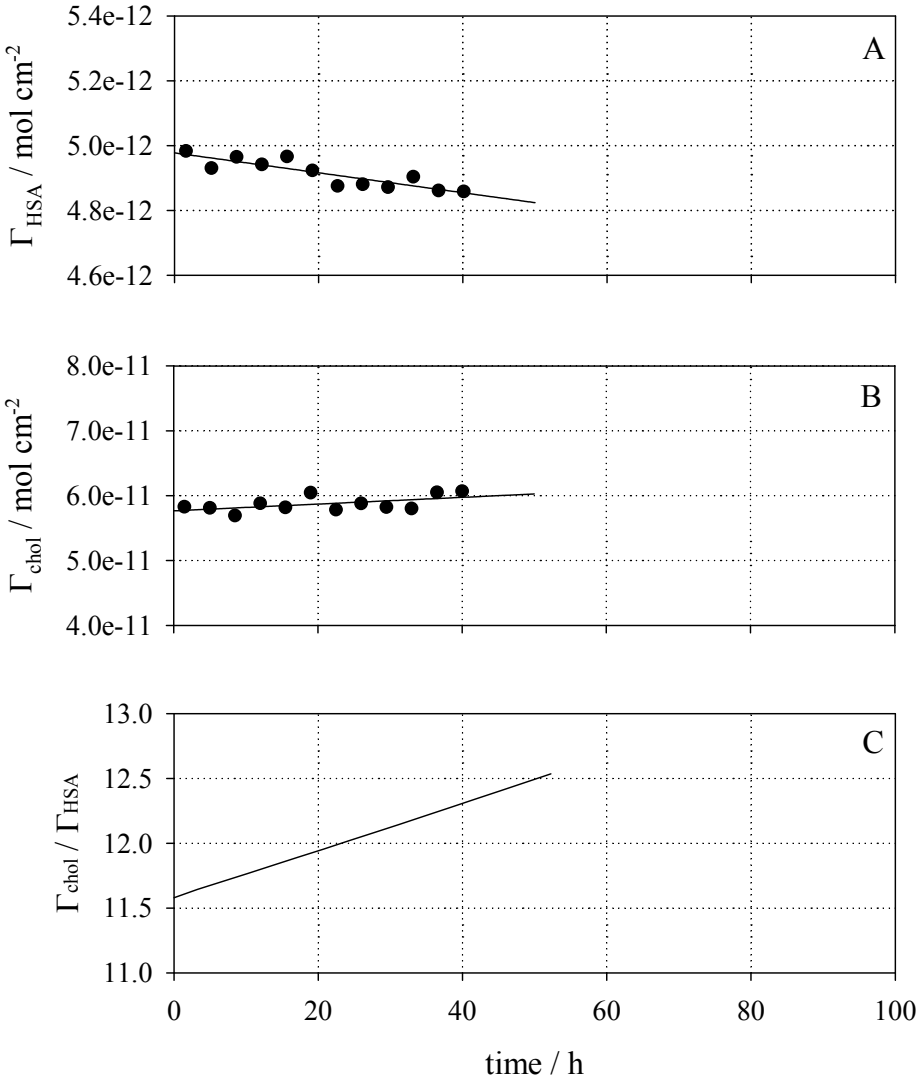

Fig. 54. Graphic representation of the evaluation of c-ME by 20.0 mM cholate solution. (A): The surface concentration of immobilized HSA decreased by about 0.6 % per 10 hours due to detachment from the Ge MIRE. (B): In the experiment with the highest cholate concentration even the surface concentration of reversibly bonded cholate Γ_{chol} increased by about 0.9 % per 10 hours despite of HSA loss. This fact can only be explained by adsorption of the cholate bonding impurity, which overcompensated by this way the loss of receptor. (C): Increase of the bonding affinity of about 1.5 % per 10 hours due to the effects depicted by (A) and (B).

8 References

[1]G. Reiter, M. Siam, D. Falkenhagen, W. Gollneritsch, D. Baurecht, U.P. Fringeli, Interaction of a bacterial endotoxin with different surfaces investigated by in situ Fourier transform infrared attenuated total reflection spectroscopy, Langmuir (2002) 18, 5761-5771.

[2]G. Reiter, N. Hassler, V. Weber, D. Falkenhagen, U.P. Fringeli, In situ FTIR ATR spectroscopic study of the interaction of immobilized human tumor necrosis factor-α with a monoclonal antibody in aqueous environment, Biochim. Biophys. Acta 1699 (2004) 253-261.

[3]C. Weber, W. Strobl, A. Krause, D. Falkenhagen, Novel detoxification device to support patients with hepatic failure, Int. J. Artif. Organs 25 (2002) 687.

[4]P. Hofer, U.P. Fringeli, Structural investigation of biological material in aqueous environment by means of infrared-ATR spectroscopy, Biophys. Struct. Mech. 6 (1979) 67-80.

[5]U.P. Fringeli, H.H. Günthard, D. Baurecht, in: H.U. Gremlich, B. Yan (Eds.), Infrared and Raman Spectroscopy of Biological Materials, Marcel Dekker, New York, 2000, pp.143-192.

[6]W. Fiers, Tumor necrosis factor. Characterization at the molecular, cellular and in vivo level, FEBS Lett. 285 (1991) 199– 212.

[7]M.J. Eck, S.R. Sprang, The structure of tumor necrosis factor-a at 2.6 Å resolution, J. Biol. Chem. 264 (1989) 17595– 17605.

[8]Oberg K. A., Fink A. L.: A New Attenuated Total Reflectance Fourier Transform Infrared Spectroscopy Method for the Study of Proteins in Solution. Analytical Biochemistry 256 (1998); 92-106.

[9]N. Hassler, Passivierung der Oberfläche eines Germanium-Kristalls für die FTIR-ATR-Spektroskopie zur Verhinderung unerwünschter Proteinadsorptionen, Diploma work, University of Vienna, 2003.

[10]T. Peters, All about Albumin, Academic Press, New York, 1995.

[11]T. Peters, Jr.: Serum Albumin. Adv. Protein Chem. 37 (1985); 161-245.

[12]D.C. Carter, J.X. Ho, Structure of serum albumin, Adv. Protein Chem. 45 (1994) 153-203.

[13]J. Figge, T.H. Rossing, V. Fencl, The role of serum proteins in acid-base equilibria, J. Lab. Clin. Med. 117 (1991) 453-467.

[14]A. Shrake, J.S. Finlayson, P.D. Ross, Thermal stability of human albumin measured by differential scanning calorimetry. I. Effects of caprylate and N-acetyltryptophanate, Vox Sang. 47 (1984) 7-18.

[15]M.J. Mura-Galelli, J.C. Voegel, S. Behr, E.F. Bres, P. Schaaf, Adsorption/desorption of human serum albumin on hydroxyapatite: A critical analysis of the Langmuir model, Proc. Natl. Acad. Sci. U.S.A. 88 (1991) 5557-5561.

[16]M.N. Jones, D. Chapman, Micelles, Monolayers, and Biomembranes, Wiley-Liss, New York, 1995.

[17]A. Roda, G. Cappelleri, R. Aldini, E. Roda, L. Barbara, Quantitative aspects of the interaction of bile acids with human serum albumin, J. Lipid Res. 23 (1982) 490-495.

[18]U.P. Fringeli, In situ infrared attenuated total reflection membrane spectroscopy, in: F.M. Mirabella (Ed.), Internal Reflection Spectroscopy, Marcel Dekker, New York, 1992, pp. 255-324.

[19]N.J. Harrick, Internal Reflection Spectroscopy, Harrick Sci. Corp.: Ossining, NY, 1979.

[20]Goos F. and Lindberg-Hänchen H., Ann. Phys, 5:251, 1949.

[21]U.P. Fringeli, H.-J. Apell, M. Fringeli, P. Läuger, Polarized infrared absorption of Na^+/K^+-ATPase studied by attenuated total reflection spectroscopy, Biochim. Biophys. Acta 984 (1989) 301-312.

[22]Born, M., and Wolf, E., Principles of Optics, Oxford: Pergamon Press, 1983, 6^{th} ed. Ch. 1, pp. 47-51.

[23]U.P. Fringeli, D. Baurecht, T. Bürgi, M. Siam, G. Reiter, M. Schwarzott, P. Brüesch, ATR spectroscopy of thin films, in: H.S. Nalwa (Ed.), Handbook of Thin Film Materials, vol. 2, chapt. 4, Academic Press, 2002, pp. 191-229.

[24]Schwarzott M., Engelhardt H., Klühspies T., Baurecht D., Naumann D., Fringeli U.P., In Situ FTIR ATR Spectroscopy of the Preparation of an Oriented Monomolecular Film of Porin Omp32 on an Internal Reflecting Element by Dialysis, Langmuir 19 (2003) 7451-7459.

[25]The MathWorks, Inc., 24 Prime Park Way, Natick, MA 01760, USA.

[26]J. Matijasevic, N. Hassler, G. Reiter, U.P. Fringeli, In Situ ATR FTIR Monitoring of the Formation of Functionalized Mono- and Multilayers on Germanium Substrate: from 7-Octenyltrichlorosilane to 7-Carboxylsilane, Langmuir 24 (2008), 2588-2596.

[27]D. Baurecht, I. Porth, U.P. Fringeli, A new method of phase sensitive detection in modulation spectroscopy applied to temperature induced folding and unfolding of RNase A, Vib. Spectrosc. 30 (2002), 85-92.

[28]M. Schwarzott, P. Lasch, D. Baurecht, D. Naumann, U.P. Fringeli, Electric Field-Induced Changes in Lipids Investigated by Modulated Excitation FTIR Spectroscopy, Biophysical Journal 86 (2004) 285-295.

[29]A. Urakawa, R. Wirz, T. Bürgi, A. Baiker, ATR-IR Flow-Through Cell for Concentration Modulation Excitation Spectroscopy: Diffusion Experiments and Simulations, J. Phys. Chem. B 107 (2003) 13061-13068.

[30]R. Wirz, T. Bürgi, W. Lindner, A. Baiker, Absolute Configuration Modulation Attenuated Total Reflection IR Spectroscopy: An in Situ Method for Probing Chiral Recognition in Liquid Chromatography, Anal. Chem. 76 (2004) 5319-5330.

[31]H.J. Böhm, G. Schneider, Protein-Ligand Interactions, Wiley-VCH, New York, 2003.

[32]SBSR equipment was obtained from OPTISPEC, Rigistrasse 5, CH-8173 Neerach, Switzerland (http://www.optispec.ch) or Portman Instruments AG, Gewerbestr. 18, CH-4105 Biel-Benken (http://www.portmann-instruments.ch).

[33]G. Reiter, Investigation of Structure-Function-Relationships of Membrane-Anchored Proteins with the Help of Fourier Transform Infrared Attenuated Total Reflection (FTIR ATR) Spectroscopy, Dissertation, University of Vienna, 2001.

[34]D. Baurecht, G. Reiter, N. Hassler, M. Schwarzott, U.P. Fringeli, Application of Special FTIR ATR Techniques for Quantitative Structural Analysis of Thin Surface Layers, Chimia 59 (2005) 226-235.

[35]C.H. Hamann, W. Vielstich, Elektrochemie I, Verlag Chemie, Weinheim, 1985.

[36] Yu.N. Chirgadze, N.A. Nevskaya, Infrared spectra and resonance interaction of amide-I vibration of the antiparallel-chain pleated sheet, Biopolymers 15 (1976) 607-625.

[37]H.H. Mantsch, W.K. Surewicz, Probing protein secondary structure by infrared spectroscopy, in: V. Renugopalakrishnan, P.R. Carey, I.C.P. Smith, S.-G. Huang, A.C. Storer (Eds.), Proteins: Structure, Dynamics and Design, ESCOM, Leiden, 1991, pp 125-132.

[38]J.L.R. Arrondo, A. Muga, J. Castresana, F.M.Goni, Quantitative studies of the structure of proteins in solution by Fourier transform infrared spectroscopy., Prog. Biophys. Molec. Biol. 59 (1993) 23-56.

[39]A. Barth, C. Zscherp, What vibrations tell us about proteins, Quart. Rev. Biophysics 35(4) (2002) 369–430.

[40]A.K. Wright, M.R. Thompson, Hydrodynamic structure of bovine serum albumin determined by transient electric birefringence. Biophys. J. 15 (1975) 137-141.

[41]M. C. Chen, R. C. Lord, Laser-excited Raman spectroscopy of biomolecules. VIII. Conformational study of bovine serum albumin, J. Am. Chem. Soc. 98(4) (1976) 990-992.

[42]Yu.N. Chirgadze, E.V.Brazhnikov, Intensities and other spectral parameters of infrared amide bands of polypeptides in the α-helical form, Biopolymers 13 (1974) 1701-1712.

[43]A. Roda, A.F. Hofmann, K.J. Mysels, The Influence of Bile Salt Structure on Self-association in Aqueous Solutions, J. Biol. Chem. 258 (1983) 6362-6370.

[44]M.J. Schwuger, Lehrbuch der Grenzflächenchemie, Georg Thieme Verlag, Stuttgart, 1996.

[45]Norbert Hassler, Dieter Baurecht, Gerald Reiter, Urs Peter Fringeli, In situ FTIR ATR spectroscopic study of the interaction of immobilized human serum albumin with cholate by means of concentration-modulated excitation, Biochim. Biophys. Acta (2008), in preparation.

[46]U.P. Fringeli, Verfahren zur simultanen, digitalen phasenempfindlichen Detektion von zeitaufgelösten, quasi-gleichzeitig erfassten Datenarrays eines periodisch stimulierten Systems. Internationale Patent Publikation, PCT, WO 97/08598 [1997].

[47]D. Baurecht, U.P. Fringeli, Quantitative Modulated Excitation Fourier Transform Infrared (ME-FTIR) Spectroscopy, Rev. Sci. Instrum. 72 (2001) 3782-3792.

[48]M. D'Alagni, A.A. D'Archivio, E. Giglio, On the Interaction of Polypeptides with Bile Salts or Bilirubin-IXα, Biopolymers 33 (1993) 1553-1565.

Lebenslauf

Persönliche Daten

Name:	Mag. Norbert HASSLER
Geburtsdatum:	15. Oktober 1966
Staatsbürgerschaft:	Österreich
Familienstand:	ledig
Adresse:	Budinskygasse 18/18 A-1190 Wien
Email:	norbert.hassler@gmx.net

Ausbildung

1973 - 1977	Volksschule in St. Andrä/Lavanttal;
1977 - 1985	Öffentliches Stiftsgymnasium der Benediktiner in St. Paul/Lavanttal; realistischen Zweig mit gutem Erfolg abgeschlossen;
1985 - 1986	Wehrdienst in Straß/Steiermark und Gratkorn;
1987 - 1989	Studium TU Wien (vier Semester Informatik);
1986 - 2003	Studium Universität Wien (Chemie mit Schwerpunkt Biochemie) mit Mag. rer. nat. abgeschlossen;
seit April 2003	Doktoratsstudium der Chemie am Institut für Biophysikalische Chemie der Universität Wien.

Berufstätigkeiten

seit 2001	Studentenbetreuer und Lehrbeauftragter im Rahmen des Lehrbetriebs am Institut für Biophysikalische Chemie der Universität Wien;
Juli 2002 – August 2003	Wissenschaftlicher Mitarbeiter am Institut für Biophysikalische Chemie der Universität Wien im Rahmen eines Forschungsprojekts des Jubiläumsfonds der Österr. Nationalbank (Titel: In situ FTIR ATR spectroscopic study of the interaction of immobilized human tumor necrosis factor-α with a monoclonal antibody in aqueous environment)
seit September 2008	Postdoc-Stelle am Ludwig Boltzmann-Institut für Osteologie im Rahmen eines Forschungsprojekts des FWF (Titel: Matrix-Cell feedback mechanisms due to altered collagen organization)